A MEASUREMENT OF THE TWO GAMMA DECAYS
OF NEUTRAL K – MESONS

IAN PETER JOSEPH SHIPSEY

DOCTOR OF PHILOSOPHY
UNIVERSITY OF EDINBURGH
1986

Declaration

This work represents the efforts of various members of the CERN-Dortmund-Edinburgh-Orsay-Pisa-Siegen Collaboration at CERN, the European Organisation for Nuclear Research; the analysis and final results are however entirely my own.

Ian F. Skippey

29th August 1986

CONTENTS

TABLES

FIGURES

v

ABSTRACT

The CERN−DORTMUND−EDINBURGH−ORSAY−PISA−SIEGEN Neutral Kaon Spectrometer at the CERN SPS has been used to study the two gamma decays of the neutral K−meson. Using a K_L beam, some 18,000 events with K−momenta between 70 GeV and 150 GeV have been collected, representing a twofold increase in the world sample for this process. We determine the ratio :

$$\Gamma(K_L \to \gamma\gamma)/\Gamma(K_L \to 2\pi^0) = 0.616 \pm 0.006 \pm 0.014$$

where the first error is statistical and the second systematic. We calculate the branching ratio for $K_L \to 2\gamma$ to be :

$$\Gamma(K_L \to \gamma\gamma)/\Gamma(K_L \to \text{all}) = 5.87 \pm 0.24 \times 10^{-4}.$$

This is to be compared with the previous world average :

$$\Gamma(K_L \to \gamma\gamma)/\Gamma(K_L \to \text{all}) = 4.9 \pm 0.4 \times 10^{-4}.$$

The ratio R of the partial widths of the K_S and K_L mesons to two photons has also been determined by a double ratio technique. Six K→γγ candidates are isolated in the K_S beam, whilst a measurement of the K_L content of this beam predicts three $K_L \to 2\gamma$ events. We find an upper limit for R :

$$\Gamma(K_S \to \gamma\gamma)/\Gamma(K_L \to \gamma\gamma) < 11.7 \text{ at } 90\% \text{ CL}$$

representing an improvement by a factor of 40 on the previous result.

1

1. INTRODUCTION

Of the many different disciplines, science at least, develops its universality by endlessly refining and generalising its own principles. As a consequence, these principles are very far removed from the intuitive ideas which gave rise to them. Physics, which is the most developed science in this sense, may be considered the universal natural science.

All pure knowledge, as opposed to Action, is concerned with answering the question, what is. For physics, which endeavours to ask this question about seemingly trivial or elementary objects, compared to structures like society or living creatures, the answer is very particular. Each discipline divides reality.

The answer that physics gives, should however be seen to supersede the traditional solutions of pure philosophy. This is because the scientific method yields a more accurate knowledge of the difficulties of understanding nature, clear demonstrations of the frailty of human reason when applied to new situations, and established procedures to overcome these obstacles.

However, the scientific method has produced contradictary world views throughout its short history; indicating that caution is necessary in raising its results to the level of principles of reality.

The equations of motion of classical mechanics possess certain invariance properties. The conservation of momentum may be viewed as the invariance of the Hamiltonian under a space translation. Similarly conservation of energy corresponds to invariance under time translation, and conservation of angular momentum to invariance under rotation about an axis. In quantum mechanics a conserved quantity is one which commutes with the Hamiltonian. One can consider a space translation operator, or a rotation operator by analogy with the classical case, and the same conservation laws are obeyed. In contrast to these continuous transformations, we may also consider discrete transformations, for example Parity (P) the operator which produces a spatial inversion of the coordinates of a system.

As a further example we consider the operation of charge conjugation which reverses the sign of the charge and the magnetic moment of a particle. Classically Maxwell's equations are invariant to a change in the sign of the charge and the current density. Quantum mechanically, this operator in addition changes the sign of the baryon number or lepton number.

Lastly there is time reversal invariance (T). Changing the sign of the time coordinate leaves Newton's third law unaltered. In quantum mechanics the T operator interchanges all final and initial states in an interaction, and reverses all momenta and spins.

One of the most important principles of quantum field theory is the CPT theorem which states that all interactions, without exception, are invariant under the succession of the three operators, C, P and T taken in any order.

Both the strong and electromagnetic interactions obey the conservation of parity, charge conjugation invariance and time reversal invariance separately. Until 1964 it was believed that the weak interaction whilst not obeying C or P individually obeyed the combined operation conserving parity and charge conjugation (CP).

One of the particles discovered in the early days of cosmic rays was the neutral kaon. This particle was subsequently produced copiously at accelerators and studied in greater detail. It was found to decay to two pions in such a way as to seemingly violate simultaneously two symmetries, charge invariance and parity. That CP−violation occurred was a totally unexpected observation, and by the CPT theorem, implies a T−violation of the same magnitude. Whilst the current synthesis has been extended to accommodate the behaviour of the kaon, at the present time the possibility that this decay is due to a completely new interaction cannot be excluded.

There have been many attempts to study the two pion decays of the neutral kaon; the rarity of this process has made it extremely difficult to measure precisely. In this work the decay of the neutral kaon to two photons is studied. This decay channel may also be expected to exhibit the phenomenon of CP−violation, and may shed new light on the unsolved mystery of CP−violation.

3

As in many previous studies of $K \to \gamma\gamma$ the data is collected in an experiment designed to measure the two pion decay modes of the neutral K−meson, for which the apparatus is optimised. The experiment has several novel features; the K_S beam is produced at a target close to the detector in contrast to the normal method of regeneration, and as the vector momentum of the neutral decay products is not measured, a kaon decay is assumed to determine the decay vertex of an event.

We present two new experimental results. The first is a determination of the ratio, P, of the partial widths of the K_L meson to two photons and two neutral pions respectively.

$$P = \Gamma(K_L \to \gamma\gamma)/\Gamma(K_L \to 2\pi^0)$$

The result is dependent on a monte carlo calculation of the relative acceptance of $K_L \to 2\gamma$ and $K_L \to 2\pi^0$. From P and the world average value of the branching ratio for $K_L \to 2\pi^0$ we obtain B, the branching ratio of $K_L \to 2\gamma$.

$$B = \Gamma(K_L \to \gamma\gamma)/\Gamma(K_L \to all)$$

There have been nine previous determinations of $K_L \to \gamma\gamma$ with various normalisations [1], [5], [6], [7], [8], [9], [10], [11], [12]. The eight measurements made prior to 1974 are all in reasonable agreement, albeit within rather large errors due to either a small number of signal events or a small number of normalisation events. Recently a more precise measurement has been made at Fermilab [1];this result is three standard deviations above the world average. Therefore another precise determination of B is valuable.

The decay $K_S \to \gamma\gamma$ has not been observed. There have been five previous searches [2], [4], [8], [10], [12]. There has been no new result since 1973, in part because of the comparative difficulty in measuring $K_S \to 2\gamma$ using a regenerated K_S beam. Our second result is a determination of the ratio, R, of the partial widths of the K_L and K_S mesons to two photons respectively:

$$R = \Gamma(K_S \to \gamma\gamma)/\Gamma(K_L \to \gamma\gamma)$$

We use an analysis identical in spirit to that normally employed to measure CP violation in two pion decays. The result is approximately independent of monte carlo.

The phenomenology of the kaon system with particular reference to the two gamma final state is reviewed in chapter two. The experiment is described in chapter three. The principles of the analysis are discussed in chapter four. Data collection and reduction are outlined in chapter five, while chapter six describes the monte carlo used to calculate acceptances and make background subtractions. In chapter seven the single rate, P, is determined. In the following chapter the ratio, R, is measured. In chapter nine previous experiments are discussed and their results compared to the current work. A comparison with theory is also made.

2. THEORY

2.1 Introduction

That C (charge conjugation invariance) and P (parity) are violated in the weak interaction is well-established. However the combined operation of CP seems, phenomenologically, to be a symmetry of the weak interaction. The only exception is the decay of the long-lived neutral kaon to two pions.

Whilst there are many possible explanations for CP-violation, the modern orthodoxy compels one to consider the standard model as the framework in which an understanding should be found. The most popular scheme, originally suggested by Kobayashi and Maskawa [18], allows CP-violation by means of mixing between the light and heavy quark sectors. The model is able to reproduce the experimental data at present however half of the parameters of the matrix are not well known experimentally. It is also economically attractive because the CP violation can occur without appeal to any new particle or interaction. Other alternative candidates include an extension of the Higgs sector, left-right symmetric models, the introduction of extra heavy neutral vector or scalar bosons and the possibility that CP violation arises from the existence of a CP-odd term in the Lagrangian of quantum chromodynamics. The first two possibilities lead to large electric dipole moment estimates which have already been contradicted by experiment. I will not discuss any of these possibilities further.

Outside the standard model, theories proposing a violation of T or C in the strong interaction (millistrong) or the electromagnetic interaction, or a T violation in the weak interaction (milliweak) have been proposed. Also a superweak interaction has been suggested by Wolfenstein [14], which is in good agreement with the data. None of these theories have the economy of the Kobayashi and Maskawa scheme however with the exception of the second possibility; at the present time they may all be considered candidates. I will only consider the superweak scheme here.

An extensive experimental programme has determined the phenomenological parameters which describe CP violation. In this chapter those parameters are defined with special reference to the 2γ system rather than the more usual 2π mode. In what follows, CPT is assumed throughout.

2.2 The kaon system and the standard model.

The neutral kaons K^0 and $\bar{K}^0$ are produced by the strong interaction, but because they are the lightest strange particles they can only decay weakly. As neither kaon is a CP eigenstate, in a CP invariant world the expected physical particles would be equal mixtures of K^0 and $\bar{K}^0$. We use the convention in which the eigenstates of strangeness are:

$$S|K^0> = |K^0>$$

$$S|\bar{K}^0> = -|\bar{K}^0>$$

These are related to each other by :

$$CP|\bar{K}^0> = -|K^0>$$

$$CP|K^0> = -|\bar{K}^0>$$

The eigenstates of CP are :

$$K_1 = 1/\sqrt{2}\,(K^0 - \bar{K}^0) \quad (CP=1) \quad (even)$$

$$K_2 = 1/\sqrt{2}\,(K^0 + \bar{K}^0) \quad (CP=-1) \quad (odd)$$

This mixing can be explained in terms of an effective $\Delta S = 2$ CP−conserving second order weak interaction in the standard model, represented by the box diagram of Figure 1 , with the u and c quarks as the intermediate quarks.

7
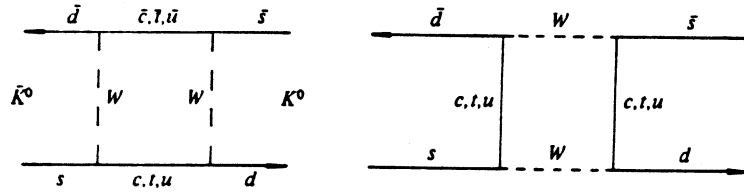
Figure 1: The box diagram.

The observed CP−violation requires, in addition, $\Delta S = 2$ CP−violating currents which give the mass eigenstates a CP impurity characterised by the complex number ϵ. The origin of this impurity is thought to be also understood by the box diagram, of Figure 1 , where the CP violation arises from the interference between the contributions from the different intermediate quarks. We may write the physical eigenstates as :

$$|K_S> = N[(1+\epsilon)|K^0> - (1-\epsilon)|\bar{K}^0>]$$

$$|K_L> = N[(1+\epsilon)|K^0> + (1-\epsilon)|\bar{K}^0>]$$

where $N = (1/\sqrt{2})(1/\sqrt{(1+|\epsilon|^2)})$. Or alternatively in terms of the CP eigenstates as :

$$|K_S> = N[|K_1> + \epsilon|K_2>]$$

$$|K_L> = N[|K_2> + \epsilon|K_1>]$$

where now, $N = (1/\sqrt{(1+|\epsilon|^2)})$

Let us now consider the decay of the K_L and K_S into two pions. The wavefunction for the final state must be symmetric with respect to particle interchange by Bose statistics, therefore the pions, which have $I = 1$, must be in an isospin state of $I = 0$ or $I = 2$. There are four amplitudes:

$$<\pi\pi, I=0 |H_{wk}|K_S>, \quad <\pi\pi, I=2 |H_{wk}|K_S>$$

$$<\pi\pi, I=0 |H_{wk}|K_L>, \quad <\pi\pi, I=2 |H_{wk}|K_L>$$

The physical pion states are superpositions of the isospin states:

$$\langle \pi^+\pi^-| = \sqrt{(1/3)} \langle \pi\pi, I=2| + \sqrt{(2/3)} \langle \pi\pi, I=0|$$

$$\langle \pi^0\pi^0| = \sqrt{(2/3)} \langle \pi\pi, I=2| + \sqrt{(1/3)} \langle \pi\pi, I=0|$$

The pions undergo a strong interaction phase shift :

$$\langle \pi^+\pi^-| = \sqrt{(1/3)}e^{i\delta_2} \langle \pi\pi, I=2| + \sqrt{(2/3)}e^{i\delta_0} \langle \pi\pi, I=0|$$

$$\langle \pi^0\pi^0| = \sqrt{(2/3)}e^{i\delta_2} \langle \pi\pi, I=2| + \sqrt{(1/3)}e^{i\delta_0} \langle \pi\pi, I=0|$$

The decay amplitudes are defined as :

$$A_0 = \langle \pi\pi, I=0 \mid H_{wk} |K^0 \rangle$$

$$A_2 = \langle \pi\pi, I=2 \mid H_{wk} |K^0 \rangle$$

The $\bar{K}^0$ decay amplitudes are then obtained from CPT :

$$-A_0^* = \langle \pi\pi, I=0 \mid H_{wk} |\bar{K}^0 \rangle$$

$$-A_2^* = \langle \pi\pi, I=2 \mid H_{wk} |\bar{K}^0 \rangle$$

The A_2 amplitude is suppressed relative to the A_0 by a factor which is experimentally determined to be 20. As the neutral kaon has $I = 1/2$ this is a statement of the $|\Delta I| = 1/2$ rule which has no adequate theoretical explanation. Using our mass eigenstates for K_L, and K_S we may now express the decay transitions in terms of ε, A_0 and A_2. Conventionally, A_0 is taken real to eliminate an arbitrary overall phase factor.

We define :

$$\eta_{+-} = <\pi^+\pi^- \mid K_L> / <\pi^+\pi^- \mid K_S>$$

$$\eta_{00} = <\pi^0\pi^0 \mid K_L> / <\pi^0\pi^0 \mid K_S>$$

In terms of which, neglecting second order terms in $|A_2|$ and ε:

$$\eta_{+-} \simeq \varepsilon + \varepsilon'$$

$$\eta_{00} \simeq \varepsilon - 2\varepsilon'$$

where :

$$\varepsilon' = 1/\sqrt{2} \, \text{Im}(A_2)/A_0 \, \exp \, i(\pi/2 + \delta_2 - \delta_0).$$

If there is a phase difference between A_0 and A_2, or equivalently a phase difference between the $I = 0$ and $I = 2$ decay channels, then ε' is not zero and CP violation occurs in the decay amplitude. This CP violation is called direct CP violation. The standard model allows $\Delta S = 1$ CP−violating processes which give rise to direct CP violation in the decay of a K_L or K_S, through the penguin diagrams [15] of Figure 2 . As these graphs involve an effective s→d transition which is $|\Delta I| = 1/2$, there are contributions to the A_0 amplitude but not to the A_2 amplitude. A_0 is no longer real in contradiction to our definition, we therefore must transform the phases of K^0 and $\overline{K}^0$. However the point to be stressed is that direct CP violation depends not on our previous isospin analysis but on the possibility that for a final state there exists two different decay amplitudes which have a phase shift between them.

There is no experimental evidence for direct CP violation. However, ε' does not depend on the fact that K_L and K_S mix.

$$X = 0, 1, \ldots, \text{gluons}$$
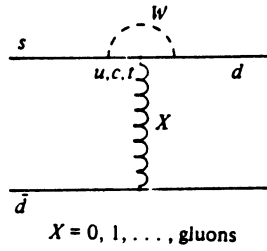
Figure 2: The penguin diagram.

It is from equation (1) that the famous relationship between the widths of the neutral kaon to two pions and ε'/ε is obtained. Empirically $\arg(\varepsilon) \cong \arg(\varepsilon')$, so that $\text{Im}(\varepsilon'/\varepsilon) \cong 0$, neglecting terms of order $|\varepsilon'|^2$ equation (1) becomes :

$$|\eta_{+-}|^2/|\eta_{oo}|^2 = 1 + 6\varepsilon'/\varepsilon$$

We close this section by stressing the very great contribution the experimental measurements of the kaon system have made, in shaping and extending the standard model. For example, the Glashow $-$ Iliopoulos $-$ Maiani (GIM) mechanism [3] introduced charm to suppress the experimentally unobserved strangeness changing neutral currents. Charm also proved necessary in order compute the mass difference between the K_L and K_S correctly [16]. Reciprocally, the observed mass difference was used to compute the charm quark mass before its discovery [19]. In order to accommodate CP $-$ violation Kobayashi and Maskawa [18] observed, that while suitably changing the unobservable phases of the states, any unitary 2x2 matrix can be made real, this is not necessarily true for higher dimensions. Their mixing matrix implied a new generation of quarks. The b $-$ quark was subsequently discovered. Indeed, even the non $-$ CP $-$ violating phenomen$\cdot$ of K^0 mixing arises from the fact that there is more than one generation of quarks, a fact the standard model is unable to explain.

2.3 The superweak theory

In 1964 when CP violation was first discovered, Wolfenstein [14] proposed a new $\Delta S = 2$ interaction to account for the $K^0 \leftrightarrow \bar{K}^0$ or equivalently $K_L \leftrightarrow K_S$ transition. $K_L \rightarrow 2\pi^0$ can then proceed via the intermediate K_S state. The amplitude is :

$$A \simeq \; <\pi\pi|H_{wk}|K_S> \; <K_S|H_{swk}|K_L>/\Delta m$$

whilst A is also given by :

$$A \simeq \; <\pi\pi|H_{wk}|K_S>$$

Solving for H_{swk} :

$$H_{swk} \simeq 2 \times 10^{-10} \; H_{wk}$$

In the superweak theory, CP violation is solely from the mass matrix, ε' is predicted to be zero. For this reason at least, the model is in excellent agreement with the experimental data.

2.4 The two gamma final state

There are two possible CP states for the photon pair produced from the decay of a neutral $K-$meson. Using the helicity basis, with the notation :

$$|+> \quad \text{for a right handed photon}$$

$$|-> \quad \text{for a left handed photon}$$

we have four possible states :

$$|++>, |-->, |-+>, |+->$$

The last two states are excluded by angular momentum conservation, as they have $J = 2$, whilst the kaon has $J = 0$.

<p style="text-align:center">left :   right :</p>
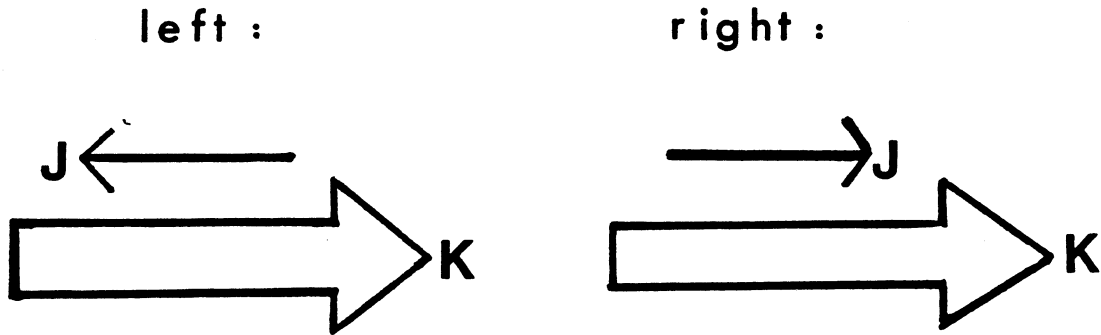
Figure 3: Photon helicities.

We form the two eigenstates of the parity operator from the remaining photon states :

$$|+> = 1/\sqrt{2}\,[\ |++> \ + \ |-->\ ]$$

$$|-> = 1/\sqrt{2}\,[\ |++> \ - \ |-->\ ]$$

$$P|+> = |+> \qquad P|-> = -|->$$

$$CP|+> = |+> \qquad CP|-> = -|->$$

We may now define four possible amplitudes :

$$A_S(+) = A[K_S \rightarrow 2\gamma(+)]$$

$$A_S(-) = A[K_S \rightarrow 2\gamma(-)]$$

$$A_L(+) = A[K_L \rightarrow 2\gamma(+)]$$

$$A_L(-) = A[K_L \rightarrow 2\gamma(-)]$$

defining the ratios :

$$\varepsilon_1 = A_L(+)/A_S(+)$$

$$\varepsilon_2 = A_S(-)/A_L(-)$$

$$\lambda = A_L(-)/A_S(+)$$

with CP invariance we would have $\varepsilon_1 = \varepsilon_2 = 0$, whilst if CP arises solely from the mass matrix $\varepsilon_1 = \varepsilon_2 = \varepsilon$.

2.5 Calculation of K_S to the CP even state of 2γ.

The dominant decay mode to $2\gamma(+)$ is expected to be from the CP even $\pi^+ \pi^-$ intermediate state. All other contributions are suppressed at least by an additional factor of α [25]. Unitarity relation calculations for this amplitude give [21], [22], [20]:

$$A(K^0 \to 2\gamma(+)) = 2\alpha A(K^0 \to \pi^+ \pi^-) \xi_{2\pi}$$

where $\xi_{2\pi}$ arises from the integration over the pion momenta and the scattering cross section to 2γ in the intermediate state. Numerically :

$$\Gamma(K_S \to 2\gamma(+)) = 2.6 \times 10^4 \ \text{sec}^{-1}$$

using the K_S lifetime from the Particle Data Group (PDG) [23]:

$$\tau_S = 0.8923 \pm 0.002 \times 10^{-10} \ \text{sec} \quad (\text{PDG})$$

14

the predicted branching ratio is :

$$\frac{\Gamma(K_S \rightarrow \gamma\gamma(+))}{\Gamma(K_S \rightarrow all)} = 2.53 \times 10^{-6}.$$

The lowest order one loop diagram, which is shown in Figure 9, does not contribute to $K_S \rightarrow 2\gamma(+)$. On making a Fierz transformation, the graph is seen to be of the same form as that for $\pi^0 \rightarrow 2\gamma$ decay, which is CP $= -1$ [19]. Also in the SU(3) limit $K_S \rightarrow 2\gamma(+)$ is forbidden by U−spin conservation [19]. In a series of four papers, Zenaida E.S.Uy [20], has considered the contribution of the vector exchange mesons ρ^0, $\rho^\pm$, ω, ϕ, ψ, $A_2(1320)$ through the process $V \rightarrow \pi\gamma$ where V is a vector meson. The enhancement to $K_S \rightarrow 2\gamma(-)$ is a few percent and can be neglected. The contribution is shown in Figure 5.
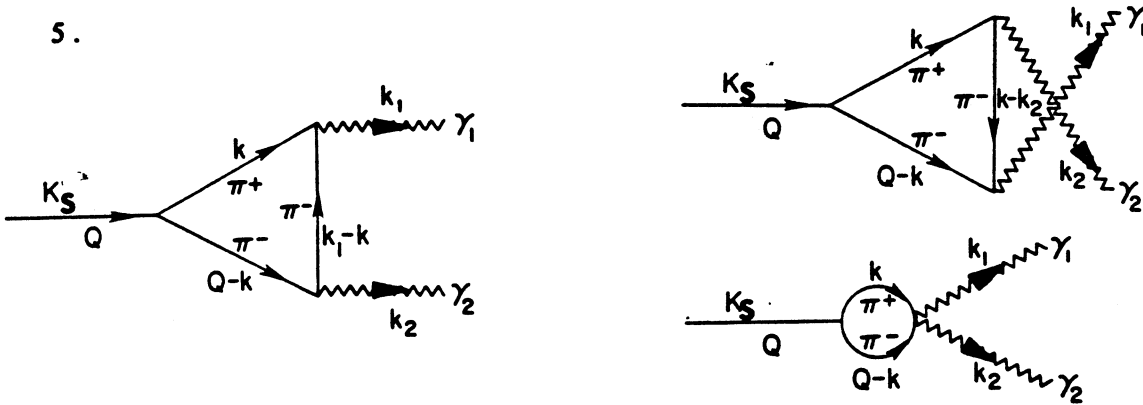
Figure 4: Processes contributing to $K_S \rightarrow \gamma\gamma$
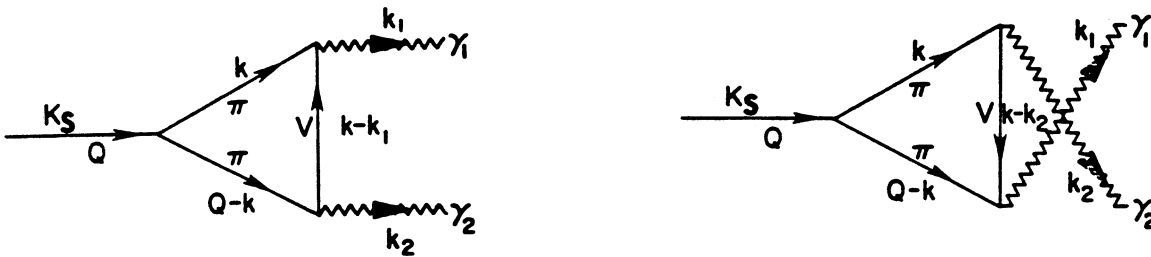
Figure 5: The vector meson exchange contribution to $K_S \rightarrow 2\gamma$.

2.6 Calculation of K_L to the CP odd state of two 2γ.

Rare kaon decays provided the experimental inspiration for the GIM mechanism which was suggested in 1970 to account for the smallness of the $K_L \rightarrow \mu^+ \mu^-$ branching ratio. It is instructive to compare that process with $K_L \rightarrow \gamma\gamma$, which is apparently not suppressed :

$$\Gamma(K_L \rightarrow \mu^+ \mu^-) \cong 2x10^{-5} \; \Gamma(K_L \rightarrow \gamma\gamma) \; .$$

First order weak decays such as $K^+ \rightarrow \mu^+ \nu$ are governed by the Fermi constant :

$$G_F/\sqrt{2} \cong g^2/(m_W)^2$$

where g is the coupling constant for charged bosons in the electroweak scheme. For second order processes, massive virtual W's can be exchanged, see Figure 6
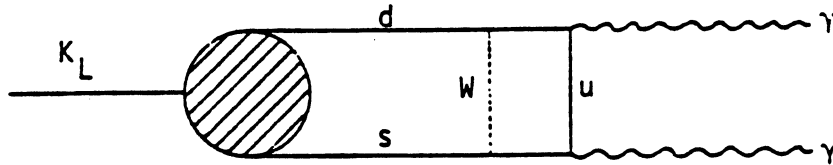
Figure 6: Second order weak process

The expected amplitude is $[g^2 / (m_W)^2] \times g^2$ where we have used the order of magnitude approximation : $e = g \sin\theta_W \cong g$. The experimental result confirms this expectation:

$$\Gamma(K_L \rightarrow \gamma\gamma) = 2x10^{-4} \; \Gamma(K^+ \rightarrow \mu^+ \nu)$$

Now consider the role of the GIM mechanism. In Figure 7 the coupling constants are equal in magnitude but opposite in sign for charmed quarks with respect to up quarks. Thus the diagrams of Figure 7 exactly cancel the graphs of Figure 6 in the limit of $m_u = m_c$, which is not the desired result.
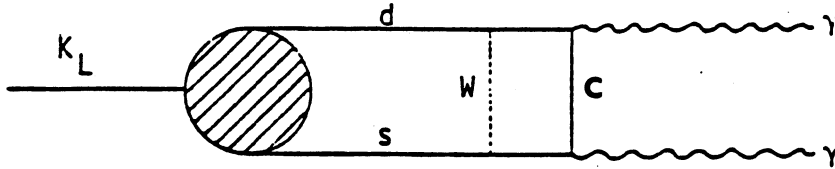
Figure 7: GIM mechanism cancellation diagram

Of course SU(4) is not an exact symmetry, $m_c \gg m_u$. Phenomenologically the difference in rates can be seen using a pole diagram, Figure 8 .
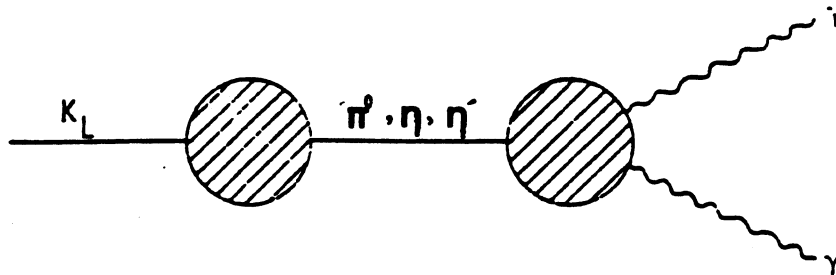
Figure 8: Pole diagrams for $K_L \to 2\gamma$.

$$A(K_L \to \gamma\gamma) \simeq A(K_L \to \pi^0)A(\pi^0 \to \gamma\gamma) \simeq G_F \, \alpha$$

The virtual $\pi^0 \to \mu\mu$ transition can occur via two photon exchange,

$$A(K_L \to \mu\mu) \simeq A(K_L \to \pi^0)A(\pi^0 \to \mu\mu) \simeq G_F \, \alpha^2$$

17

or via the exchange of a Z^0 :

$$A(K_L \rightarrow \mu\mu) \cong A(K^0 \rightarrow \pi^0)A(\pi^0 \rightarrow \mu\mu) \cong G_F^2 \, m_k^2$$

Thus the desired suppression factor is obtained. Having established the order of magnitude for $K_L \rightarrow \gamma\gamma(-)$, we can now attempt a more precise estimate. In the quark model we form the sum of all diagrams like :
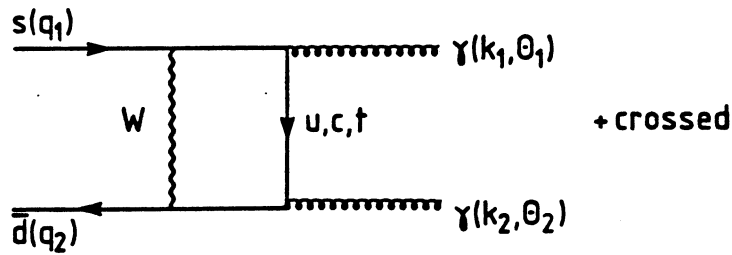
Figure 9: *Quark model diagrams contributing to* $K_L \rightarrow \gamma\gamma(-)$

Where θ_1, θ_2 and k_1, k_2 are the polarisation and momentum vectors respectively of the two photons. The quark model gives [19]

$$A_Q(K \rightarrow \gamma\gamma) = (G_F\alpha/\sqrt{2}\pi)f_K \, \Sigma_i V^*_{is} V_{id} A_i(m_q^2/m_K^2) \quad (1)$$

Where the A_i's are a function of the quark masses. When $(m_q^2/m_K^2) > 3$, $A_i < 0.005$. Therefore $|A_u| \gg |A_c|$, $|A_t|$ so that the only sizeable contribution is from u quark. CP−violation may occur through the complexity of the V_{ij} although these amplitudes are highly suppressed, and from A_u itself which has an absorptive part ImA_u. Calculating the sum yields :

$$|A_Q(K_L \rightarrow 2\gamma(-))/A_{exp}(K_L \rightarrow 2\gamma)| \cong 10\% - 27\%$$

for $m_u = 330$ MeV and 0 MeV, respectively [38].

2.7 Phenomenological pole – dominance model for $K_L \rightarrow \gamma\gamma$

In order to obtain better agreement with experiment the u–quark contribution in the quark model can be represented by individual particles. We then assume that the $K_L \rightarrow \gamma\gamma$ amplitude is described by a sum over one particle intermediate states [19] [24]:

$$A(K_L \rightarrow \gamma\gamma) = \Sigma_i \frac{A(P_i \rightarrow \gamma\gamma) <P_i|H_W|K_L>}{m_K^2 - m_i^2} \qquad (1)$$

where the pseudoscalar meson P_i refers to π^0, η, η'. The masses of these particles and amplitudes to two photons are well known, therefore only the matrix element involving the kaon needs to be computed. Using the soft pion reduction of $K \rightarrow 2\pi$ one obtains [24]:

$$<\pi^0|H_W|K_L> = 2f_\pi <\pi^0\pi^0|H_W|K_S> = -6.93 \times 10^{-2} \text{ MeV}^2 \qquad (2)$$

where $f_\pi = 0.95\ m_\pi$ The physical states, η and η', are mixtures of the SU(3) octet and singlet pseudoscalar meson states η_8 and η_0 :

$$\eta = \eta_8 \cos\theta + \eta_0 \sin\theta \qquad (3)$$

$$\eta' = -\eta_8 \sin\theta + \eta_0 \cos\theta \qquad (3)$$

where $\theta = -10.6 \pm 0.5$ degrees. From SU(3), U–spin conservation gives:

$$<\eta_8|H_W|K_L> = 1/\sqrt{3} <\pi^0|H_W|K_L> \qquad (4)$$

The singlet is outside the scope of SU(3) octet relations. Its amplitude and phase can only be fixed by making assumptions which can lead to interesting consequences for CP violation.

19

The most common choice is to assume the SU(4) analogue of SU(3), that is to assume that the H_W operator is 15 dominant in analogy to the octet dominance in SU(3) [24]:

$$<\eta_0|H_W|K_L> = 1/\sqrt{6} <\pi^0|H_W|K_L> \tag{5}$$

which follows with the definitions:

$$\eta_0 = -1/\sqrt{3}(\bar{u}u + \bar{d}d + \bar{s}s)$$

$$\eta_8 = 1/\sqrt{6}(\bar{u}u + \bar{d}d - 2\bar{s}s) \tag{6}$$

$$\pi^0 = 1/\sqrt{2}(\bar{u}u - \bar{d}d).$$

Using :

$$A(\eta_8 \rightarrow \gamma\gamma) = 1/\sqrt{3} \, A(\pi^0 \rightarrow \gamma\gamma)$$

and (3) :

$$\cos\theta \, A(\eta \rightarrow \gamma\gamma) - \sin\theta \, A(\eta' \rightarrow \gamma\gamma) = 1/\sqrt{3} \, A(\pi^0 \rightarrow \gamma\gamma) \tag{7}$$

using the known value of θ, the sign of the various amplitudes can be fixed relative to one another such that (7) is satisfied. We have from the PDG :

$$A(\pi^0 \rightarrow \gamma\gamma) = 2.535 \times 10^{-5} \text{ MeV}^{-1}$$

$$A(\eta \rightarrow \gamma\gamma) = 1.98(\pm 0.14) \times 10^{-5} \text{ MeV}^{-1}$$

$$A(\eta' \rightarrow \gamma\gamma) = -.35(\pm 0.6) \times 10^{-5} \text{ MeV}^{-1}$$

and $m_{\pi^0} = 134.96$ MeV, $m_\eta = 548.8$ MeV, $m_{\eta'} = 958$ MeV. Substituting into eq. (1) we have 3 terms :

$$A(K_L \to \gamma\gamma)_{theory} = (\pi^0) + (\eta) + (\eta')$$

$$A(K_L \to \gamma\gamma)_{theory} = -7.66 + 12.63(\pm 0.89) - 1.84(\pm 0.34)$$

$$A(K_L \to \gamma\gamma)_{theory} = 3.13 \pm 0.33 \times 10^{-12} \ MeV^{-1}$$

Using the world average branching ratio for $K_L \to \gamma\gamma$ of $4.9 \pm 0.4 \times 10^{-4}$:

$$A(K_L \to \gamma\gamma)_{exp} = 3.19 \pm .33 \times 10^{-12} \ MeV^{-1}$$

$$A(K_L \to \gamma\gamma)_{theory}/A(K_L \to \gamma\gamma)_{exp} = 1.0 \pm 0.3$$

Of course the agreement between theory and experiment is somewhat fortuitous, relying heavily on cancellations between the different amplitudes. The calculation should be regarded as an order of magnitude estimate according to the authors [24]. It is interesting to note that whilst the $\Delta I = 1/2$ rule is not well described by the contribution of the $I = 3/2$ and $I = 1/2$ amplitudes in $<\pi^0|H_W|K_L>$ these components are automatically incorporated in the correct amounts using the experimental value for $K_S \to 2\pi^0$ in the soft pion approximation. The $\Delta I = 1/2$ enhancement is missing in the quark model, which is one of the reasons for the smallness of the result with that method. We conclude that a simple pole model describes the data very well.

2.8 The calculation of R.

We have now calculated both the numerator and the denominator of R. In the literature R is defined in two different ways:

$$R = \Gamma(K_S \to 2\gamma(+))/\Gamma(K_L \to 2\gamma(-))$$

or:

$$R = \Gamma(K_S \to 2\gamma)/\Gamma(K_L \to 2\gamma)$$

explicitly this is :

$$R = \frac{\Gamma(K_S \to 2\gamma(+)) + \Gamma(K_S \to 2\gamma(-))}{\Gamma(K_L \to 2\gamma(-)) + \Gamma(K_L \to 2\gamma(+))}$$

we will use the second definition, because we do not determine the CP of the final state. Using our previously determined width :

$$\Gamma(K_S \to \gamma\gamma) = 2.53 \times 10^{-6}$$

and the world average for $\Gamma(K_L \to 2\gamma)/\Gamma(K_L \to \text{all}) = 4.9 \times 10^{-4}$ we obtain :

$$R = \frac{\Gamma(K_S \to 2\gamma) \times \tau_L}{\Gamma(K_L \to 2\gamma) \times \tau_S} = 3.0$$

where we have used $\tau_L/\tau_S = 581$. The earliest calculation of R was made by Dreitlein [29] using results obtained by Cabibbo [26]. The authors were the first to point out that the process $K \to \gamma\gamma$ should proceed at a rate proportional to the product of a weak interaction and an electromagnetic interaction. Where the K_L and K_S decay into a photon pair by internal annihilation of intermediate state pions produced by the weak interaction. The ratio of the rates is then obtained purely from phase space considerations.

$$\Gamma(K_S \to \gamma\gamma) \cong \alpha\, G_F\, 1/\tau_S$$

$$\Gamma(K_L \to \gamma\gamma) \cong \alpha\, G_F \frac{(2-\text{body phase space})}{(3-\text{body phase space})}\, 1/\tau_L$$

therefore :
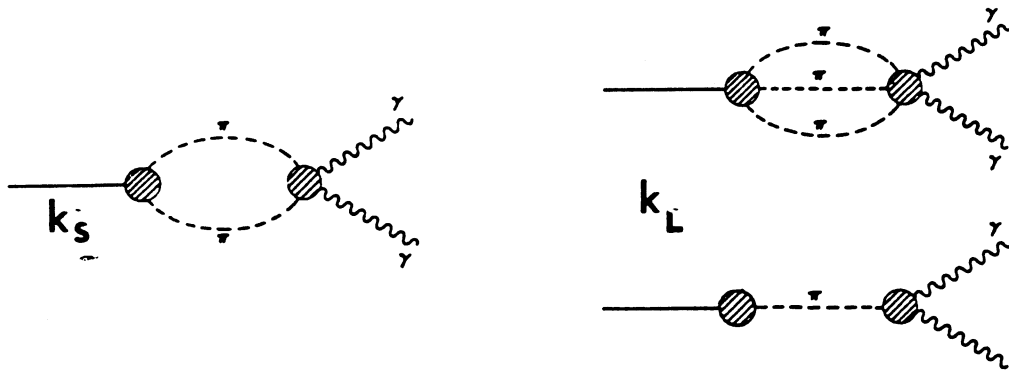
Figure 10: Decay of K_L and K_S into 2γ by internal annihilation

$$\frac{\Gamma(K_S \rightarrow \gamma\gamma)}{\Gamma(K_L \rightarrow \gamma\gamma)} = R = \frac{(3-\text{body})}{(2-\text{body})} \times \frac{\tau_L}{\tau_S} = (1/300)\text{x}586 \cong 2.0$$

The experimental status of R is largely unchanged since 1973, when Barmin determined the upper limit for $K_S \rightarrow \gamma\gamma$ which sets the upper limit for the ratio. Using the world average branching ratio $K_L \rightarrow \gamma\gamma$, we calculate the experimental upper limit :

$$R \leq \frac{4\text{x}10^{-4}}{4.9\text{x}10^{-4}} \times 586$$

$$R \leq 474 \text{ at } 90\% \text{ C.L.}$$

Clearly there is considerable room for improvement in the experimental limit if the theoretical expectation is to be tested.

An upper limit for R may be derived from the experimental value of ϵ, in the following way. We express the total decay rates for $K_S \rightarrow 2\gamma$ and $K_L \rightarrow 2\gamma$ in terms of the amplitudes introduced in section three as :

$$\Gamma(K_S \rightarrow 2\gamma) = N_S[|A_S(+)|^2(1 + |\epsilon_2|^2|\lambda|^2)]$$

$$\Gamma(K_L \rightarrow 2\gamma) = N_L[|A_S(+)|^2(|\epsilon_1|^2 + |\lambda|^2)]$$

23

where the phase space factor $N_{L,S} = (1/32 \pi)m_{L,S}$ and $m_{L,S}$ are the masses of the K_L and K_S respectively. These rates constrain ϵ_1 and ϵ_2 :

$$|\epsilon_1|^2 \geq 1/R \quad \text{and} \quad |\epsilon_2|^2 \geq R$$

or :

$$0 \leq |\epsilon_1|^2 \leq 1/R \quad \text{and} \quad 0 \leq |\epsilon_2|^2 \leq R$$

in the superweak case $\epsilon_1 = \epsilon_2 = \epsilon$. Using the experimental value for ϵ, R is bounded :

$$|\epsilon|^2 \leq R \leq 1/|\epsilon|^2$$

or.:

$$5.3 \times 10^{-6} \leq R \leq 2.5 \times 10^{+5}$$

2.9 CP violation in K_L and K_S to 2γ

From the definition of K_L and K_S in the mass matrix CP violation occurs at least to $O(\epsilon)$ in the process $K \rightarrow \gamma\gamma$. The amount of CP violation from the mass matrix is well known, and when determined from charged or neutral 2π final states, or from semi−leptonic charge asymmetries the agreement is good :

$$\text{Re}(\epsilon) = 1.536 \pm 0.062 \times 10^{-3} \quad (K_{L,S} \rightarrow 2\pi)$$

$$\text{Re}(\epsilon) = 1.620 \pm 0.088 \times 10^{-3} \quad (K_L \rightarrow \pi \ell \nu)$$

The observation of CP violation in a single decay of a kaon into two gammas requires the measurement of the polarisation of the two photons. The equivalent of the observation of Christenson et al. [30] of $K_L \rightarrow \pi^+ \pi^-$ would be the determination of the planes of polarisation of the two pairs of elec-

trons in the double Dalitz decay of a $K \rightarrow \gamma\gamma$ analogous to the measurements which determined the parity of the π^0. Whilst the measurement could be conceived for K_L, the low branching ratio for K_S would make the technique extremely difficult.

An alternative method is to measure interference in the 2γ partial widths between K_L and K_S. In what follows we have used results from two papers [27], [38]. We write the partial decay difference :

$$\Delta(t) = \frac{\Gamma(K^0 \rightarrow 2\gamma)(t) - \Gamma(\bar{K}^0 \rightarrow 2\gamma)(t)}{\Gamma(K^0 \rightarrow 2\gamma)(t) + \Gamma(\bar{K}^0 \rightarrow 2\gamma)(t)}$$

and the time integrated rate :

$$\Delta_I(T) = \frac{[I(T) - \bar{I}(T)]}{[I(T) + \bar{I}(T)]}$$

where :

$$I(T) = {}_0\!\int^T dt\ \Gamma(K^0 \rightarrow 2\gamma)(t)$$

$$\bar{I}(T) = {}_0\!\int^T dt\ \Gamma(\bar{K}^0 \rightarrow 2\gamma)(t)$$

$\Delta(t)$ and $\Delta_I(T)$ are not vanishing and of the order $O(\epsilon)$.

Using the definition of K^0 and $\bar{K}^0$:

$$|K^0> = \frac{1 + |\epsilon|^2}{\sqrt{2}(1+\epsilon)} \{|K_S> + |K_L>\}$$

$$|\bar{K}^0> = \frac{1 + |\epsilon|^2}{\sqrt{2}(1-\epsilon)} \{|K_S> - |K_L>\}$$

consider the time evolution of a K^0 state which is some mixture of K_L and K_S :

$$|K^0> \; = \; \alpha|K_S> \; + \; \beta|K_L>$$

decaying to some state f which has CP = 1. We have :

$$<f|H|K^0> \; = \; \alpha <f|H|K_S> \; + \; \beta <f|H|K_L>$$

Putting in the time development :

$$<f|H|K^0> \; = \; T\{\alpha exp(-M_S t) \; + \; \epsilon\beta \, exp(-M_L t)\}$$

where $M = im + \Gamma/2$ with m the mass and Γ the width, and T is a transition amplitude. The intensity I is given by :

$$I \; = \; |<f|H|K^0>|^2 \; = \; |T|^2\{\alpha^2 exp(-\Gamma_S t) \; + \; |\epsilon|^2\beta^2 exp(-\Gamma_L t) \; + \; \alpha\beta|\epsilon|exp(-(\Gamma_S+\Gamma_L)t/2)cos(\Delta m t - \theta)\}$$

For initially pure beams of K^0 and $\bar{K}^0$, A = B. Considering $f = 2\gamma$ and the definitions of $|K^0>$ and $|\bar{K}^0>$:

$$I(t)(K^0 \rightarrow 2\gamma) = \frac{1+|\epsilon|^2}{2(1+2Re\epsilon+|\epsilon|^2)}\{X(t)+Y(t)\}$$

$$I(t)(\bar{K}^0 \rightarrow 2\gamma) = \frac{1+|\epsilon|^2}{2(1-2Re\epsilon+|\epsilon|^2)}\{X(t)-Y(t)\}$$

where :

$$X(t) = [|A_L(-)|^2 + |\epsilon_1|^2|A_S(+)|^2]exp(-\Gamma_L t)$$

$$+ [|A_S(+)|^2 + |\epsilon_2|^2|A_L(-)|^2]exp(-\Gamma_S t)$$

$$Y(t) = [2|\epsilon_1|^2|A_S(+)|^2cos(\theta_1 - \Delta m t)$$

$$+ [|\epsilon_2|^2|A_L(-)|^2cos(\theta_2 + \Delta m t)]exp[-(\Gamma_L + \Gamma_S)t/2]$$

Neglecting terms of order $|\varepsilon|^2$, we obtain :

$$\Delta(t) = \frac{Y(t) - 2Re(\varepsilon)X(t)}{X(t) - 2Re(\varepsilon)Y(t)}$$

This method can also be used to determine ε'/ε for two pion decays. However, the method of using the time integrated rate $\Delta_I(\tau)$ is less subject to systematic errors, especially vertex resolution, and will be used by the CP−LEAR experiment at CERN [17]. It can be shown that for $\pi^+\pi^-$:

$$\Delta_I(T) = Re\varepsilon' + 2Re\varepsilon$$

and for $2\pi^0$:

$$\Delta_I(T) = 2Re\varepsilon - 8Re\varepsilon'$$

In addition to the three amplitudes defined in terms of K_L and K_S in section 2.2 we now define two more :

$$r_+ = -\frac{A(K^0 \rightarrow 2\gamma(+))}{A(\bar{K}^0 \rightarrow 2\gamma(+))}$$

$$r_- = \frac{A(K^0 \rightarrow 2\gamma(-))}{A(\bar{K}^0 \rightarrow 2\gamma(-))}$$

Let us consider the K_S and K_L decays to two photons allowing for CP violation. As we now have the possibility of CP−non−conserving effects in the decay amplitudes, in equation 2.3.1 $A(K^0 \rightarrow \pi^+\pi^-)/A(\bar{K}^0 \rightarrow \pi^+\pi^-)$ is no longer real however because of the $\pi^+\pi^-$ dominance in $K_S \rightarrow 2\gamma(+)$:

$$r_+ = \frac{A(K^0 \to 2\gamma(+))}{A(\bar{K}^0 \to 2\gamma(+))} = \frac{2\,\alpha\,\xi_{2\pi}\; A(K^0 \to \pi^+\pi^-)}{2\,\alpha\,\xi_{2\pi}\; A(\bar{K}^0 \to \pi^+\pi^-)}$$

or equivalently $\epsilon_1 = \eta_{+\,-}$. The CP−violation is to a very good approximation, from the mass matrix alone.

We have shown in section 2.5 that the pole dominance model gives the correct order of magnitude for $K^0 \to 2\gamma(-)$. As stated then, the singlet η_0 is outside the scope of SU(3) octet relations. Following [35] and [36] we now relate the singlet amplitude to the π^0 amplitude via a complex parameter ρ :

$$<\eta_0|H_{WK}|K^0> \;=\; -2\,(\sqrt{2/3})\,\rho\; <\pi^0|H_{WK}|K^0> \qquad (1)$$

Using equation 2.5.1 as before and (1) there are two possible values of ρ which give the experimentally determined amplitude. These values are $\rho = 0.94$ and $\rho = 0.06$. It has been shown in [36] [37] that the two parts of ρ are related to f, which is the fraction of the $\Delta I = 1/2$ transition amplitude that is explained by the penguin diagram:

$$\mathrm{Re}\rho = (3f-1)/2 \qquad \mathrm{Im}\rho = -3(1-f)t_0/2$$

where $t_0 = \mathrm{Im}\, A_0\, /\, \mathrm{Re}\, A_0$. Our two solution for ρ give :

$$\rho \approx 1 \Rightarrow f = 1 \qquad \rho \approx 0 \Rightarrow f = 1/3.$$

When $f = 1$, $\mathrm{Im}\rho = 0$ and :

$$\arg <\eta_0|H_{WK}|K^0> \;=\; \arg <\pi^0|H_{WK}|K^0>$$

when $f \neq 1$, the phases of the two amplitudes are different. There is evidence from D−meson decay that the penguin diagram cannot be the sole graph responsible for the $\Delta I = 1/2$ rule [28]. Using :

$$\arg <\pi^0|H_{WK}|K^0> \;=\; \arg <\pi^0\pi^0|H_{WK}|K^0> \;=\; t_0$$

we have from equation 2.5.1 :

$$\arg A(K^0 \to 2\gamma(-)) = t_0[1 - 3.4(1-f)] \equiv t'_0$$

From the sum of the pole contributions and the quark model we have :

$$A(K^0 \to 2\gamma(-)) = A_p + A_q$$

$$= A(K^0 \to 2\gamma(-))(1 + i\, t'_0) - i(G_F\alpha\,/\sqrt{2}\pi)f_K V^*_{us}V_{ud}\,\mathrm{Im}A_u$$

$$= A(K^0 \to 2\gamma(-))(1 - it'_0 - 0.3\,i\,\mathrm{Im}\,A_u) \qquad (2)$$

from the definition of r_-, using (2) :

$$|r_-| = 1 - 0.6\, t'_0\,\mathrm{Im}\,A_u$$

and from:

$$r_- = |r_-|\exp(i\theta_-)$$

we have :

$$\theta_- = -2t'_0$$

The partial difference at $t = 0$ is :

$$\Delta(t=0) = \frac{|r_+|^2 - 1 + R(|r_-|^2 - 1)}{2(1+R)} \qquad (3)$$

Using the current value of ϵ'/ϵ :

$$t_0 = -\sqrt{2}\,20\,e^{-i\pi/4}\,\epsilon' \approx -\sqrt{2}\,20\,(\epsilon'/\epsilon)\,2.3\mathrm{x}10^{-3} \approx -7.4\mathrm{x}10^{-4}$$

For $\rho = 0.06$ we find $|r_-| 1 + 1.7\, t_0$, $\theta_- = 2/6\, t_0$ or equivalently $\epsilon_2 = 3.65\mathrm{x}10^{-3}$. The effect is large :

$$\frac{\text{Kobayashi} - \text{Maskawa}}{\text{superweak}} = \frac{\varepsilon_2}{\varepsilon} = 1.6$$

The time evolution of the partial rate difference is shown in Figure 11 [27], where the dashed lines are for the KM model. As R increases, the deviation from the superweak expectation decreases. The feasibility of performing this experiment will be discussed in the final chapter. A determination of R is clearly necessary before embarking on such an undertaking.

To summarise; in all final states involving pions the $\Delta I = 1/2$ rule suppresses ε' by a factor twenty compared to ε. In the decay $K \to \gamma\gamma$ we have seen that this suppression factor is absent and CP violation arising from the decay amplitudes is expected to be comparable to the mass matrix effects.
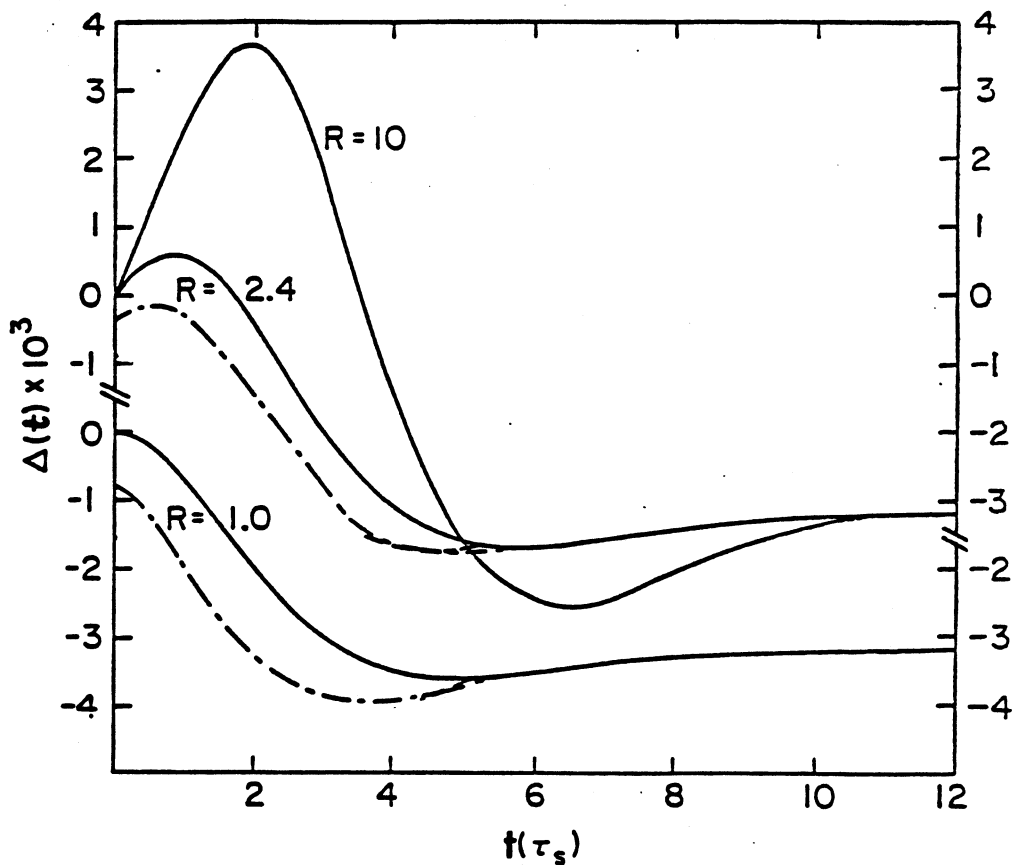
Figure 11: The time evolution for the partial rate difference $\Delta(t)$

3. THE EXPERIMENT

3.1 Introduction

In recent years there has been a renewed interest in the study of CP violation, prompted both by theoretical predictions that ε'/ε could be as large as one percent [31] and by the advance in detector and electronics technology promising an improvement in the accuracy with which the parameters describing CP violation can be determined. Already the experiments of Adair et al. [32] and Winstein et al. [1] have indicated that ε'/ε is smaller than one percent.

The NA31 experiment [13], is in the North Area of CERN, the European Centre for High Energy Physics in Geneva, Switzerland. It is designed to measure ε'/ε to precision of a few per mille, by determining the double ratio $|\eta_{00}/\eta_{+-}|^2$ Thus four modes have to be measured, each with a precision of about 0.3%. The numerators of the double ratio are heavily suppressed with respect to the CP−allowed channels for a K_L decay. The rarest mode is $K_L \rightarrow 2\pi^0$; with N events of this type detected the statistical error on ε'/ε is :

$$\Delta(\varepsilon'/\varepsilon) = 17\%/\sqrt{N}$$

Thus 30,000 $K_L \rightarrow 2\pi^0$ decays are required to reach the required precision, whilst it is planned to record about 200,000. Therefore the experiment will not be limited by statistics; the precision with which it is possible to determine ε'/ε will depend on the efficiency with which background can be rejected online and the remaining backgrounds subtracted offline. The magnitudes of these backgrounds should be small; however only an understanding of the origins of these backgrounds will guarantee that the systematic error in the background subtraction can be controlled. To summarise the backgrounds involved both for the ε'/ε and this analysis, a list of branching ratios is presented in Table 1.

In the experiment the charged and neutral two pions decays, as well as 2γ and other rare modes are detected simultaneously in beams dominated alternatively by K_L or K_S. To increase the acceptance for

Table 1: Principal branching ratios of neutral K − mesons.

K_L	mode	fraction
$c\tau = 1554$ cm.	$\pi^0\pi^0\pi^0$	21.5%
	$\pi^+\pi^-\pi^0$	12.39 %
	$\pi^\pm\mu^\pm\nu$	27.1%
	$\pi^\pm e^\pm\nu$	38.7%
	$\pi^+\pi^-$	0.203%
	$\pi^0\pi^0$	9.4×10^{-4}
	$\pi^0\gamma\gamma$	$< 2.4 \times 10^{-4}$
	$\gamma\gamma$	4.9×10^{-4}
	$\pi e\nu\gamma$	1.3%
	$\mu^+\mu^-$	9.1×10^{-9}
K_S		
$c\tau = 2.675$ cm.	$\pi^+\pi^-$	68.61%
	$\pi^0\pi^0$	31.39%
	$\pi^+\pi^-\gamma$	1.8×10^{-3}
	$\gamma\gamma$	$< 4 \times 10^{-4}$

the charged decay mode, energy is determined by wire chambers and calorimetry only, without the use of a magnet. In the neutral mode, an electromagnetic calorimeter with excellent energy and spatial resolution is used. The photon vector momenta are not measured, the decay vertex of an event being determined by the assumption that it has the kaon mass. A number of $3\pi^0$ events survive energy and moment cuts, whilst only having four detected photons; however these events appear shifted downstream of the true decay position because of the missing photons. In the remaining part of this chapter the various parts of the experiment are described. For this analysis the wire chambers and hadron

calorimeter are only used peripherally and brief outlines are given. A paper [33] is to be published in which a more detailed account may be found. The design of the experiment is shown in Figure 12.
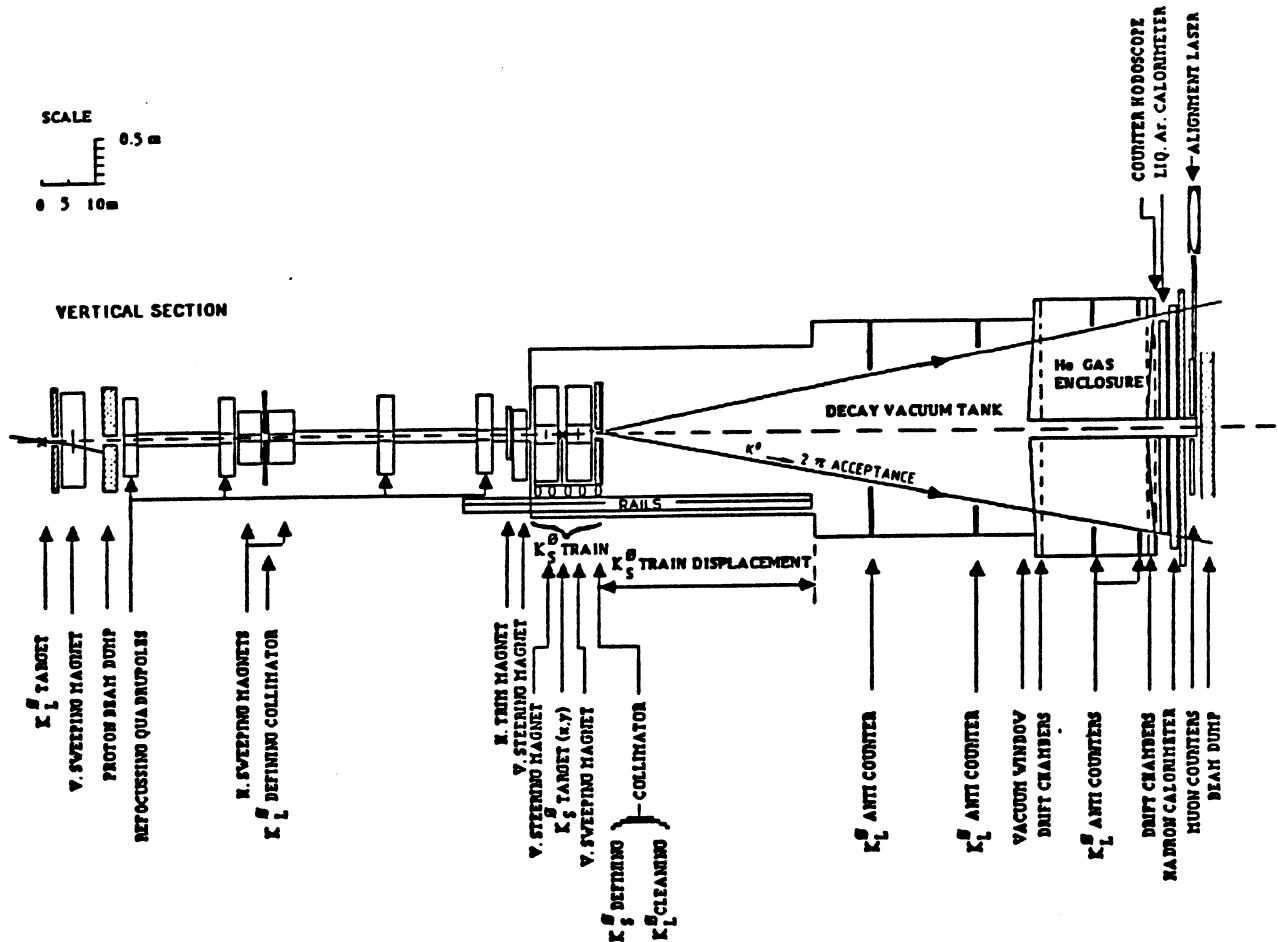
Figure 12: Experimental design

3.2 The K_L beam.

For K_L running, primary protons from the CERN SPS derived from target station T2 are transported along the H4 beam line to a target at the entrance to the experimental hall, 240 metres upstream of the detector. The K_L target station is shown in Figure 13. The target head consists of beryllium rods 100mm. in length and 2.0 mm. in diameter aligned along the axis of the resulting K beam.

The target is preceded and succeeded by instrumentation boxes containing secondary emission monitors, used principally for steering. A magnet immediately upstream of the target permits the direction of the incident proton beam to be inclined in the vertical plane. The production angle of 3.62 mrad. yields a neutron to kaon flux ratio of six. The target is followed by a collimator and vertical sweeping magnet which deflect the proton beam and charged secondaries from the neutral beam line, and dump them in iron blocks. The assembly, from target T2 to the dump is shielded to allow a nominal intensity of 10^{11} incident protons at 450 GeV/c on the target per SPS pulse every 14.4 seconds.

After this first section, the neutral beam is transported in vacuum until it passes through a central hole in the detector before being absorbed in a beam dump 252 m. from the target.

The defining collimator of 1 m. length is 48 m. from the target (acceptance ± 0.2 mrad.). The assembly again includes sweeping magnets. The K_L beam then passes through the K_S beam train, which is parked in its most upstream station with K_S target, collimator and anti$-$counter displaced.

A final collimator, with aperture greater than the K_L acceptance is located 120 m. after the target, its function to stop particles produced on the jaws of the defining collimator from entering the detector.

The profile and relative intensity of the beam are monitored by the conversion of neutral particles at the exit of the vacuum tube, in front of the beam dump. A wire chamber profile is shown in Figure 14. Typical rates are shown in Table 2, whilst the spectrum is shown in Figure 15.
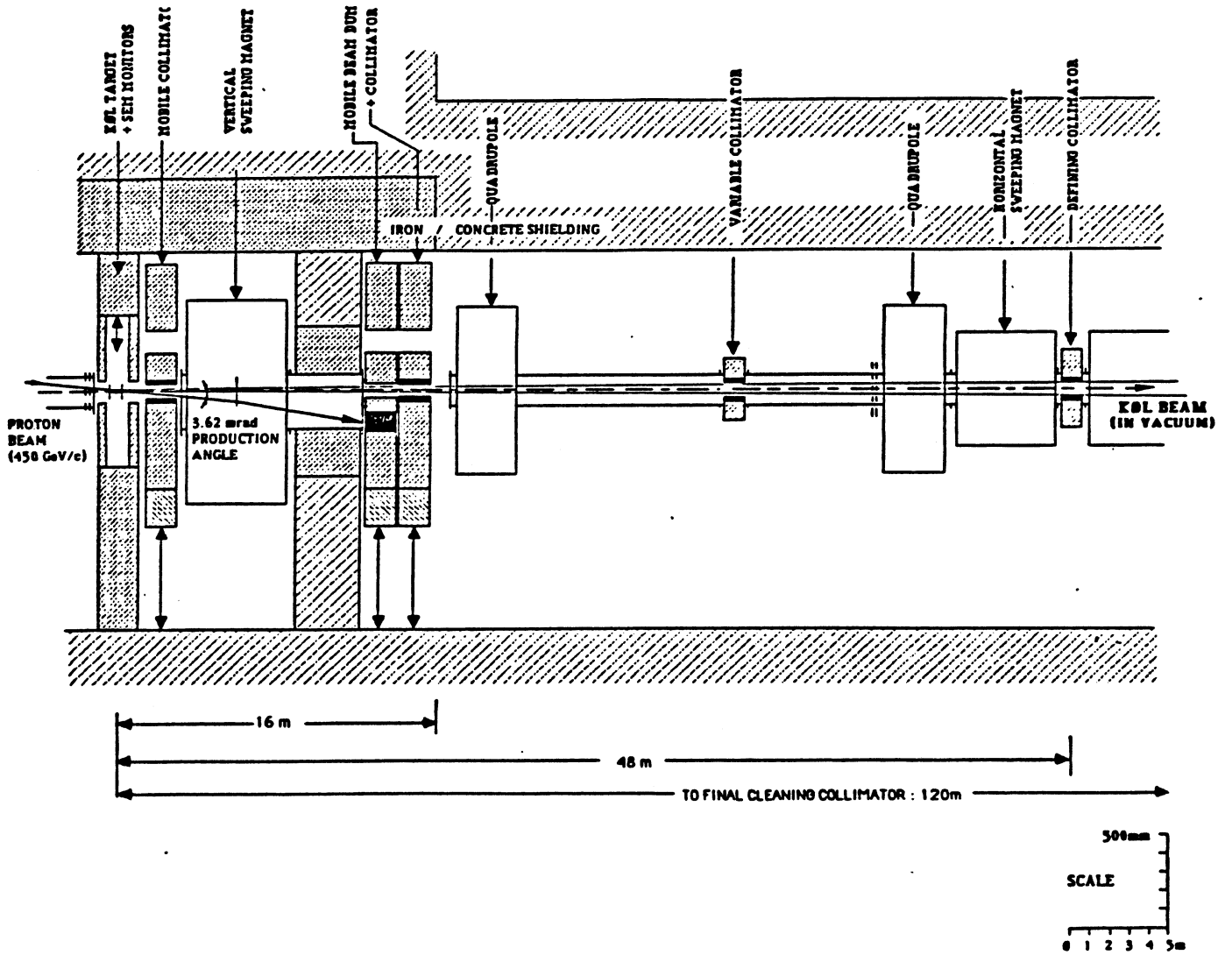
Figure 13: K_L target station
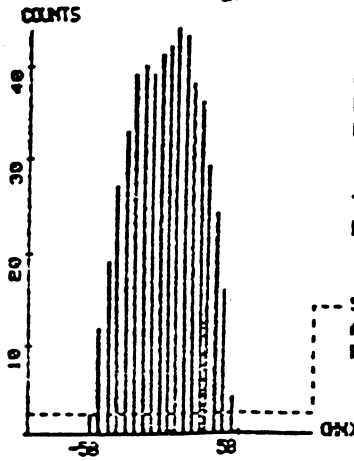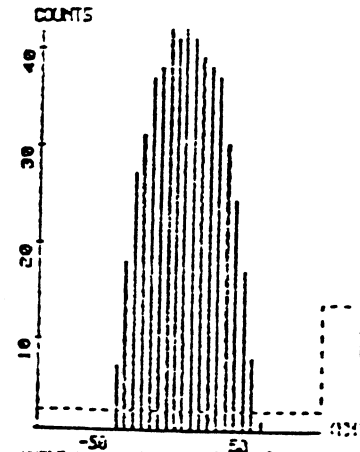
Figure 14: Beam profile at production.

Table 2: Rates at per burst

	K_L	K_S
primary protons	3×10^{10}	1.8×10^7
decays in 50m	6×10^3	190
$\pi^+\pi^-$	12	130
$\pi^0\pi^0$	6	60
$\gamma\gamma$	4	—
accepted $\pi^+\pi^-$	2.5	40
accepted $\pi^0\pi^0$	0.8	10
accepted 2γ	1.2	—

3.3 The K_S beam

The primary beam from the H4 beam line may be attenuated by a beryllium absorber and collimated to 2×10^7 protons per pulse. This beam is then transported along the K_L beam line to the K_S target which is no longer displaced. The incident protons may be directed such that the production angle is the same as in K_L beam.

TOTAL KOL= 1.75 10**6
<P> KOL = 95.9 GEV/C
PRODUCTION ANGLE= 3.62 MRAD.
ACCEPTANCE = 4πx10⁻⁸ SR
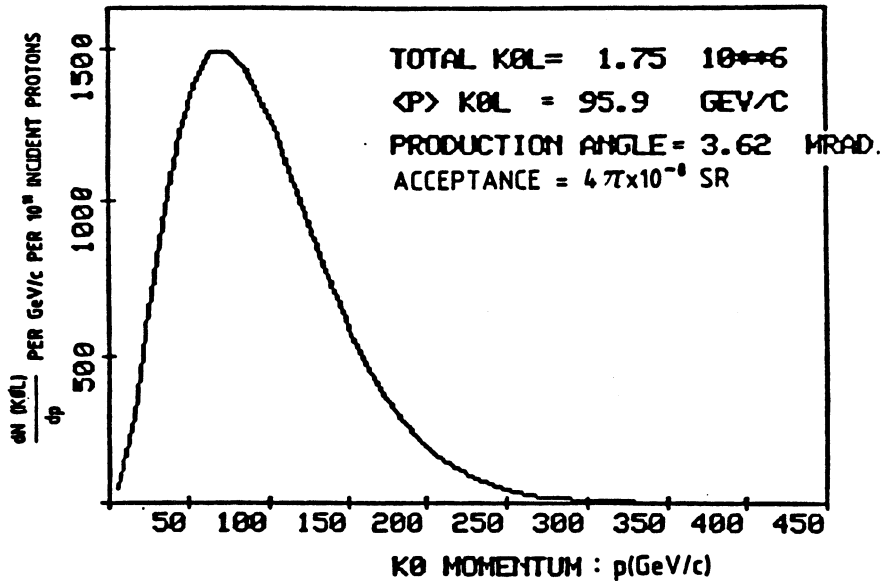
Figure 15: Beam at production.

After the target the charged secondaries and remaining protons are swept by a 5 m. magnet and dumped in a beam— dump/collimator assembly. The central part of this device is the 1.2 m. long K_S collimator which defines the beam (acceptance ±.5 mrad.) 7.1 m. from the target. An anticounter with 1.5 radiation lengths of lead converter mounted on the downstream face of the collimator, is used to define the beginning of the K_S decay region and ultimately the neutral decay length scale.

The magnets, target, steering instruments, beam dump and collimator comprising a total length of 14.4 m. are mounted on a motorized train, 'XTGV', which travels at 3.6 m./min. on rails aligned parallel to the beam axis, over a distance of 48 m. inside an evacuated tank which comprises the K − decay region. The XTGV is shown overleaf. The train may stop at any of 41 different stations spaced 1.2 m. apart. Thus K_L and K_S decays can be observed throughout the whole decay region, as illustrated in Figure 17

37
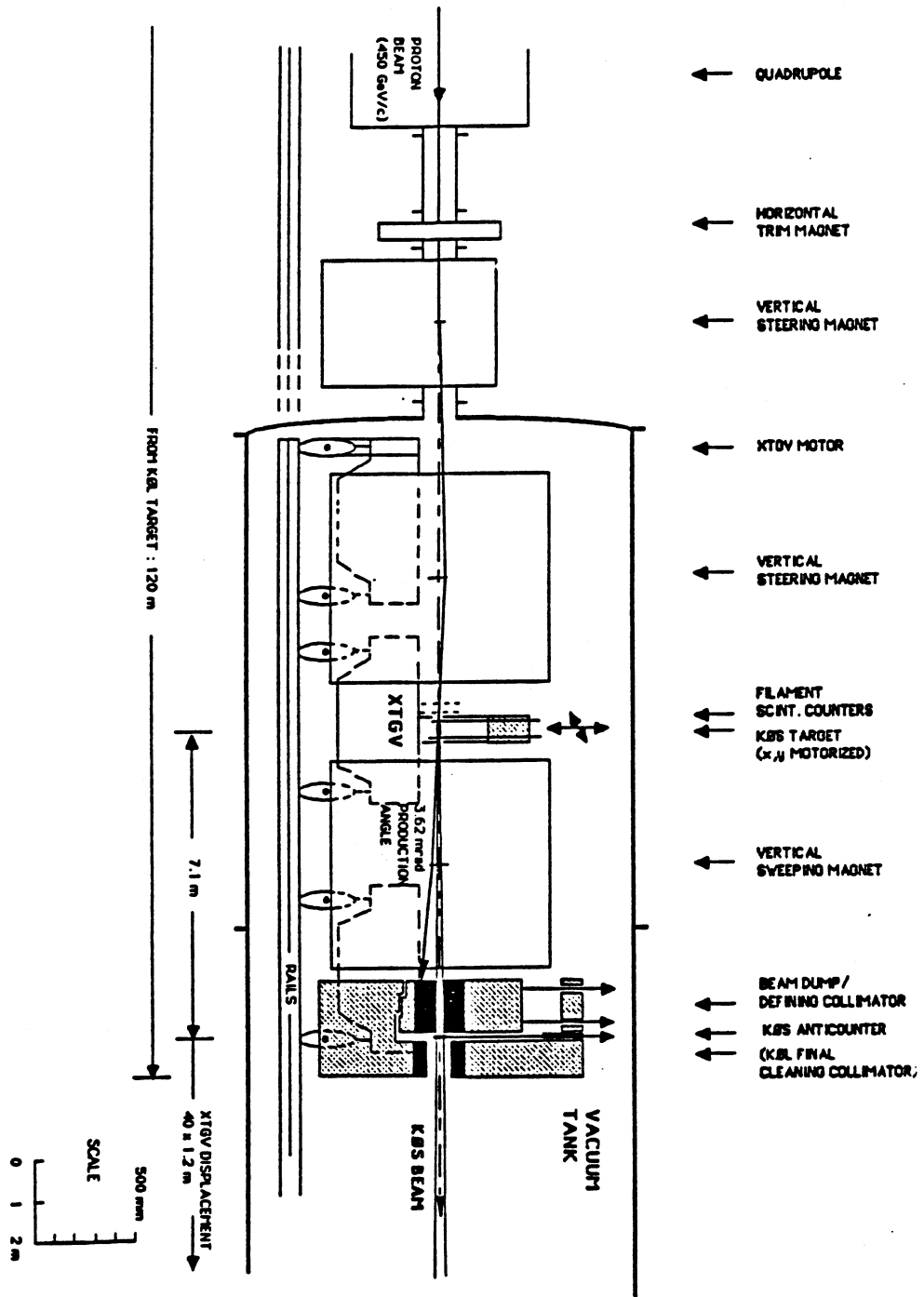
Figure 16: The XTGV (K_S beam assembly)

3.4 The decay region

The K decay region consists of a cylindrical vacuum vessel 111 m. long of volume 400 m.^{3} divided in two sections of internal diameter 1.92 m. and 2.40 m. respectively. The pressure inside the tank is $< 10^{-2}$ Torr. Four rings of scintillators which surround the acceptance cone of the beam at fixed points along the decay region, are used as anticounters to reject the copious 3 − body neutral decays, giving particles outside the acceptance of the principal detectors.
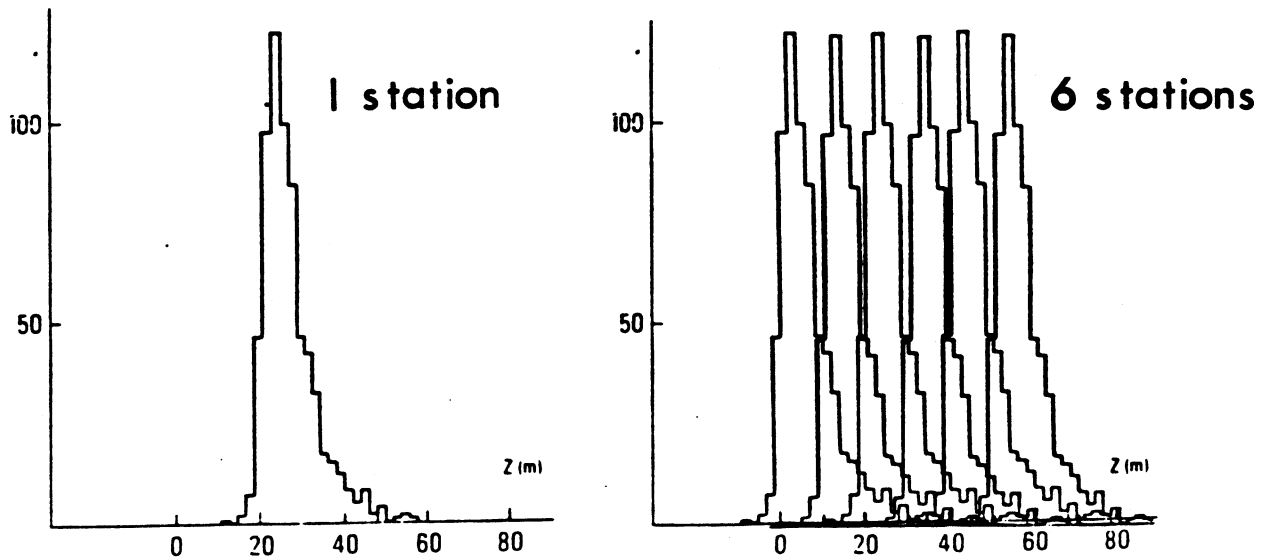
Figure 17: *Role of the train.*

The downstream end of the vacuum vessel is a spherical window composed of resin impregnated Kevlar fibre cloth, 3×10^{-3} of a radiation length thick. The beam pipe of diameter 164 mm. passes through this window into a further vessel filled with helium at atmospheric pressure. The drift chambers used to measure the coordinates of charged tracks, are housed in this tank, which is closed by a 12mm. thick aluminium alloy end − cap preceding the calorimeters.

3.5 The liquid argon calorimeter

All information about decay products for neutral events is provided solely by the liquid argon calorimeter (LAC). The calorimeter is segmented in depth (2 x 12X$_0$) to facilitate e/π rejection and to

provide near total electromagnetic containment. It is a fine grain device, with a strip size of 1.25cm. and spatial resolution of better than 1mm. The calorimeter structure is shown in Figure 18
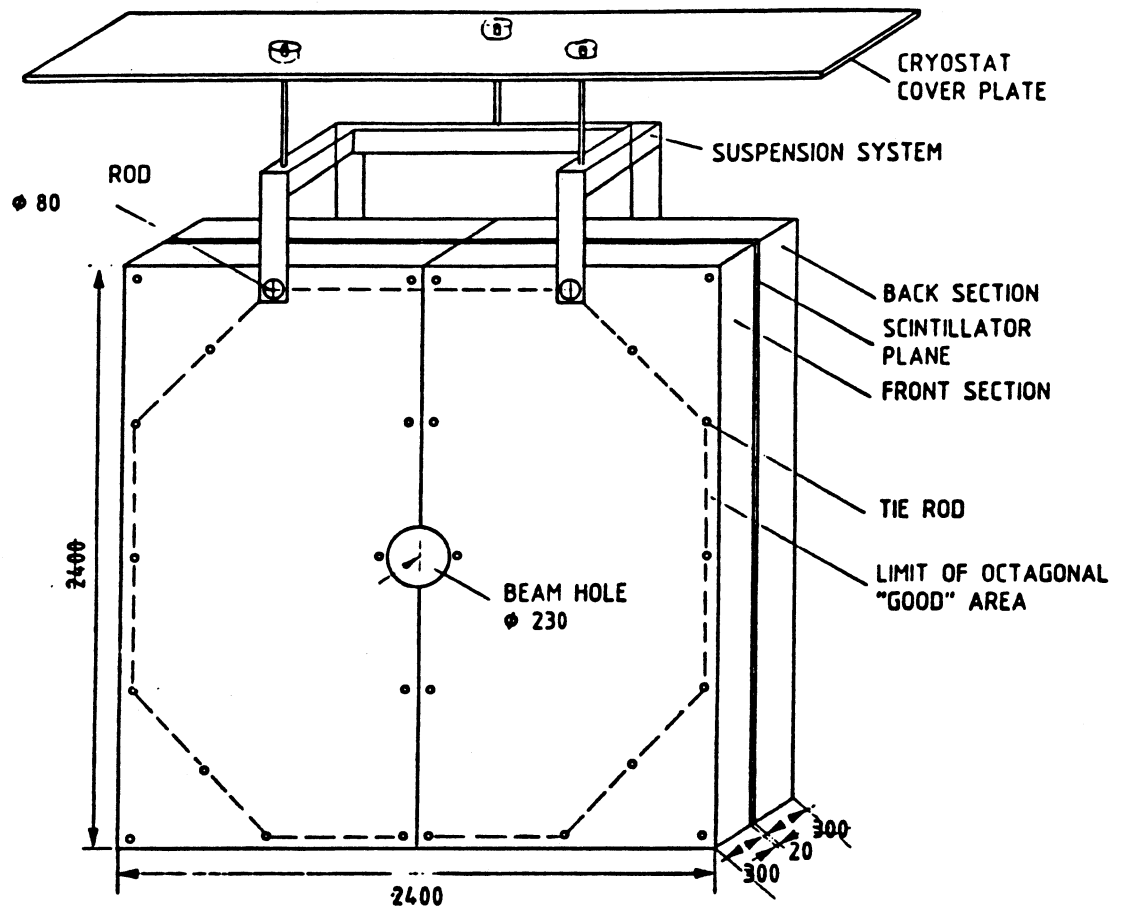
Figure 18: The liquid argon calorimeter.

The calorimeter has an active area of 1.2m.^{2} however the useful area is somewhat less. The projection of the wire chamber frames onto the plane of the calorimeter limits the area used for measuring events to an inscribed octagon of diameter 118 cm. A flange around the beam hole at the first chamber further limits the acceptance. For this analysis a circular region of radius 16cm. centred on the beam axis is excluded.

Figure 19 shows the cell structure, of alternating metal conversion plates and double—sided copper clad readout plates. The conversion plates consist of 1.5 mm. of lead sandwiched between two sheets of 0.3 mm. thick aluminium alloy which affords the necessary rigidity for machining. The read-out plates are G10 printed circuit board 0.8 mm. thick including 2 X 0.35μm. of copper. Each strip is 11.3 mm. wide, the space between strips is 1.2 mm. Altogether there are 80 such cells.
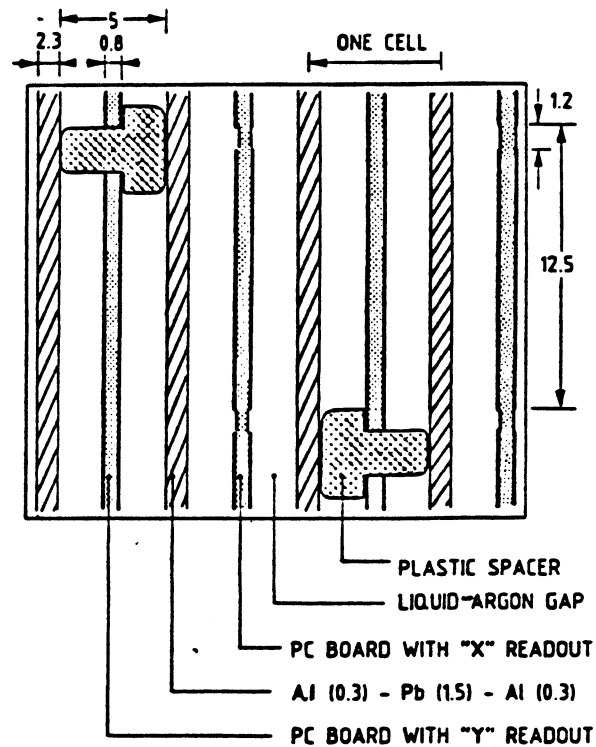
Figure 19: The electromagnetic calorimeter cell structure.

Spacing between layers of the cells is maintained by a system of plastic blocks, so ordered that they do not introduce a systematic effect in the energy measurement. The long—range order is given by tie rods mounted with G10 washers. The readout is in two halves, front and back. Readout is alternately horizontal (X) and vertical (Y). Cells are longitudinally connected in groups of 20 such that for any particle at impact point (X,Y) four energies are measured; E_x, E_y in the front, and similarly in

the back. The mechanical construction is further subdivided about the line $X = 0$ making four half-planes. The readout reflects this subdivision and an artificial one about $Y = 0$. Each quadrant so created, consists of 96 X channels and 96 Y channels. The total number of channels is 1536, composed of 30,270 strips.

The longitudinal connection of corresponding readout strips is achieved with a special connector and bus-bar made of printed circuit board. The resulting channel of 20 strips is connected to a preamplifier outside the cryostat. The signal bus-bar is also used to send calibration pulses from a capacitor into selected channels.

3.6 The electromagnetic calorimeter cryogenics

The cryostat is composed of an inner (liquid argon) vessel, an outer (vacuum) vessel and a cover plate. The assembly is in stainless steel. After insertion of the calorimeter, the two holes in the inner vessel are connected by a tube allowing the beam-pipe to pass through the calorimeter. The inner vessel has a thickness of 0.28 X_0. The outer vessel has an entry (exit) thickness of 0.31 (0.46) X_0. The signal and calibration cables,transfer line for the argon and emergency cooling loop for the liquid nitrogen pass through the cryostat cover plate. The whole assembly is gas tight.

The liquid argon is supplied by a heat exchanger using nitrogen. During the cooling down, the temperature gradient throughout the entire volume was less than 20^0 Celsius. Oxygen is removed from the argon by a commercial absorber. During the run, the average oxygen contamination measured in the gas phase was 1.1 ppm.

3.7 The electromagnetic calorimeter electronics

The LAC electronics is divided into three parts; the HV and preamplifier cards, the Sample and Hold Card (SHC) and the FASTBUS ADC system.

The HV card contains a transformer, providing power for 8 LAC channels, a blocking capacitor and two calibration capacitors per channel. The preamplifier, which has two outputs, is used to drive 30 m. twisted pair cables to the control room. The two cards are plugged into a single board. On each card one output from each channel is used to form a sum. Groups of twelve cards are then added. The resulting signal is shaped and used by the trigger for the total energy sum and e/π rejection.

The signal arriving at the SHC is sampled at three different times, 700 ns. apart, in order to be insensitive to baseline slope. The sampling times A,B and C define Q :

$$Q = Q_A + Q_C - 2Q_B$$

Thus Q is a well−defined voltage. The signal rise time is 400ns ,whilst the preamplifier decay time is 1.6 μs. Analogue signals are stored in a capacitor acting as a buffer, enabling the trigger which also receives the LAC channel signals to determine if an event should be kept or not before the ADC'S are opened. As the SHC receives a signal later than the first level trigger it is always possible to sample at time A.

The signals from the SHC enter FASTBUS ADC's of 96 channels each. Adjacent calorimeter strips are given to different ADC input blocks. In order to reduce the number of words being written to tape, channels below a certain threshold are set to zero; however the four channels closest to a channel above threshold are preserved. The ADC conversion time is 35 μs. The average number of channels per event is about 200.

The ADC's are readout by the fastbus system, and fed into the Fast Buffering and Arithmetic Processing (FBAP) module. It is this module which transmits reformatted data to the Arithmetic FASTBUS Interface (AFBI) in which hardwired cuts are performed on the data and the results returned to the FBAP to reject or accept an event.

3.8 Electromagnetic calorimeter performance

The energy resolution is determined with electron beams at 15, 25, 35, 50, and 80 GeV. A gaussian distribution is fitted to the measured energy deposition from -3σ to $+4\sigma$ around the most probable energy yielding a resolution of better then $8\%/\sqrt{E}$ (in GeV) for all electron beams.

Using an electron beam of 80 GeV a scan was made over the whole fiducial area of the calorimeter. The response was independent of impact position within $\pm 0.5\%$.

From random triggers and events where a known charge is injected to every fourth channel the r.m.s. of the pedestal values has allowed a study of the noise and inter−channel pick−up. The electronic noise per channel is 16 MeV and is uncorrelated. For photons of several GeV the noise contibution is important; typically $40-60$ channels are summed giving 16 MeV $*\sqrt{no.channels}$ = $100-150$ MeV. The energy resolution then is the sum of three contributions:

$$\sigma = \{(0.1 GeV)^2 + (7.3\%\sqrt{E})^2 + (.5\%E)^2\}^{0.5}$$

$$\sigma = \{(noise) + (sampling) + (inhomogeneity)\}^{0.5}$$

Using electrons and the chamber information the spatial distribution was obtained from a gaussian fit and found to be $\sigma = 0.75$ mm. No correction has been made for the chamber resolution or multiple scattering. From $K_S \rightarrow 2\pi^0$ decays the π^0 mass resolution is determined to be 2 MeV. The contribution from energy resolution is greatest at the lowest photon energies whilst at higher energies the spatial resolution increases in importance, however it remains much the smaller term.

From electronic calibration events the measured response to an injected charge reveals a significant drift of $\pm 0.4\%$ with a periodicity of 24 hours. This is attributed to the temperature variation in the experimental hall from day to night and is corrected for in the final analysis.

Calibration events taken inside and outwith the beam gate are not significantly different indicating the absence of a rate effect.

The amount of charge seen in a calibration event compared to the amount of charge injected is a well known function of the electric field and gap width. The presence of electronegative species such as oxygen or fluorine (from freon) change the overall energy scale by about 5 % for 1.0 ppm and 5 % for 0.1 ppm respectively. From the known electric field the mean free path in argon is determined and found to be explicable only if the impurity is 4.4 ppm. in disagreement with the oxygen analyser. The energy normalisation is observed to change by 1 % per month. Both of these effects are assumed to arise from a diffusion of electronegative ions into the argon, and are corrected for in the final analysis.

The electron data is also used in conjunction with the hadron calorimeter, amplifying every channel, to determine leakage. The leakage is ⁓⁓⁓⁓ at all energies, and whilst undetermined, is expected to be up to a factor of four higher for photons. The leakage for electrons is described by the curve :

$$E_{leakage} = (1.72 \times 10^{-4}) \times E_{nominal}^{1.645} \text{ (in GeV)}$$

3.9 The hadron calorimeter

The hadron calorimeter (HAC) is situated immediately behind the LAC. It is an iron−scintillator sandwich of depth 120 cm., divided longitudinally into two halves consisting of 24 steel plates, each of area 2.7 m^2.

Between the plates, scintillator planes are inserted, each consisting of separate strips of dimensions $130 \times 11.9 \text{ cm}^2$ and thickness 4.5 mm. The scintillator is BIS−MSB. There are 24 (25) scintillator planes in the front (back) module. In consecutive planes the strips are aligned alternately horizontal or vertical. In each module consecutive strips at the same lateral position are coupled to a single 3″ SLC L75 B07 phototube by plexiglass light−guides.

There are 176 channels to be read out. The analogue signals are fed to linear mixers which allow an optional amplification of 25 for calibration with muons or electronic test pulses. After the mixers the readout chain is identical to the LAC.

A laser calibration system continuously monitors the performance of the readout chain by distributing converted laser light to all phototubes. Channels are calibrated relative to each other; however because an average hadronic shower deposits 35% of its energy in the LAC the absolute hadron calibration is performed with the combined calorimeters. Using pion beams of 20 − 120 GeV, the energy resolution for pions is:

$$65\%/\sqrt{E_\pi} \text{ in GeV for } E_\pi > 30 \text{ GeV.}$$

3.10 The multi − wire proportional chambers

The experiment has two identical chambers located in the helium tank and separated by about 25 m. There are four wire planes in each chamber. To avoid left − right ambiguities, the wire orientation is successively vertical, horizontal, and at arctan ± 4/3, that is 53^0 and 143^0 respectively. The two orthogonal coordinate systems are offset such that a crossing of more than two wires in the projection perpendicular to the beam is avoided everywhere.

All wires in the anode plane are at the same potential. The wires are 30 μm diameter gold − plated tungsten and are 6 mm. apart. The distance between the cathode planes is 16mm. They consist of 25 μm. Mylar foils coated with graphite operated at 2.85kV. Wires and graphite foils end on Vetronite rings of external diameter 20 cm. and 22.4 cm in chambers one and two respectively. The rings are mounted on aluminium cylinders allowing the beam − pipe to pass through the chambers. The gas mixture is 70% argon + 30% isobutane. The drift velocity is 55 μm/ns.

The signal from each wire is amplified and shaped to a standard ECL pulse. One output for each wire is fed to a separate coincidence register. A hit is recorded if it occurs less than 180 ns after the trigger hodoscope has fired. For drift time measurements the second output of the amplifier is connected to a FASTBUS TDC.

Each wire was timed with respect to the trigger hodoscope using muons. The efficiency was then determined using K_L and K_S charged decays with a reconstructable vertex. To form a space point, hits in three out of four planes are required. The frequency of missing hits in a plane determines the inefficiency; however only if two hits corresponding to the same space point are missing will the event be lost. The average efficiency per plane was better than 99.3%. The loss due to inefficiency or from events where too many space points are found is a few per mille.

3.11 Scintillators

There are four scintillator arrays in the detector. They are all used in the generation of the pretrigger which provides a gate pulse to the wire chambers and the calorimetry.

The charged trigger hodoscope (CTH) is immediately in front of the calorimeters. It is a single plane of scintillators divided into four quadrants. It provides a trigger for charged two−body decays which give a hit in each of two opposite quadrants. The signal is defined to be QX.

The neutral trigger hodoscope (NTH) is a single plane of scintillator in between the front and back halves of the electromagnetic calorimeter. It consists of two half−planes divided at X = 0. A left−right coincidence defines the trigger signal LACX which is shown in figure 20. Explicitly LACX is ·

$$LACX = (1+2+3)_R \cdot (1+2+3)_L + (1.2)_R + (1.2)_L$$

Four rings of scintillators situated along the decay region, are used as anti−counters in the pretrigger, to reject the copious three− body neutral decays, giving particles outside the acceptance of the principal detectors. A logical OR of the rings define the signal (ANTI).

In order to reject $K_{\mu 3}$ events, two planes of scintillator behind the detector, and separated from it by an iron wall, are used in conincidence to define a muon (MU). The Edinburgh group built the

47
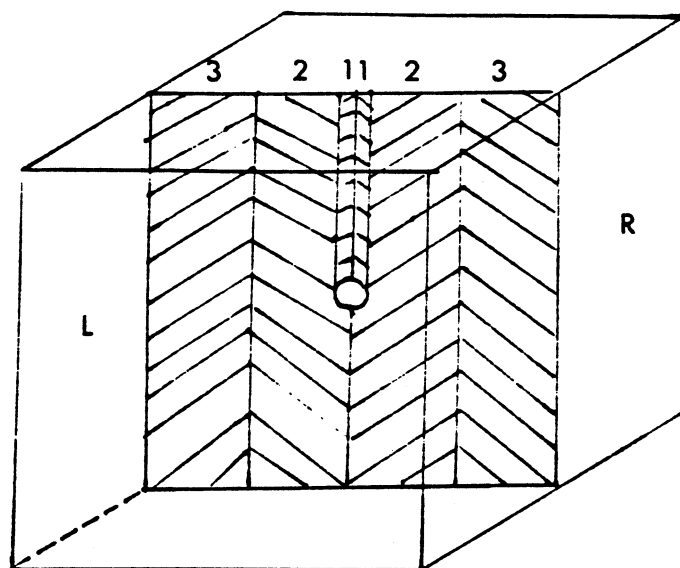
Figure 20: The neutral trigger hodoscope.

muon counters and they remained my responsibility throughout the experiment. I will therefore describe them some detail in the following section.

3.12 Muon − counters.

The detector consists of two planes of NE110 plastic scintillator, shown in figure 21. Each plane has ten double−ended components of 2.7m length and two single−ended components of about 1.25m. All the scintillator is 1cm. thick. Adiabatic lucite light−guides are used for light collection and EMI 9813 14 stage phototubes for light detection. There is a hole in the centre of each plane for the beam−pipe. The two planes of scintillator are orthogonal so that position information from the muon, to within 25cm x 25cm,can be provided if required by the experiment. Each plane of the detector is preceded by an iron wall 0.8m thick.

The construction of a muon veto component involves firstly the wrapping of all parts through which light will travel, in silver foil, cobex and black tape. This reduces the background light, at least

48

in theory, to zero. Next the light – guides are fixed with a high quality optical glue to the scintillator. The phototubes are encased in a spring – loaded mu metal housing to ensure good physical contact to the light – guide and protection from high magnetic fields. An optical grease is applied between the photosensitive window and the end of the light – guide.

The phototube base is a standard resistor chain with decoupling capacitors over the last four stages.
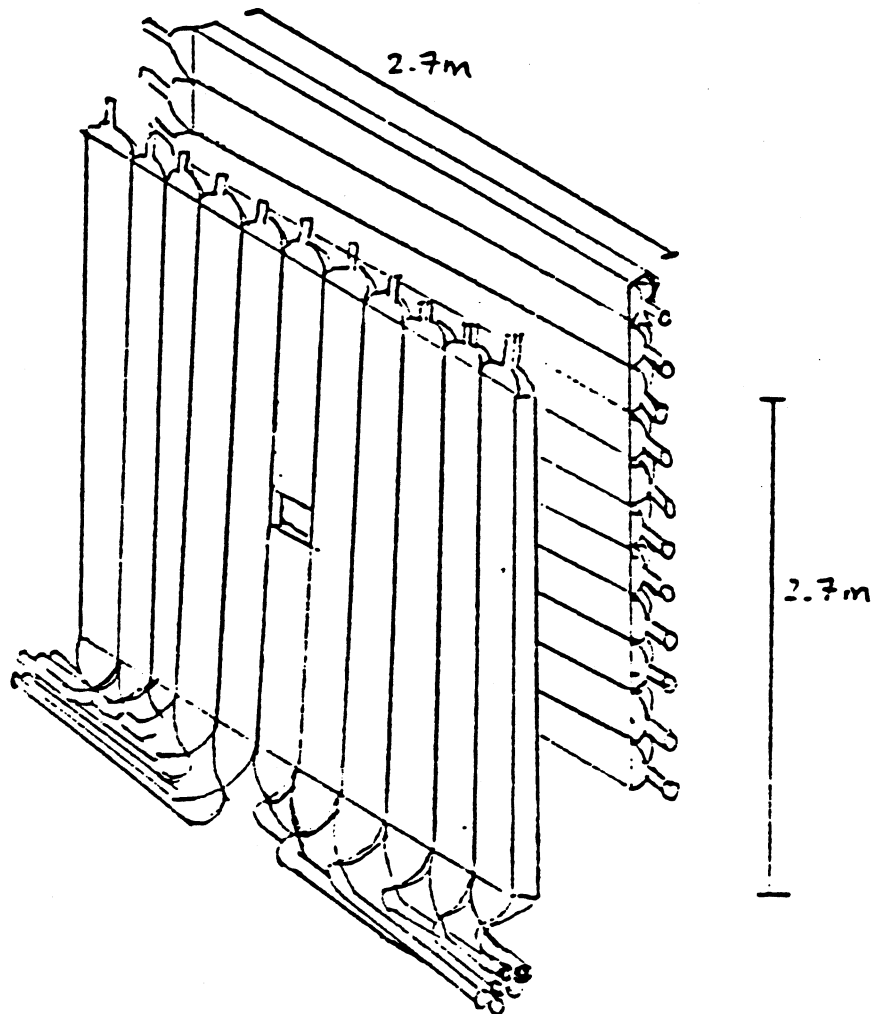
Figure 21: The muon – veto.

The detector is required to be as efficient as possible, and whilst the average muon will deposit 2.16 MeV in the scintillator, which is a fifty photoelectron signal, the variation in pulse height depends on several factors:

- The muon deposits energy according to a Landau distribution.

- The scintillator attenuates the light produced by the scintillation process.

- The light − guide/scintillator interface is a potentially troublesome absorber.

- The light − guides are not better than 10% efficient.

- The phototubes have widely differing gains for a given voltage.

To measure the efficiency of each scintillator light − guide combination the experimental arrangement shown in figure 22 is used. The betatron, an old medical cyclotron, produced bursts of electrons of approximately 35 MeV energy. The beam was defined by a collimator. T_1, T_2 and T_3 are the trigger counters, they were small pieces of scintillator with air light − guides. If a coincident signal is seen in T_1, T_2 and T_3 a particle is deemed to have traversed the test scintillator. An iron shield acts as a second collimator to reduce the rate at which electrons hit the test device and define where they hit it.

The logic for the trigger is shown in figure   23. The 4684 and 821 are discriminators. The semi − circles represent coincidence units. The squares containing numbers are delay boxes, necessary to compensate for the different time of arrival of the electron at each counter. The 'gate' boxes are an ADC, analogue to digital converter, and a TDC, time to digital converter. Another feature of the logic stops, for example, several electrons which have arrived at the test scintillator almost simultaneously from being confused as a single particle. The data acquisition was on a PDP11 computer. Figure 24 shows two of the 44 efficiency curves and a typical tube spectrum. The efficiencies η_L and η_R are defined as the AND of the two ends divided by the left or right rates respectively.

The average efficiency was better than 99%. This was felt to be satisfactory as the electron is not a clean signal. In principle, an electron may traverse T_1 and T_2 and then it or another electron close to it in time, may scatter from the iron wall into T_3 never passing through the test scintillator.

From the ADC spectra the attenuation length of the scintillator was calculated. If this was found to be too long the glue joint between the scintillator and light − guide was suspected as a possible cause. In those cases it was found that the glue had not set properly giving less than perfect optical

$$p \cos \lambda \simeq 3 \times 10^{-4} \, \beta R$$
$$\beta \simeq .23 \, T$$

35 MeV β-tron

BENDING MAGNET

COLLIMATOR

10cm

2m

T_1

T_2

10cm

SHIELD

10cm

R   L

10cm

T_3
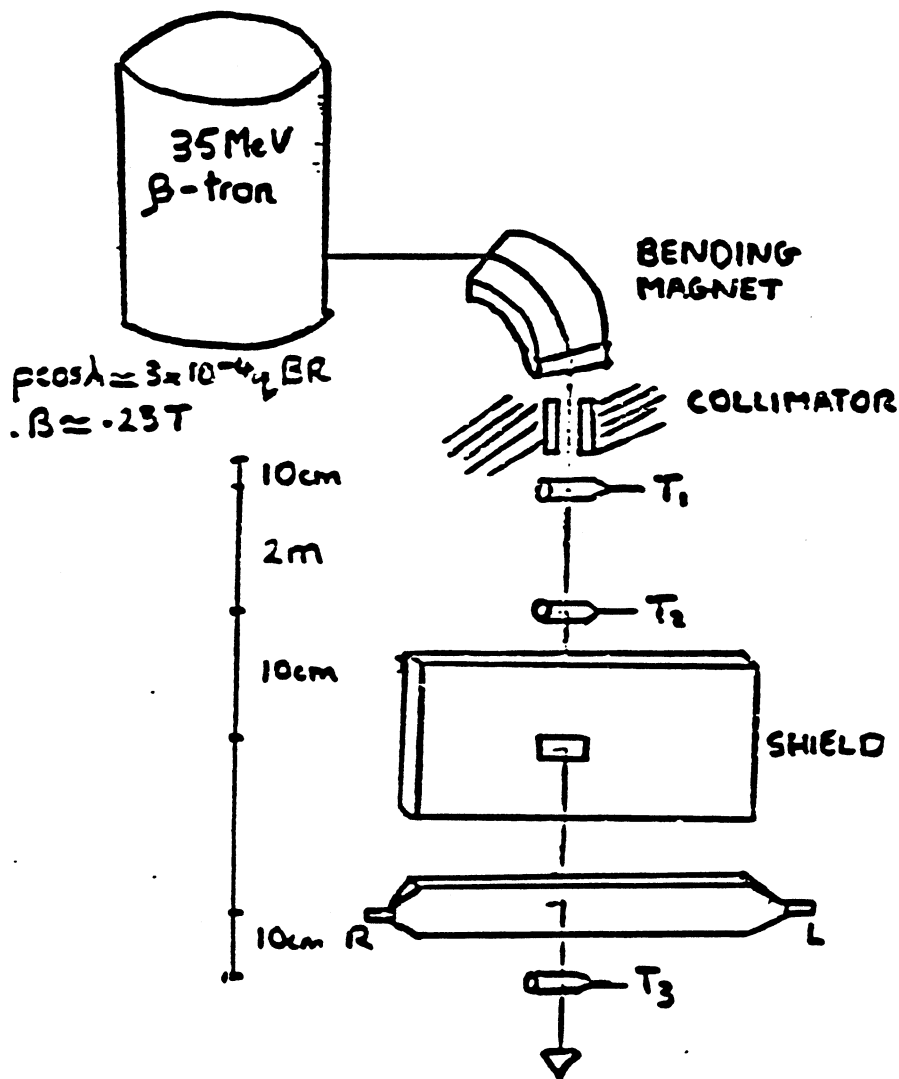
Figure 22: *The experimental arrangement to measure muon efficiencies*

contact. Of the 84 tubes tested, 28 were rejected either because of their low efficiency, high intrinsic noise or because their spectra were too broad. Twelve tubes were kept as spares.

The components were mounted on aluminium support frames which had been especially constructed in Edinburgh, in order for a long HT soak test to be performed on part of the detector before transport to CERN. Five light-guides separated from their respective scintillators during assembly, and these, of course, had to be re-tested. However no problems with tube stability and joint degradation were observed over a one month period. Prisms were glued to each scintillator so that, by in-

51
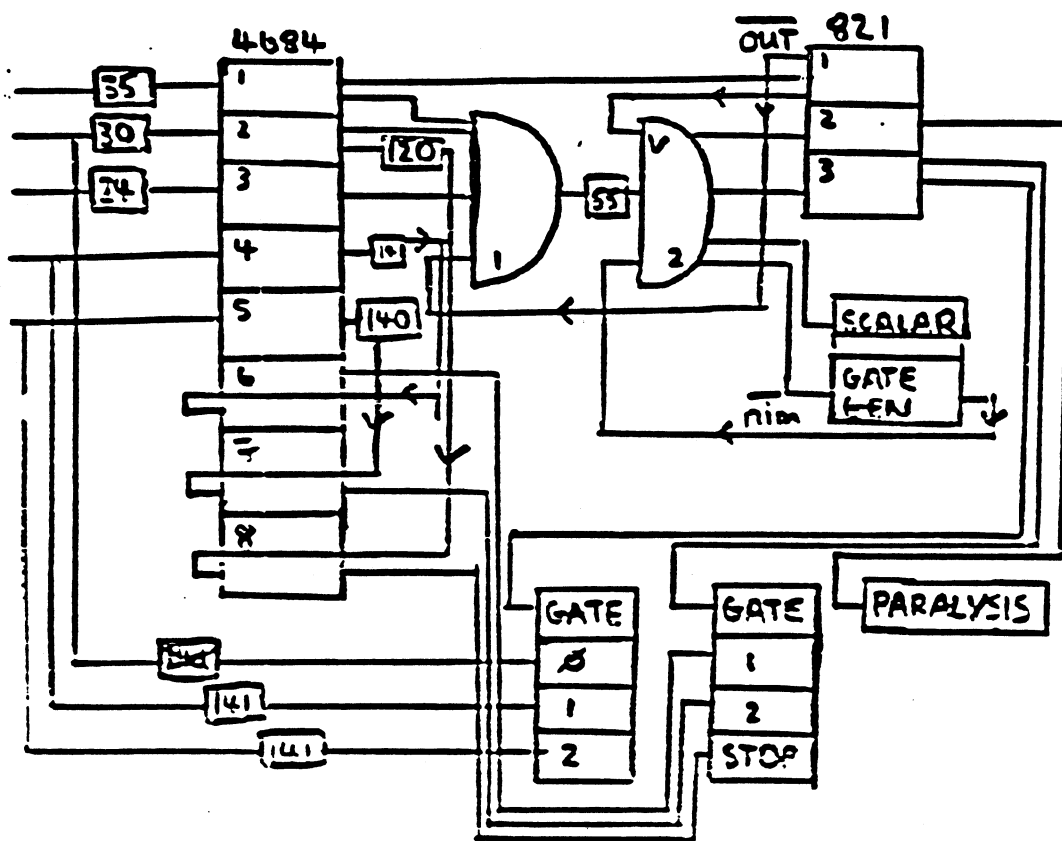
Figure 23: The trigger logic

ternal reflection, laser light may be introduced to monitor response when there is no beam in the experimental hall.

To obtain a muon signal we require that both planes of scintillator detect a particle simultaneously; the presence of the two iron walls then ensures that the particle was a muon. To achieve this signature one cannot compare analogue signals from the pmts, instead one must generate a standard level logic signal for each component. The phototubes at each end of the scintillator pass through an analogue mixer. In this way the signal from a genuine particle which is seen by both ends is enhanced relative to processes like random noise or the passage of a particle through a light guide which will generally produce a signal at one tube of a component only.
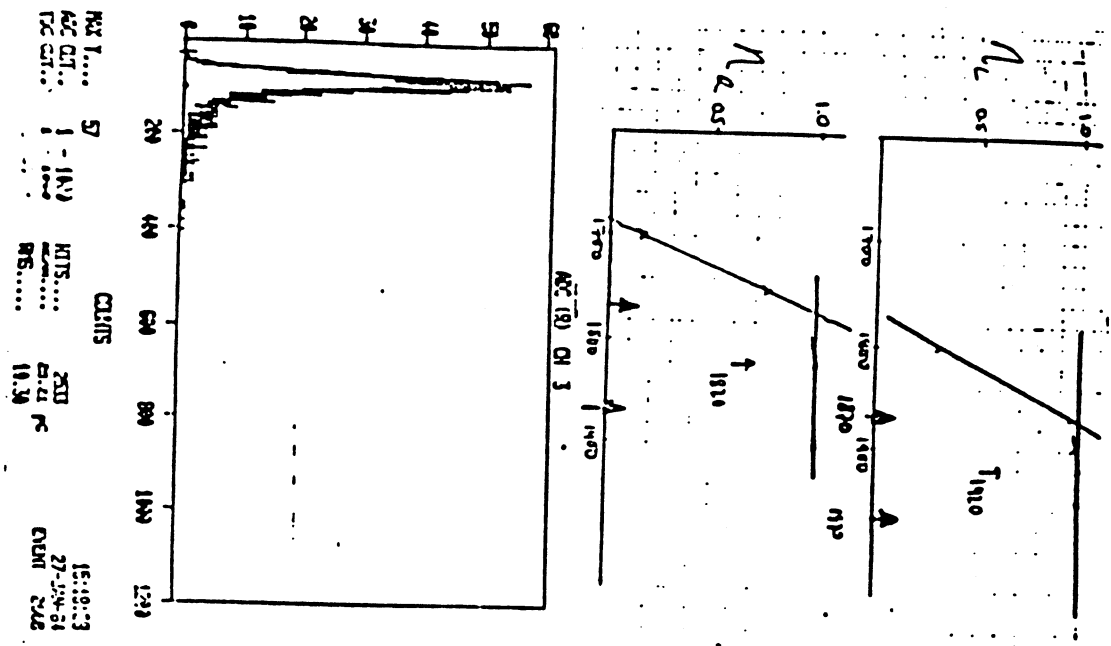
Figure 24: Muon counter efficiency determination
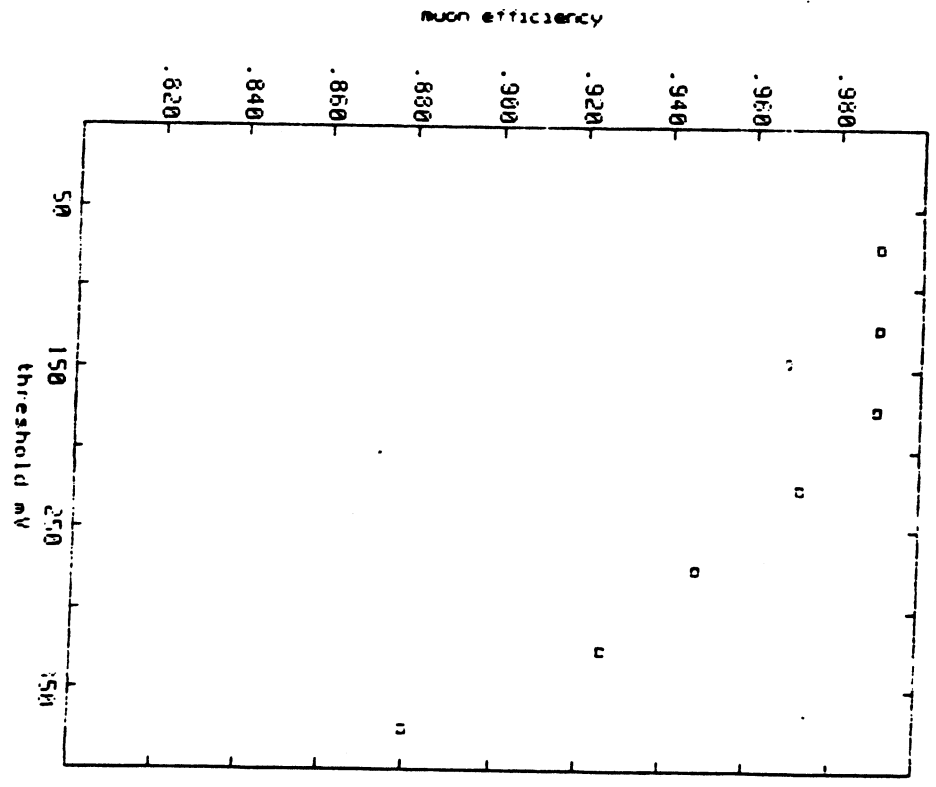
A Ruthenium 106 beta emitter was used to produce minimum ionising particles. Each tube was set such that its spectrum observed on an oscilloscope was equal. The individual tube signals were mixed and the resulting pulseheight and efficiency of detection were measured as a function of source position. It was found that several iterations were necessary to determine the optimum voltage for each tube, such that the efficiency and pulseheight of the mixed signal were large enough and reasonably constant over the scintillator. All components of the veto were then made as similar as possible.

The mixed signal then enters a discriminator. This device has a threshold voltage and only produces a signal if the analogue input is greater than the threshold setting. Clearly if the thresholds are not carefully chosen an inefficiency will exist for muons that produce a small signal. Finally the twenty two outputs from the discriminators enter a LRS4564 logic unit to provide an AND of the 11 − fold OR from each plane.

By using the charged trigger hodoscope and the second muon plane in coincidence to define a particle, the efficiency curve shown in Figure 24 of the whole first plane was obtained for different thresholds as a function of voltage. The maximum efficiency achieved was 99.8%. The threshold applied to each signal was set to 50mV, one sixth of the pulseheight from a minimum ionising particle.

All voltages are set and monitored by a caviar microcomputer. The 44 unmixed analogue signals are divided by a resistor chain before the muon logic is made, and one half sent to ADC's which are read every burst by the caviar. In this way deviations in the spectra can be reported to the shift crew by an alarm, and long term drifting of the phototube response may be studied. Figure 25 shows the caviar display monitoring the voltages, while Figure 26 shows some typical spectra taken in the kaon beam.

With $3x10^{10}$ protons per pulse from the SPS striking the target, more than 30,000 muons from decaying kaons and background from neighbouring beams are produced every two seconds. The muon veto generates a 40ns pulse for almost every muon, which is received by the overall experimental trigger as an anti − coincidence, and the event is rejected.

HORIZ. MUON-ANTI

LEFT   VOLTAGES   RIGTH

VOLTAGE
STATION
MODULE

VERT.MUON-ANTI
TOP

BOTTOM
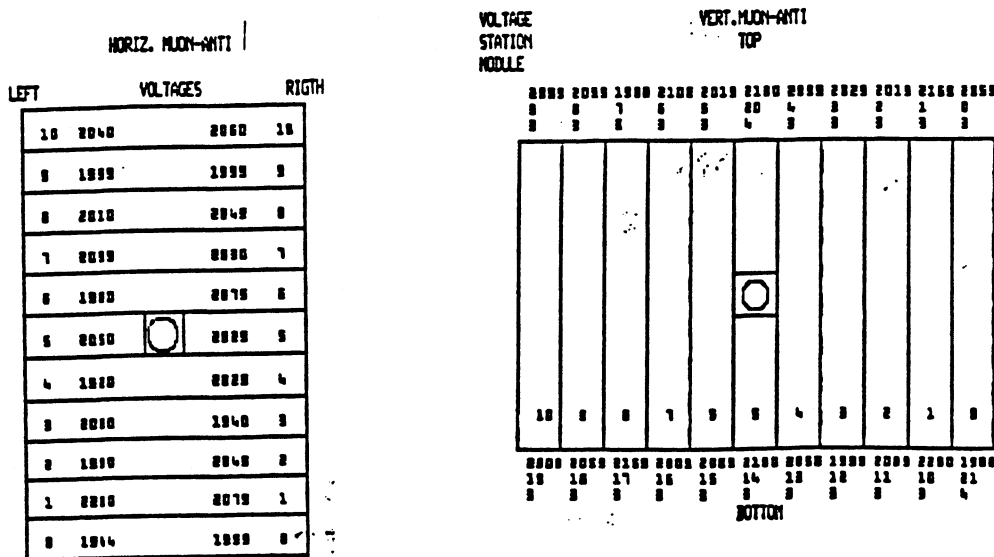
Figure 25: Voltage monitoring

3.13 The peak−finder.

The number of energy clusters deposited in the front half of the electromagnetic calorimeter is measured online by the peak−finder and used in the trigger. As the lateral electromagnetic shower width is comparable to the channel width in the calorimeter, a cluster is defined by comparing the digital output of the strips in the vertical and horizontal views. A bit is set whenever one strip is greater than 2 GeV and greater than the two adjacent strips. The 384 bits are read out by a FASTBUS pattern unit and used by the 168/E processor for the rejection of $K_L \to 3\pi^0$ events if more than four clusters are found. The peak−finder generates a current proportional to the number of clusters found 1.5μs. after an event. This is used to reject single track events and to reject neutral events in the third level trigger.
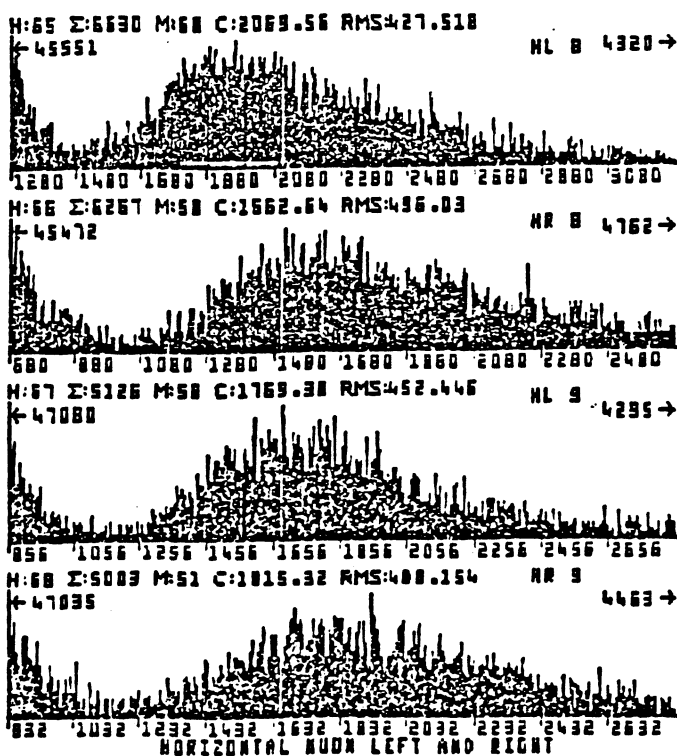
Figure 26: Muon spectra

3.14 The trigger

The trigger is designed to recognize and accept two pion decays, although it also accepts two gamma and some other rare decay modes of the kaon. Because all of these modes together, represent only $\approx 1\%$ of the possible decays of a K_L, a powerful rejection of events is required online if the data tapes are to contain a substantial percentage of useful events.

To achieve this, the trigger is divided into two parts. The first synchronous part has three levels :

- The pretrigger, defines the starting signal T0 using the scintillator arrays to indicate that a likely two−body decay has been detected. T0 opens the gate for the wire chambers and blocks subsequent events.

- The second level uses the fast energy sums from the calorimeters to determine if an event is above the total energy threshold and defines the event categories charged and neutral. If the longitudinal shower development is consistent with the presence of an electron, or the anti− counter on the K_S train has fired, the event is rejected and the trigger re−enabled.

56

- The third level trigger provides additional constraints on the event types. For neutral events, the current generated by the peak−finder is required to correspond to greater than one and less than four energy clusters. For charged events, at least two hits in at least two planes of WC1 are required.

If either a charged or neutral trigger is satisfied, a signal is sent to the second part of the trigger. In this asynchronous part an intermediate buffer reduces the trigger dead time by allowing two events to be present at one time. Each event enters the analogue memories of the calorimeter encoders to be digitised. As soon as the previous event has been readout by the FASTBUS from the intermediate buffer into the 168/E system, the current event is transferred to the intermediate buffer.

We define E and H to be the energy sums for the electromagnetic hadronic calorimeters respectively. The thresholds used by the trigger to define the two event categories are :

- Neutral : $H < 12$ GeV and $E > 35$ GeV.
- Charged : $H > 12$ GeV and $(E + H) > 30$ GeV.

The synchronous trigger logic is shown schematically in the flowchart of Figure 27.

3.15 The Arithmetic FASTBUS Interface.

The arithmetic FASTBUS interface (AFBI) rejects events on−line using the ADC information from the calorimeters which it receives from the FBAP.

Energy sums, first and second moments, and hence the vertex of an events are determined in accumulation cards. The stored results are then compared with cut−off values loaded into registers at initialization, to determine if an event should be rejected.

WC

PK

ENERGY SUMS

QX

LACX

ANTI

MU

TO

PO

$\text{I} \quad 100 \quad \text{I} \quad 250 \quad \text{I} \quad 1500\,\text{ns} \quad \text{I}$
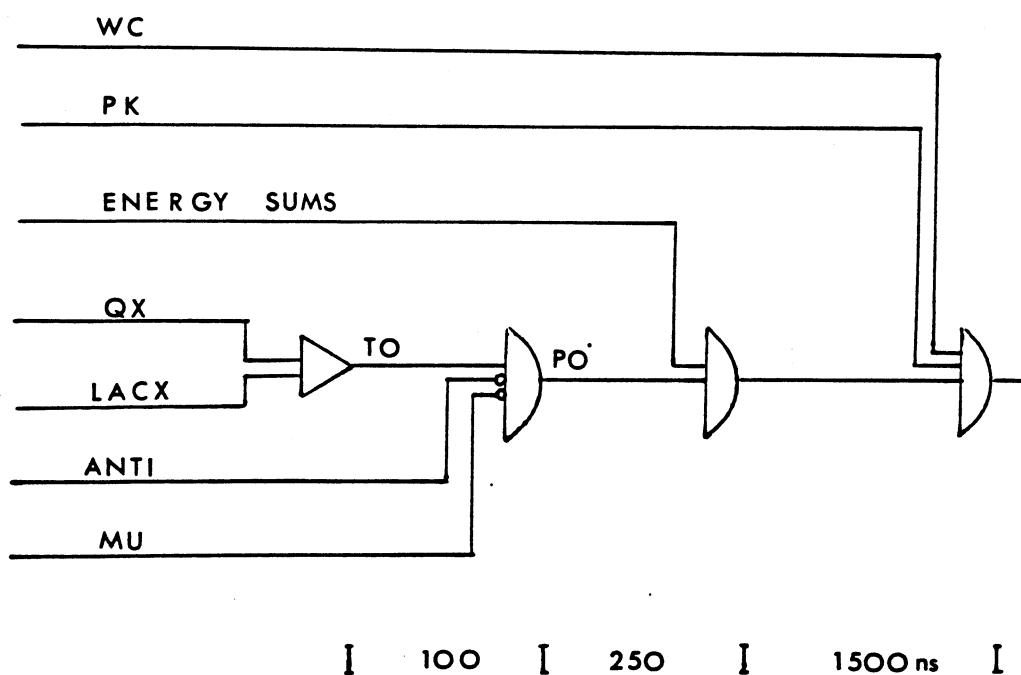
Figure 27: The synchronous trigger logic

The contents of the accumulation cards, the vertex of an event and rejection flags are returned to the FBAP. Using downscaled data, the rejection power of the AFBI was determined to be 1/5 of all neutral triggers and 1/2 of all charged triggers.

3.16 The 168/E processors

The final on−line rejection is made by two 168/E emulators, which receive data from the FASTBUS system.

Each emulator operates the same filter algorithm. Using the information from the AFBI and the peakfinder, the following cuts are made for the neutral category :

- peakfinder cut
- $E_{LAC} -$ cut   40 GeV

- first moment cut   15 cm.

- z−cut   < 70 m.

The complete algorithm for neutral and charged events lasts 500 μs. The filter rejects two−thirds of the data, but one quarter of the events are kept without reference to the filter decision, so that half of the data read into the 168/E's is transferred to the buffer memory.

3.17 The data−taking sequence

The data acquisition system is the FASTBUS standard controlled by a VAX11/750 computer. It is described in reference [34].

During each burst of the SPS, which lasts 2.8 s, all the data from each event is read into the 168/E, without intervention from the VAX. During the 11.6 s between beam bursts, the data in the buffer memory are tranferred to the VAX. There is a calibration gate, about two seconds before the beam gate. Calibration events used to monitor the calorimeters are read directly by the VAX at this time. The data are reformatted by the VAX and written onto 1600 bpi tapes in the CERN standard EPIO format.

3.18 Time History Module

The status of all trigger input signals is latched every 50 ns. into a group of registers. Because of the high beam flux two kaon decays may arrive close in time or an unassociated particle may confuse or contaminate an event. The experimental memory is composed of the LAC drift time (400 ns) and the readout electronics (1.2 μs). By analysing the time history module (THM) data offline, one may investigate the purity of an event in a window 3.2 μs about the T0.

4. PRINCIPLES OF THE MEASUREMENT

4.1 Introduction

In this chapter the principles used in the analysis to extract the signal and normalisation from the various backgrounds are discussed. To begin the backgrounds are listed.

We have seen that there are three main neutral decay modes of the K_L meson: $3\pi^0$, $2\pi^0$ and 2γ. Therefore the principal sources of background for the 2γ mode in this experiment are:

- $K_L \rightarrow 3\pi^0$ where four photons miss the detector and anti$-$counters, or otherwise go undetected.

- $K_L \rightarrow 2\pi^0$ where two photons miss the detector and anti$-$counters, or otherwise go undetected.

Other sources of two photons are :

- $K_L \rightarrow \pi^+\pi^-\pi^0$ where neither charged pion is seen

- neutron interactions in the collimator or other matter in the beam line, producing π^0's

- a coincidence of two unrelated photons in the detector

- a coincidence between a neutron and a photon in the detector

In the K_S beam we expect three additional backgrounds for 2γ:

- $K_S \rightarrow 2\pi^0$ where two photons miss the detector or otherwise go unrecorded.

- $K_L \rightarrow 2\gamma$ where both photons are detected.

- The decay of a lambda, $\Lambda \rightarrow n\pi^0$, where only two of the final products are detected.

For the $2\pi^0$, which we shall use for normalisation, the backgrounds are :

- $K_L \to 3\pi^0$ where two photons miss the detector and anti-counters, or otherwise go undetected.

- $K_L \to 3\pi^0 \to 3\gamma$ or $K_S \to 2\pi^0 \to 3\gamma$ with an additional unassociated photon.

4.2 The first moment.

The only information recorded from a neutral decay is the energy and position of each converted photon at the detector. Using these the nth moment of an event in which there are N particles may be defined as :

$$X_n = \Sigma_{i=1,N} E_i x_i^n \quad \text{and} \quad Y_n = \Sigma_{i=1,N} E_i y_i^n$$

Normalising by the total energy the centre of gravity (COG) of the event is obtained:

$$(COG)^2 = (X_1/X_0)^2 + (Y_1/Y_0)^2$$

For a decay of a particle which comes from the beam in which all photons are observed, the first moment just measures the beam size in the calorimeter, or put another way: the position of the kaon at the calorimeter had it not decayed. From the distance of the target, distance and aperture of the collimator and position of the calorimeter it is expected that the beam size and hence first moment should always be less than 5 cm. and in any case certainly within the beam-pipe as shown in Figure 28, where t is the target, and C and CC are the defining and cleaning collimators respectively. The energy resolution of the lowest energy photon in an event determines the error in the first moment, typically ±1 cm. A first moment distribution should therefore be limited to about 6 cm. For events with undetected photons, the first moment will be generally larger than the diameter of the beam-pipe. The first moment will be used to ensure that events originate from kaon decays in the beam.

61
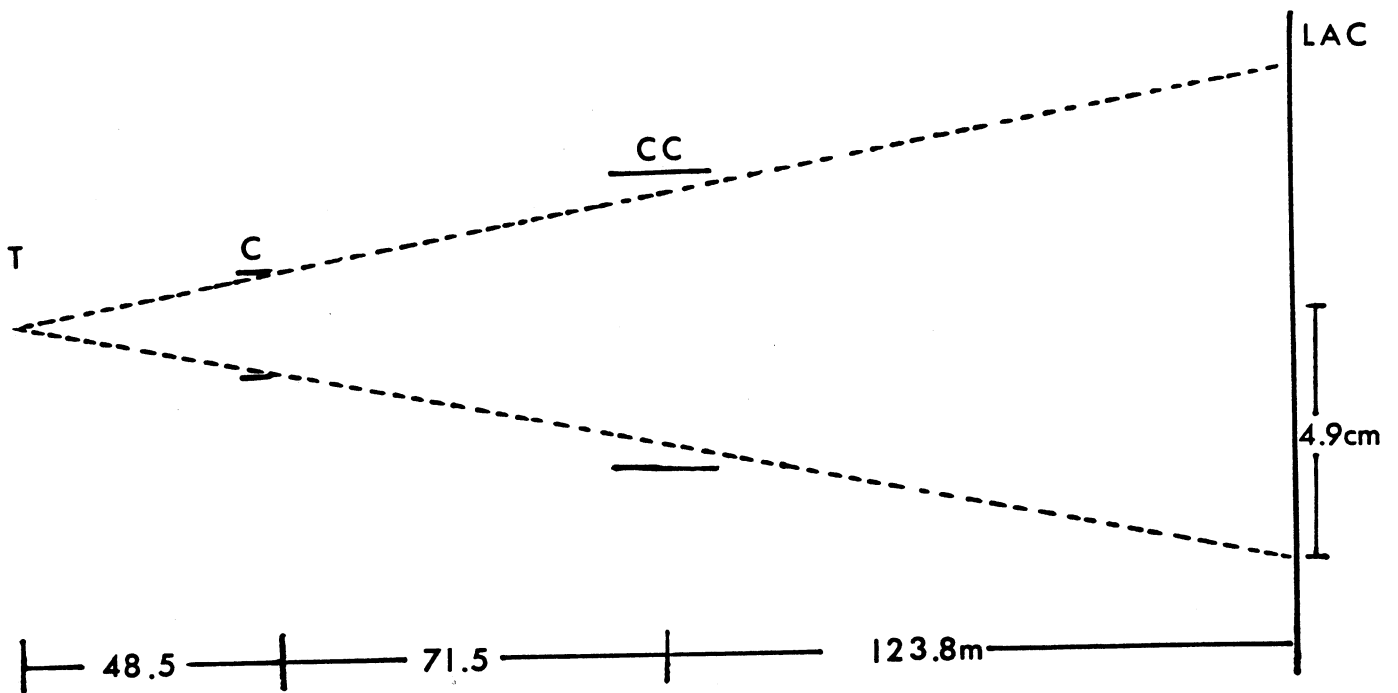
Figure 28: The beam divergence at the calorimeter.

4.3 The mass constraint.

The mass constraint is now introduced. Using the second moment and the constraint that the decaying particle is a kaon the $Z-$vertex of an event is:

$$Z^2 = (1/m_k^2) \{ X_0.X_2 - X_1^2 + Y_0.Y_2 - Y_1^2 \} \qquad (3)$$

Let us look at this determination of Z in greater detail.

We first derive the relationship for the two photon case, considering Figure 29 in the centre of mass.

62
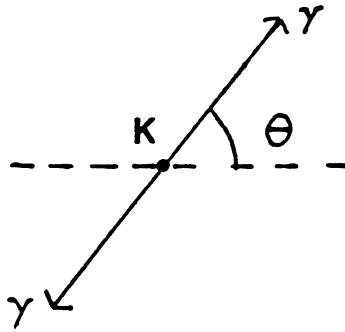
Figure 29: The decay $K \to 2\gamma$ in the kaon rest frame.

$$P_K{}^2 = (P_{\gamma 1} + P_{\gamma 2})^2$$

$$= P_{\gamma 1}{}^2 + P_{\gamma 2}{}^2 + 2P_{\gamma 1} \cdot P_{\gamma 2}$$

therefore :

$$m_k{}^2 = 2E_1 E_2 (1 - \cos\theta)$$

In the laboratory where θ becomes small for high energy kaons :

$$m_k{}^2 = E_1 E_2 \theta^2 \qquad (4)$$

now θ in the laboratory is just :

$$\theta = r/Z$$

where r is the separation of the two photons at the detector as shown in Figure 30

Explicitly the square of the vertex is measured by inverting equation (4):

$$Z^2 = E_1 E_2 \{ (x_1 - x_2)^2 + (y_1 - y_2)^2 \}/m_k{}^2 \qquad (5)$$
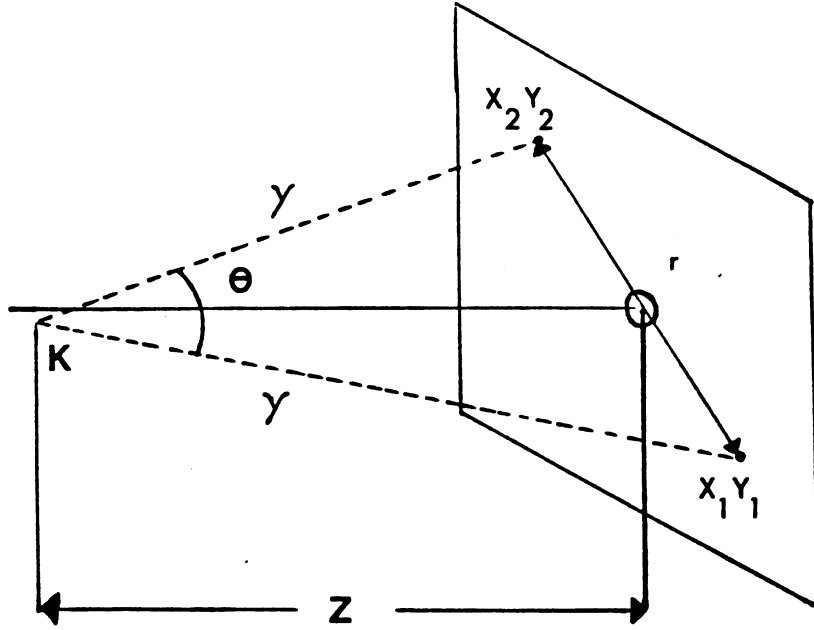
which is just equation (3), with x_i and y_i the coordinates of the ith photon. This equation is the mass constraint for two photons. We shall determine the vertex for each two photon event using equation (5). Note that all distances are determined at the detector, and therefore the vertex is measured from the detector, which is defined to be at $Z = 0$.

As a further example the four photon case is obtained. Analagously to the two photon case :

$$m_K{}^2 = (P_1 + P_2 + P_3 + P_4)^2$$

$$= P_1{}^2 + P_2{}^2 + P_3{}^2 + P_4{}^2 + 2(P_1P_2 + P_3P_4 + P_1P_3 + P_2P_4 + P_1P_4 + P_2P_3)$$

$$m_K{}^2 = \Sigma_{i,j\,=\,1,4} E_i E_j (x_i - x_j)^2 + (y_i - y_j)^2 \, /Z^2$$
$$i > j$$

It is clear that there is a reciprocal relationship between the vertex of an event and the effective mass of two photons; that is to say for any combination of E_1, E_2 and r, a Z is determined for an assumed mass and vice versa. This invariance can be seen in terms of cms quantities. The four momentum of each γ in the cms is:

$$P_{\gamma_1} = m_K/2 \, (1,1,0,0) \qquad P_{\gamma_2} = m_K/2(1,-1,0,0)$$

For a kaon with a momentum $m\beta\gamma$ in the laboratory, we have for the decay $K_L \to 2\gamma$:

$$E_{lab_1} = \gamma m_K/2(1-\cos\theta)$$

$$E_{lab_2} = \gamma m_K/2(1+\cos\theta)$$

$$\sqrt{(E_{lab_1} E_{lab_2})} = \gamma m_K/2 \, \sin\theta$$

the angle in the laboratory is :

$$\frac{r_1}{z} = \frac{P_{T_1}}{P_{Z_1}} = \frac{(m_K/2 \, \sin\theta)}{\gamma m_K/2(1-\cos\theta)}$$

$$\frac{r_2}{z} = \frac{P_{T_2}}{P_{Z_2}} = \frac{(m_K/2 \, \sin\theta)}{\gamma m_K/2(1+\cos\theta)}$$

The invariance is manifest:

$$\sqrt{(E_{lab_1} E_{lab_2})}\theta_{lab} = m_K$$

Consider the effect of the mass constraint when the two detected photons are from a π^0. The situation is shown in Figure 31 .

The true vertex is related to the measured quantities by :

$$Z_\pi = \sqrt{(E_1 E_2)}r/m_{\pi^0}$$

The Z we obtain from the mass constraint however is :

$$Z_k = \sqrt{(E_1 E_2)}r/m_k$$

The shift between the two vertices is :
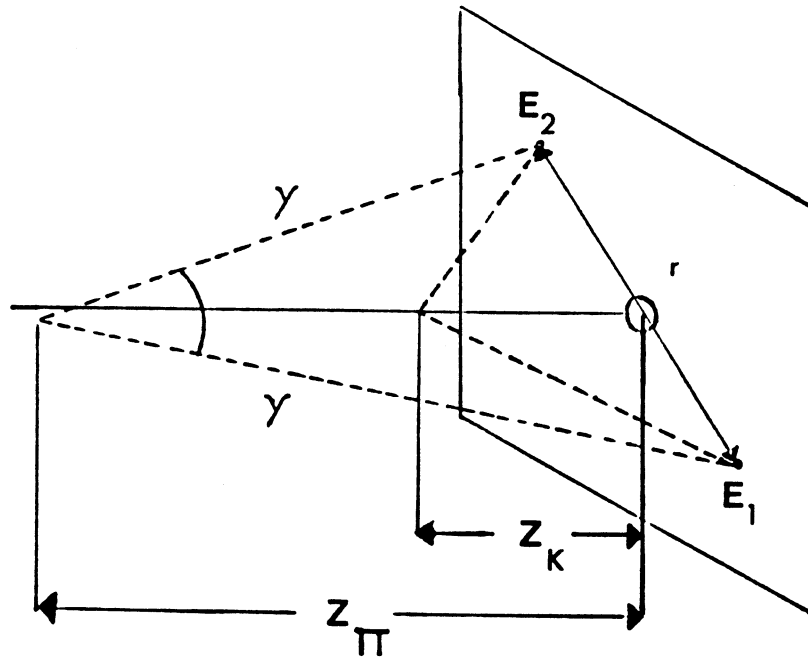
Figure 31: The mass constraint for a π^0 decay.

$$\Delta Z = (Z_\pi - Z_k)/Z_\pi$$

$$\Delta Z = 1 - m_{\pi^0}/m_k$$

$$\Delta Z = 1 - 0.27 = 0.83$$

The one–to–one relation between mass and vertex is demonstrated. Note that this result is not dependent on the energy scale. The centre of our fiducial volume is about 100 m. from the calorimeter, but for backgrounds which give two photons from a π^0 which decayed at the centre of decay tank the vertex we determine is only 27 m. We conclude that the background from these sources is not a problem.

Let us consider the background from $2\pi^0 \rightarrow 2\gamma$. Now the two photons may not come from the same π^0; in general we may form six different pairs of two photons in the cms frame of the kaon. Any one of these pairs might be the only pair seen from that decay in the apparatus; however the effective mass of any pair from a $2\pi^0$ decay may not exceed 458 MeV. This value arises from the following considerations. For the K decay into $2\pi^0$, each pion has an energy in the kaon rest frame of:

66

$$P_\pi^{\ 2} = (m_K/2)^2 - m_\pi^{\ 2}$$

$$P_\pi = 209.1 \text{ MeV} \qquad E_\pi = 248.8 \text{ MeV}$$

The invariant mass for any combination of two photons, γ_A and γ_B, from the four photons produced in the subsequent decay of the π^0's is :

$$m_{AB}^{\ 2} = 2 E_A E_B (1 - \cos\theta_{AB})$$

This has a maximum value when γ_A and γ_B are back to back in the rest frame of the kaon. To conserve momentum each γ, from a π^0 decay, receives:

$$P_\gamma = (248.8 - 209.1)/2 = 19.9 \text{ MeV}$$

in the kaon rest frame. Therefore the maximum momentum/energy a photon can have in the kaon rest frame is :

$$P_{\gamma max} = E_{\gamma max} = 209.1 + 19.9 = 229$$

$$m_{AB}^{\ 2} = (2)\,(229)\,(229)\,(2)$$

$$m_{ab} = 458 \text{ MeV}$$

Therefore by assuming the kaon mass the systematic shift in Z, δZ, will be :

$$\delta Z/Z \geq 458/m_k \text{ (in MeV)}$$

$$\delta Z/Z \geq 0.920$$

$$1 - \delta Z/Z \geq 0.080$$

As the decay volume starts 124 metres upstream of the detector, the first 8.0% (9.9 m.) of the region is completely background free. In practice measurement errors reduce this region. The neutral vertex resolution is typically 1%, given by the energy resolution. The effective mass distribution for a pair of photons in a $2\pi^0$ decay is shown in Figure 32.The largest effective mass combination is plotted for each event.
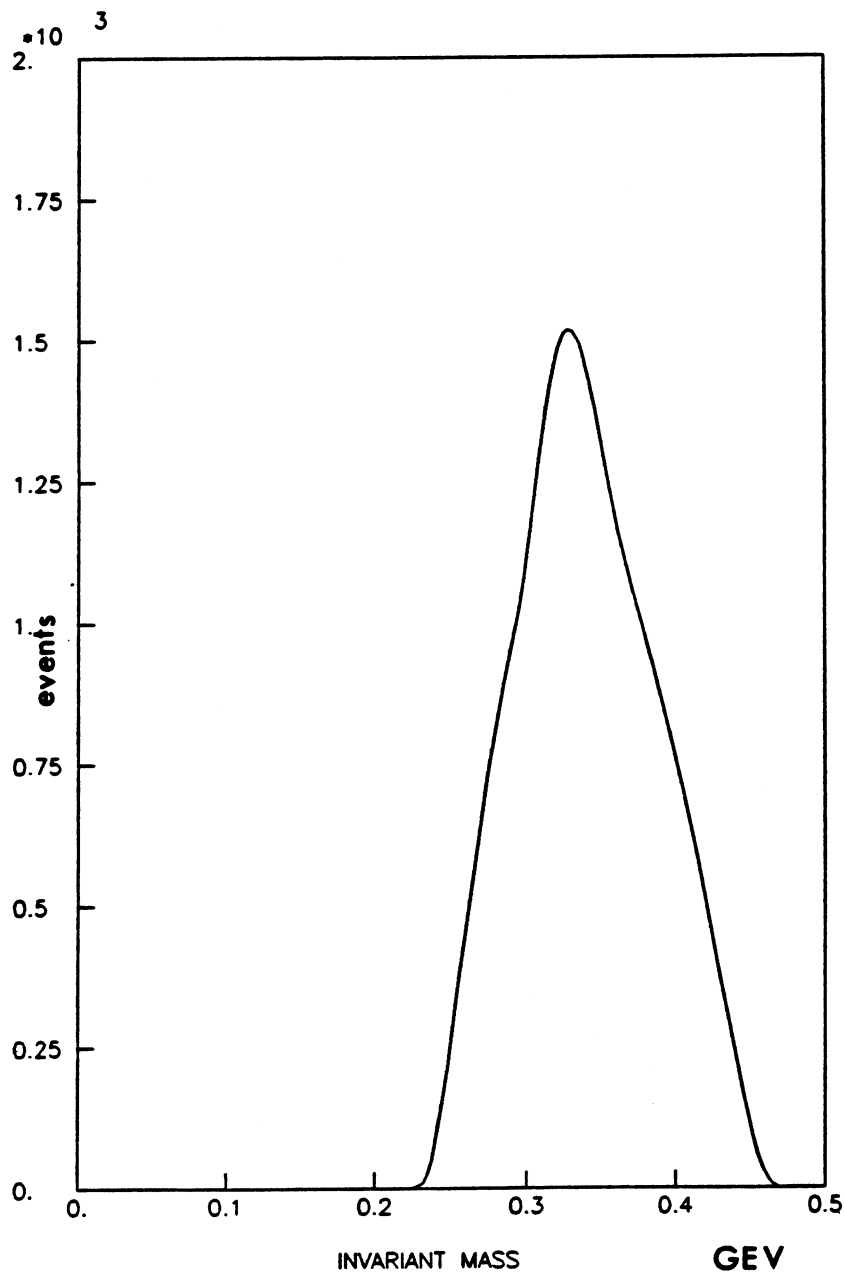
Figure 32: Effective mass in a $2\pi^0$ decay of the highest mass photon pair.

The corresponding plot for a $3\pi^0$ decay is shown in Figure 33 The cutoff mass is less than for $2\pi^0$ and the consequent shift in the determination of z is larger.

$$\delta Z/Z \geq 300/m_k \text{ (in MeV)}$$

$$\delta Z/Z \geq 0.603$$

$$1 - \delta Z/Z \geq 0.397$$

Indeed for the $3\pi^0$ decay it is clear that no background is expected in the first 49 m. of the decay tank. Consequently the fiducial volume for this measurement will end at 47 m.

From the shape of the effective mass distributions, which are always plotted for the worst case from the point of view of 2γ background, it follows that the background falls rapidly with increasing Z, approaching the kinematical cutoff with zero slope. To summarise, using the mass constraint it is possible to work in a region of Z sufficiently far from the detector to ensure that only a small background remains.

As an example of the power of the mass constraint consider data taken in the K_S beam. The neutral background is dominated by $2\pi^0$ decays. The effective mass may be artificially measured by fixing Z with the approximation that all K_S decays are at the collimator. The mass obtained from this constraint is shown in figure 34 for all two photon events. A m_{π^0} peak is clearly visible, its exponential tail coming from the K_S lifetime. The peak below 400 MeV is from $2\pi^0$ decays where the photons are from different π^0's. There is no evidence for a long mass tail, the cutoff is at $\simeq$ 450 MeV.
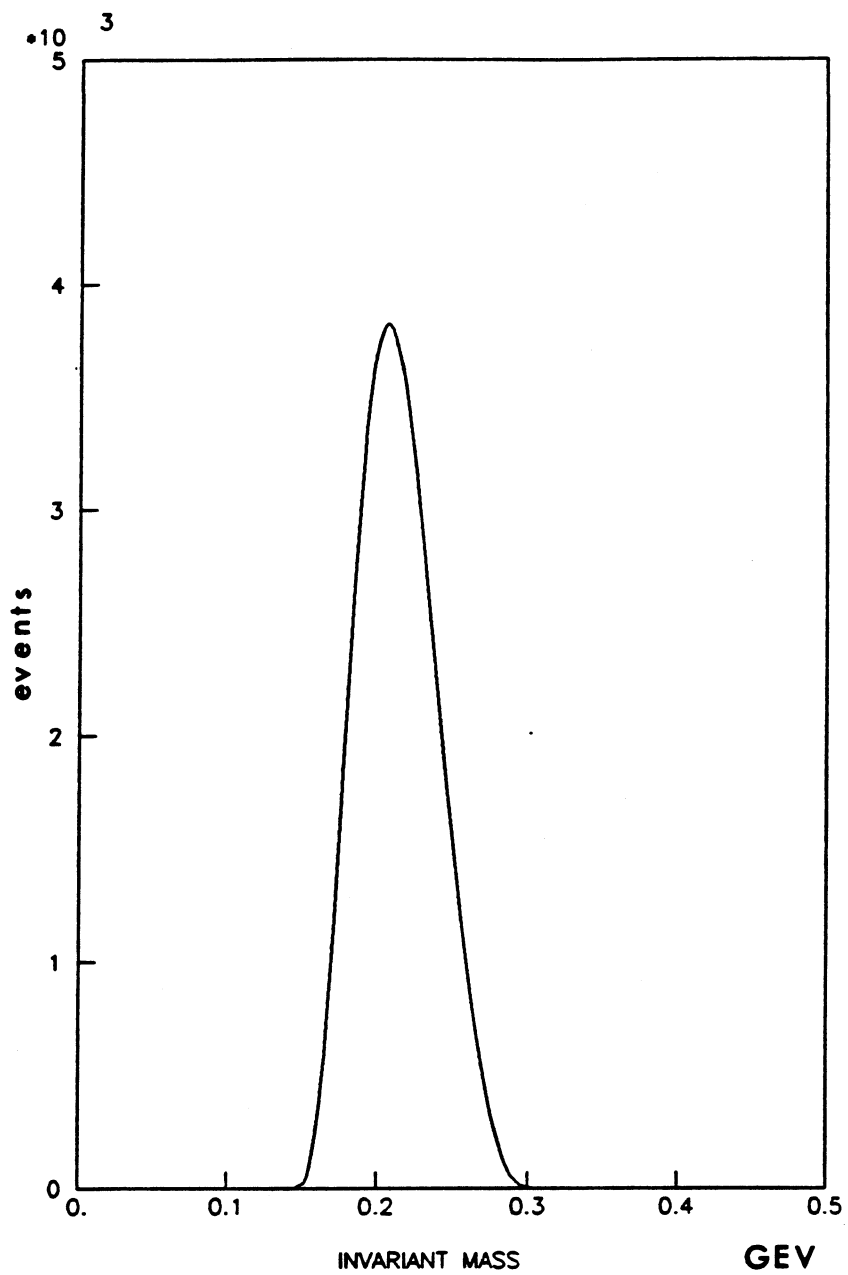
Figure 33: Effective mass in a $3\pi^0$ decay of the highest mass photon pair
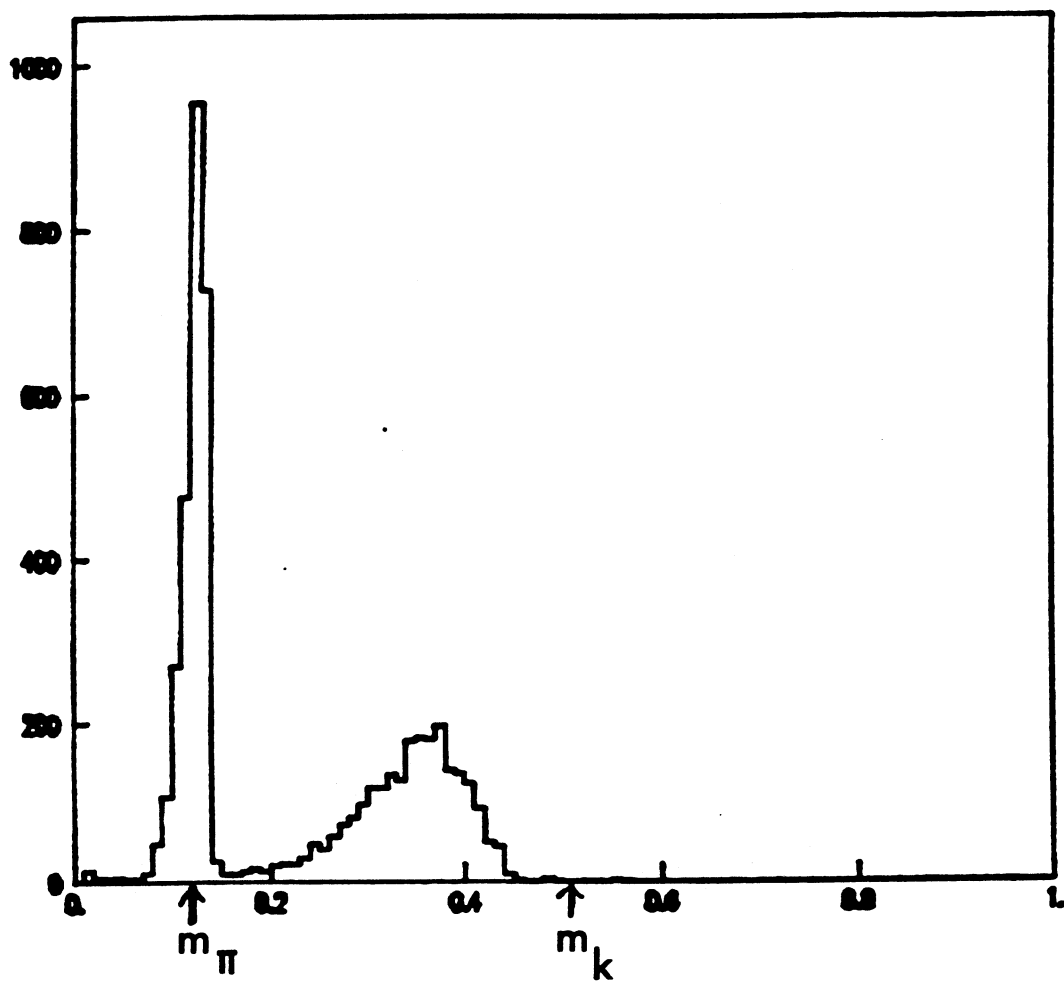
Figure 34: Effective mass distribution of 2 photon events in K_S

5. DATA REDUCTION

The data analysed for this work consists of the total data sample collected during the 1985 run. The run commenced in the middle of April and ended in August. The data presented here was taken in July and August after the experiment had reached a stable configuration.

Normally, during data taking the beam is K_L, however every two days the beam is switched to K_S and data is taken at every fourth station. The stations are selected such that each is chosen every fourth K_S period. A period of K_S running and about half the preceding and succeeding K_L data defines a mini − period. The total data sample represents twelve such mini − periods.

The data is written directly onto tape in the control room using 1600 bpi tapes in EPIO format. These are copied, at the earliest opportunity, onto 6250 bpi tapes and the calibration events written onto separate tapes. The high − density tapes were then passed through the reconstruction program KORECT.

5.1 The reconstruction program KORECT

KORECT is the work of many physicists in the collaboration. The program reads an event and decodes the raw data blocks; the ADC's, TDC's, HTM's, PU's and wire chamber addresses.

At this stage an event will only be rejected if a readout error occurred online such that a data block is completely absent. All events are then passed through a charged reconstruction. If there are two space points in each chamber and a vertex can be made the event is treated as a charged decay; however if the neutral trigger is set a neutral reconstruction will be made later if the charged reconstruction is unsuccessful. A series of cuts is then performed to determine which output stream the event should go to.

For the production there are two output streams; one containing all input events and another with a selected sample of 2γ , 2π and 3π events. For each event the data blocks and the reconstruction blocks, containing energies and coordinates of the particles , are written to tape in EPIO format.

72

5.2 Charged reconstruction

The charged reconstruction starts by using the wire chamber addresses to make space points. If there are at least two space points in each chamber all possible combinations of one pair of space-points in each chamber are made to find the best fit to a plane, provided that the space points are at least 20 cm. apart. If the most coplanar combination has an acceptable χ^2, the TDC data is used to improve the precision of the vertex. If a space point is closer than 12 (18) cm. from the beam axis at WC1 (WC2) the vertex will be rejected.

Each track is extrapolated to the calorimeters and its energy and width are determined from a well–defined region around the track. After the determination of the charged track energies the neutral reconstruction, that is a photon search, is applied to the whole LAC area. Due to hadronic shower fluctuations many 'photons' are found. To distinguish real photons from fakes a minimum energy and good separation from the charged track is required. If any photon remains the event is flagged as it is most likely a $K_L \to \pi^+ \pi^- \pi^0$ event.

Finally electron rejection criteria are applied. Electrons are those tracks which satisfy the following criteria:

- the energy in the HAC is less than 5 GeV

- the distance of the centre of gravity of the shower to the extrapolated impact point from the chambers is less than 1 cm.

- $E_{LAC} / E_{HAC} > 6$

- E_{LAC} (front) / $(E_{LAC} + E_{HAC}) > 0.46$

- The width of the shower is between 1.77 and 2.21 cm.

These cuts are tested with the K_S data and reject only a few per mille of $K_S \to 2\pi^0$ events whilst rejecting $90-95\%$ of all electrons as determined in electron beams.

For the principal aim of the experiment, only $K \to \pi^+ \pi^-$ are interesting in the charged category. For this analysis however our concern is that a neutral event should not be labelled as a charged event, under which circumstances a neutral reconstruction will not be made and the event consequently lost. In conclusion, if an event has two well-separated space-points in each chamber far from the rings, if either or both tracks are identified as pions or electrons or a combination of the two, or if a isolated additional photon is found, the event will be labelled as charged and for our purposes lost.

5.3 Neutral Reconstruction

For all events with a neutral trigger the neutral reconstruction may be called only if the charged reconstruction has failed. The neutral reconstruction uses only the LAC information.

Energies are calibrated using pedestals and sensitivities determined for every K_L and K_S period separately and read from a database. Sensitivities are obtained from the electronic calibration which is corrected for a nonlinearity. There are several dead channels, and energies in these regions are obtained by interpolation from neighbouring strips assuming an electromagnetic shower profile.

Firstly one-dimensional clusters are found with a software peakfinding algorithm; summing the energies in the front and back halves of the calorimeter a peak is defined for the kth strip if :

- $E_K > 0.5*(E_{K-1} + E_{K+1}) + 0.15 \text{ GeV}$
- $E_{K-1} + E_K + E_{K+1} > 0.6 \text{ GeV}$
- $E_{K-1} > 0.15 E_K$ and $E_{K+1} > 0.15 E_K$

Peaks on neighbouring strips are merged. The number of peaks in any quadrant side is limited to 10. For isolated peaks the cluster energy is determined by summing over the fifteen strips adjacent to the peak. The cluster position is determined from the energy ratios of the central three strips only. For overlapping showers the strip energy is weighted according to the profile

$$E(x) = \Sigma A_i / \{abs(x - x_i) + 0.65\}^{2.5} \text{ GeV.}$$

where the parameters A_i and x_i are taken either from a full least squares fit, if the peaks are only separated by one strip, or from a parametrisation.

The one−dimensional clusters are now associated with the other projection. Pairs are made starting at the boundaries of the quadrants and then inside the quadrants, when there is an ambiguity clusters of the most similar energy are paired. The program is written such that a maximum of three photons per quadrant and eight in the whole detector will be accepted.

Corrections are now applied to the photon energy.

5.4 The zero suppression correction to the data

A typical photon has a width of about one channel in the calorimeter, however the energy is derived from the sum over 15 strips. The zero suppression clips the wings of almost all photon showers reducing the measured energy recorded by the ADC's by about 3% with respect to the true energy . Moreover the zero suppression is uncorrelated between the front and the back of the LAC; it is therefore possible that no information whatsoever is available for a photon in one or more projections. A correction has been determined by taking $K_S \rightarrow 2\pi^0$ decays with and without the suppression implemented in the ADC's. Whilst this correction recovers most of the energy loss a residual non−linearity of about 1% over the whole energy scale remains.

The strip threshold is determined offline to be 80MeV on average. The spread in the pedestals contributes 35 MeV rms to this average. The measurement error of the thresholds and the intrinsic variation of the thresholds contribute a further 20 MeV rms. The average noise per channel is 16 MeV.

Showers have only 15% of the total energy of the photon in the back of the calorimeter, where they are also broader. Thus channels are in general much closer to the zero suppression threshold in

the back. This is particularly important when $E_\gamma < 20$ GeV. Zero suppression losses for the various categories of isolated photons are shown in Table 3.

Table 3: Zero suppression energy losses for $K_S \rightarrow 2\pi^0$ events

(Energy in MeV)	All photons	Back strips read out	Back X or Y not read out	Back X and Y not read out
Fraction of events	100%	76%	9%	15%
Total E_{Lost}	560 ± 220	500 ± 160	790 ± 230	670 ± 320
Front E_{Lost}	170 ± 80	170 ± 80	170 ± 80	160 ± 160
Back E_{Lost}	400 ± 200	340 ± 130	620 ± 210	520 ± 290

The energy lost decreases with increasing photon energy as shown in Figure 35. The losses induce a 10% nonlinearity in the photon energy spectrum, whilst the energy resolution deteriorates by up to 20% for $E_\gamma < 20$ GeV, thereby affecting the mass and vertex resolution adversely.

The correction for these serious losses is made to each photon projection individually. The correction uses the following shower shape:

$$f(x) = E_\gamma/2 \times (\lambda^2/\{x^2 + \lambda^2\}^{1.5})$$

$$E_\gamma(X_{low}, X_{high}) = \frac{E_\gamma}{2} \left[\frac{X_{low}}{\sqrt{(X_{low}^2 + \lambda^2)}} + \frac{X_{high}}{\sqrt{(X_{high}^2 + \lambda^2)}} \right]$$

Where : $\lambda = 1.2 - .0075E_\gamma$ (front half)

and : $\lambda = 3.2 - .011E_\gamma - .06E_{\gamma back}$ (back half)

The X_{low} and X_{high} are the positions of the shower edges.
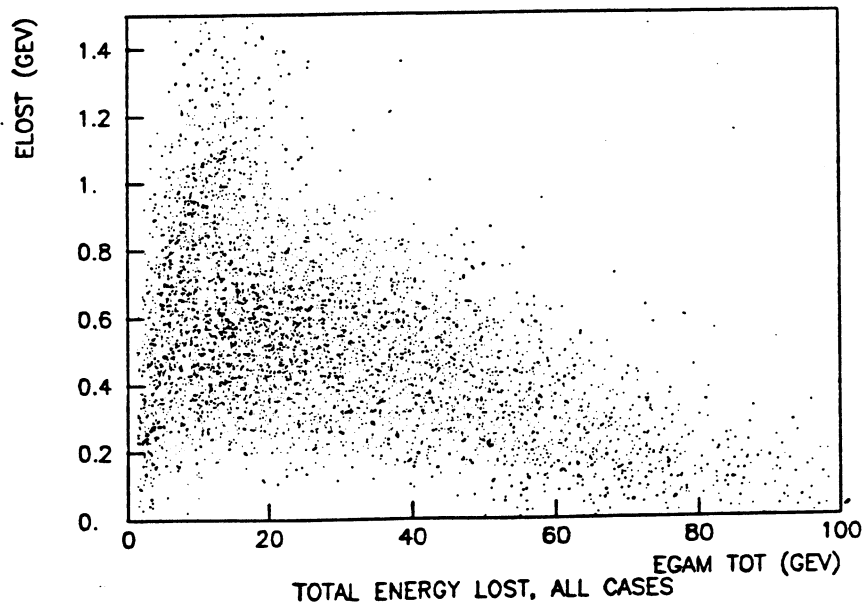
Figure 35: Energy loss as a function of γ energy due to zero suppression

When one or two projections in the back of the calorimeter are completely suppressed, the back energy is estimated both from a knowledge of the zero suppression thresholds and the observed energy in the front of the calorimeter or from the other projection in the back if it exists. For photons which strike the border between two quadrants there are separate tail corrections for the part of the shower in each quadrant. This occurs because the zero suppression is only correlated on a quadrant edge. When the energy across a border is absent, the observed corrected energy is extrapolated across the border.

By using data which had been taken without zero suppression (ZS) the effects could be simulated offline and the correction parameters optimised. In Figure 36 a comparison between the offline corrected energies and the energies, before the offline suppression was made, is shown. The effect on the π^0 mass resolution is recorded in table 4. The correction is applied to all photons before energy cuts are made.
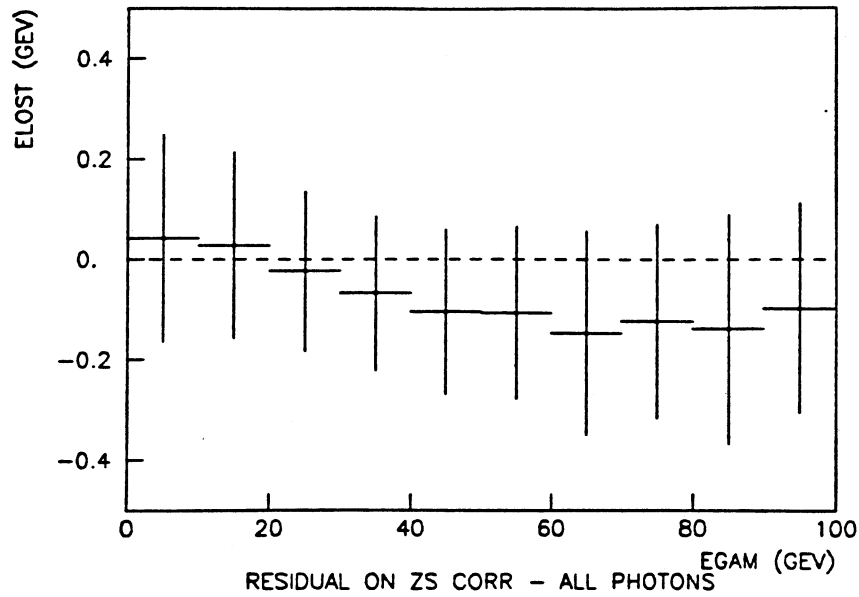
Figure 36: Residuals for offline simulated zero suppression

5.5 Correction to photon energy near the hole

For photons closer to the beam axis than 18 cm. the leakage of energy into the beamhole is corrected for. The correction was determined using an electron beam scan made around the hole in the calorimeter. The size of the correction is shown in Figure 37. Events are only accepted in this analysis which are greater than 16 cm. from the beam axis; as the correction diminishes with distance from the hole its systematic effect on the final result is neglected.

5.6 The neutral energy scale.

All corrections to the photon energy scale are now applied. One may ask how the measured energy corresponds to the true energy. To establish this, the vertex distribution of $K_S \rightarrow 2\pi^0$ decays is used to determine the position of the anti−counter on the K_S train at the front face of the collimator.

Cuts: E_γ < 5 GeV
120 MeV < m_{π^0} < 150 MeV

| | Uncorrected for ZS | | Corrected for ZS | |
	offline ZS	online ZS	offline ZS	online ZS
Total sample				
# π^0's	6444	11534	6808	12188
$RMS_{m_{\pi^0}}$	2.64	3.05	2.38	2.73
Isolated γ's	734	1226	770	1302
	2.28	2.76	1.72	2.41
No γ overlap	2226	4040	2384	4320
	2.37	2.79	1.90	2.38
Not on border	1160	2088	1250	2278
	2.45	2.89	2.19	2.56
Complete overlap	290	644	314	674
1 view	3.36	3.56	3.37	3.25

Because there are insufficient events at any one station to do this, data from several stations are merged. The anti-counter position is found to be reconstructable to within a few tens of centimetres, corresponding to an accuracy of a few per mille in the energy scale. This can be seen in Figure 38 for each of the twelve mini-periods of data. No time dependence is seen. A dependence on Z was also looked for but not found.

5.7 Event selection.

The reconstruction program looks for the decays $K^0 \rightarrow 2\pi^0, 3\pi^0$ and 2γ. If 4 (6) photons are found, the Z-position is computed from the kaon mass, and an angular correction is then applied to the re-
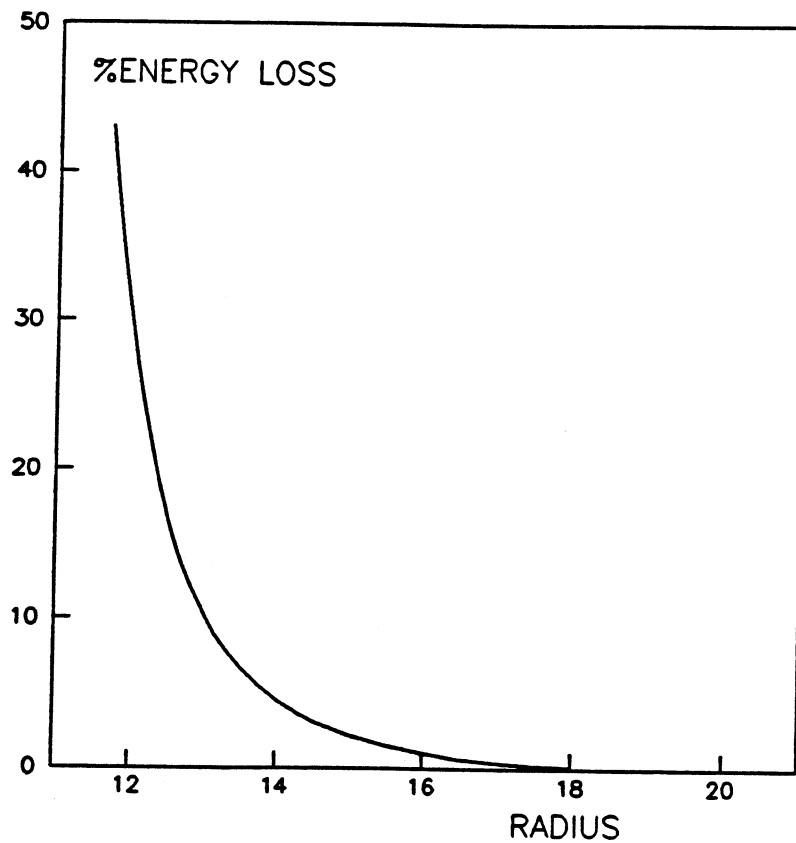
Figure 37: Energy loss correction for photons near the hole

constructed photon position, adjusting it by typically 1 mm. The best pairing of two photons into π^0's is then made by minimising a χ^2 condition :

$$\chi^2 = \{(m_{\pi^0} - m_{ij})/\sigma m_{ij}\}^2 + \{(m_{\pi^0} - m_{kl})/\sigma m_{kl}\}^2$$

Where i,j,k,l are the four photons in the event. For an event to be selected as a candidate, it must fulfill the following kinematic cuts:

- $E_K > 45$ GeV

- -10 m $< Z_{vertex} < 65$ m

- $X_{cog}^2 + Y_{cog}^2 < (15 \text{ cm})^2$

- 100 MeV $< m_{\gamma\gamma} < 170$ MeV
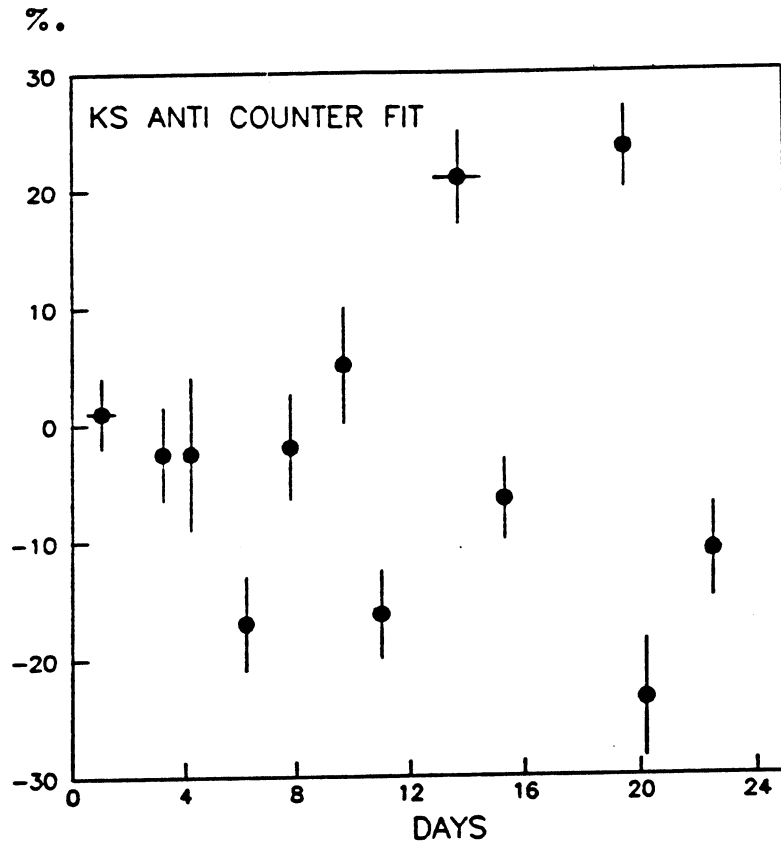
Figure 38: The reconstruction of the K_S anti − counter.

For events with only 2 photons, the vertex is calculated and the position correction is similarly applied. The two photon events must then pass all kinematic cuts except the mass cut.

In addition, for all events with an odd number of photons n, all combinations of n − 1 photons are made. If a combination is found which passes all the appropriate kinematic cuts, and the photon which is not included in this combination has an energy of less than 10 GeV, then the event is kept.

These cuts are deliberately loose and designed only to reject events which are background far from the signal. Background from $3\pi^0$ and $2\pi^0$ decays survives in quantities sufficently large to make extrapolations into the signal region.

The following events are included in the selected data sample :

- All $2\pi^0$ candidates

- All 2γ candidates

- All $3\pi^0$ events where all photons have an energy greater than 5 GeV

81

- All 7 and 8 photon events

- 4γ events which fail the mass cut but have a second acceptable X/Y cluster combination

- 6γ events failing the mass cut but having a second acceptable X/Y cluster combination and no photon with energy less than 5 GeV

- Events flagged with a reconstruction error if the total electromagnetic energy is greater than 45 GeV.

All categories except the first two are required to have no peak near the dead region in the LAC and to have less than ten peaks.

5.8 Split photons

In the K_S beam of all neutral events with more than three photons, 2.4% have five photons. This is too high to be explicable by K_L decays in the K_L beam. A distribution of the distance between showers in their X and Y projections reveals a peak at zero in 72% of these events. One of the two photons which shares a common coordinate has an energy of less than two GeV. Spurious noise and a few consistently active channels are identified as the cause of the fifth photon. The same phenomena has been observed in 3γ events. As the neutral reconstruction is designed to pair as many projections as possible, it mistakenly pairs this spurious activity with part of the energy of a genuine photon as illustrated in figure 39 . An algorithm has been prepared to correct this problem for all events with an odd number of photons. If two photons are in the same quadrant and closer than 0.5 cm in one projection and 10 cm. in the other the two photons are completely merged, if the unshared projection is more distant only the energy of the shared projection is merged. This correction is applied to the selected event sample at the DST production stage.
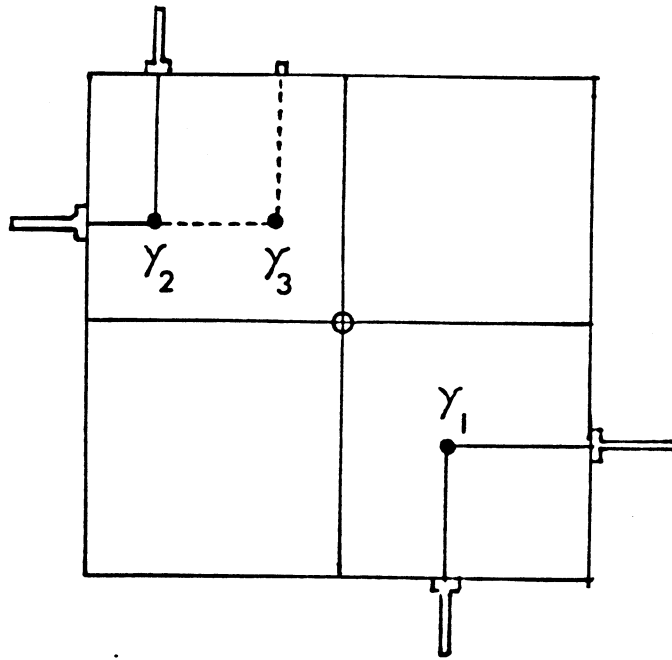
Figure 39: Origin of the extra photon

5.9 Event selection for the DST.

The selected data sample produced by KORECT occupies a considerable amount of tape, and because of the format of the data, an analysis performed on these tapes would be time consuming and the CPU time would largely be spent reading the tapes. The selected sample was therefore further compressed by a combination of slightly harder cuts, downscaling and the exclusion of all charged triggers.

All 2γ, $2\pi^0$ and $3\pi^0$ candidates in the selected event sample are required to satisfy the following cuts :

- $-10 < Z < 57$ m

- Total Energy > 48 GeV

In addition for $3\pi^0$ events :

- $E_\gamma > 6$ GeV

A downscale factor of five (that is only 1/5 of all candidates passing all cuts are kept) is applied to $3\pi^0$ events in K_L and to $2\pi^0$ events in K_S

The remaining events are written with a FORTRAN unformatted write to mass storage on the IBM. Each event record contains only the coordinates of each photon, the corresponding energy and sufficient ancillary information to trace the event back to the data tapes if necessary.

Altogether 24 data sets are created in this way, 12 for each beam corresponding to the 12 mini-periods of data. The anaylsis is performed with these data sets without further reduction. The whole data reduction chain is summarised in Figure 40
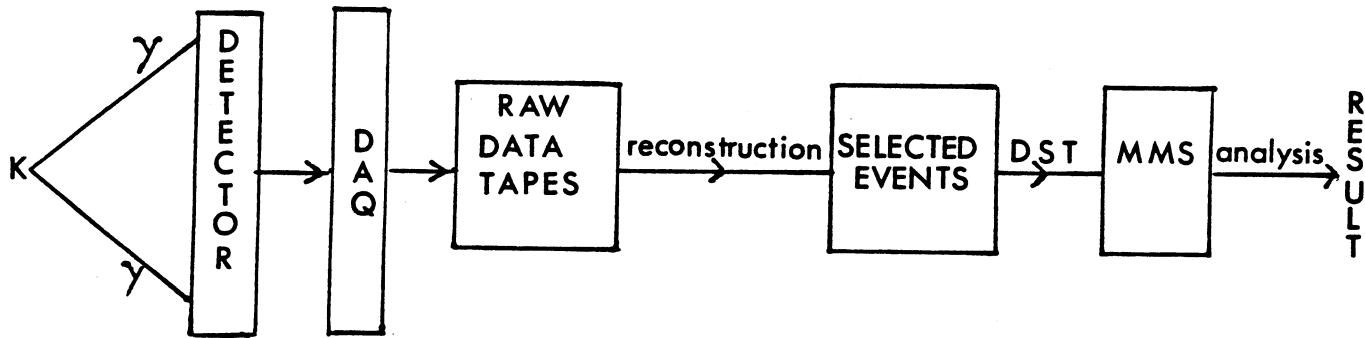
Figure 40: The data reduction chain

6. MONTE CARLO

The number of events of a given type detected in the apparatus is not the total number of that type which decayed in the fiducial volume. The geometrical acceptance of the apparatus, the efficiency of the hardware and the ability of the reconstruction program to find photons together determine the total number of detected photons and hence the total number of each event type observed. The ratio of the number of events observed to the number of events which decayed is defined to be the acceptance. In principle the acceptance is just an integral over the solid angle of the detector taking into account all relevant variables; the kaon momentum spectrum, the n−body phase space, the exponential decay distribution, the smearing of the measured quantities in the apparatus, and the efficiencies for detection and reconstruction. This integral in general cannot be evaluated explicitly. Instead a numerical integration is performed using random numbers distributed according to the variables in the integral.

The simplicity of the events in kaon physics obviates the need for the usual complicated event generator which has to deal with jets and their hadronisation. For the monte carlo program MCCP event generation is simply conservation of 4−momentum in the rest frame of the decaying particle and a Lorentz boost into the lab frame. Each particle is then tracked to the detector. The trigger is simulated by rejecting most events where a particle passes through an anti−counter. The anti−counter efficiency, which has been determined by a photon shower simulation package, is a function of photon energy and is normally greater than 95%. This efficiency does not enter into acceptance calculations, but only in the level of background produced. Whilst there is no direct way to measure the anti−counter efficiencies in the experiment, from the projection of the last anti−counter onto the plane of the calorimeter, and the photon distribution over the surface of the calorimeter it is possible to conclude that the estimated efficiency is in reasonable agreement with data.

Events where one or more particles have struck the electromagnetic calorimeter are digitised to simulate the ADC readout. The energy to be deposited is gaussianly smeared with the resolution which has been determined with an electron beam to be:

$$\sigma = \{(0.1)^2 + (7.3\% \sqrt{E})^2 + (.5\% E)^2\}^{0.5} \text{ in GeV}$$

The digitisation is based on a parametrisation determined from real $2\pi^0$ decays. This includes simulated longitudinal and lateral development of the showers, and the merging of showers which are close together. After digitisation a simulated zero − suppression is performed and the surviving channels are written to tape in exactly the same format as the data. In addition a block containing the generated vertex and energy is written to tape for each event even when the event would not have been accepted by the detector. These monte carlo tapes are then treated exactly as if they were raw data tapes. They are passed through KORECT, the statistics of event generation are made, that is the distributions of true energies and Z−vertices are recorded, and a tape is produced, containing all the normal reconstructed quantities. This, in turn is passed through the DST program and the event records are written to MSS. Finally the analysis program reads these data sets thus ensuring that for acceptance calculations exactly the same cuts are made to data and monte carlo.

The ratio of generated to accepted events is defined as the acceptance. The acceptance automatically includes the efficiency of the reconstruction program. Any software bugs remaining in KORECT should also cancel in their effect between data and monte carlo.

6.1 Monte carlo acceptance calculations.

We have calculated the acceptances for both 2γ and $2\pi^0$ decays in a K_L beam. The vertex distribution is given by the lifetime of the K_L. The spectrum is generated at the target according to a simple power law :

$$F(P) = P^{C1} \exp(-PC2)$$

Where C1 = 1.68 and C2 = 33.08. The resultant decay spectrum is in good agreement with the data for $2\pi^0$ decays measured in the K_S beam.
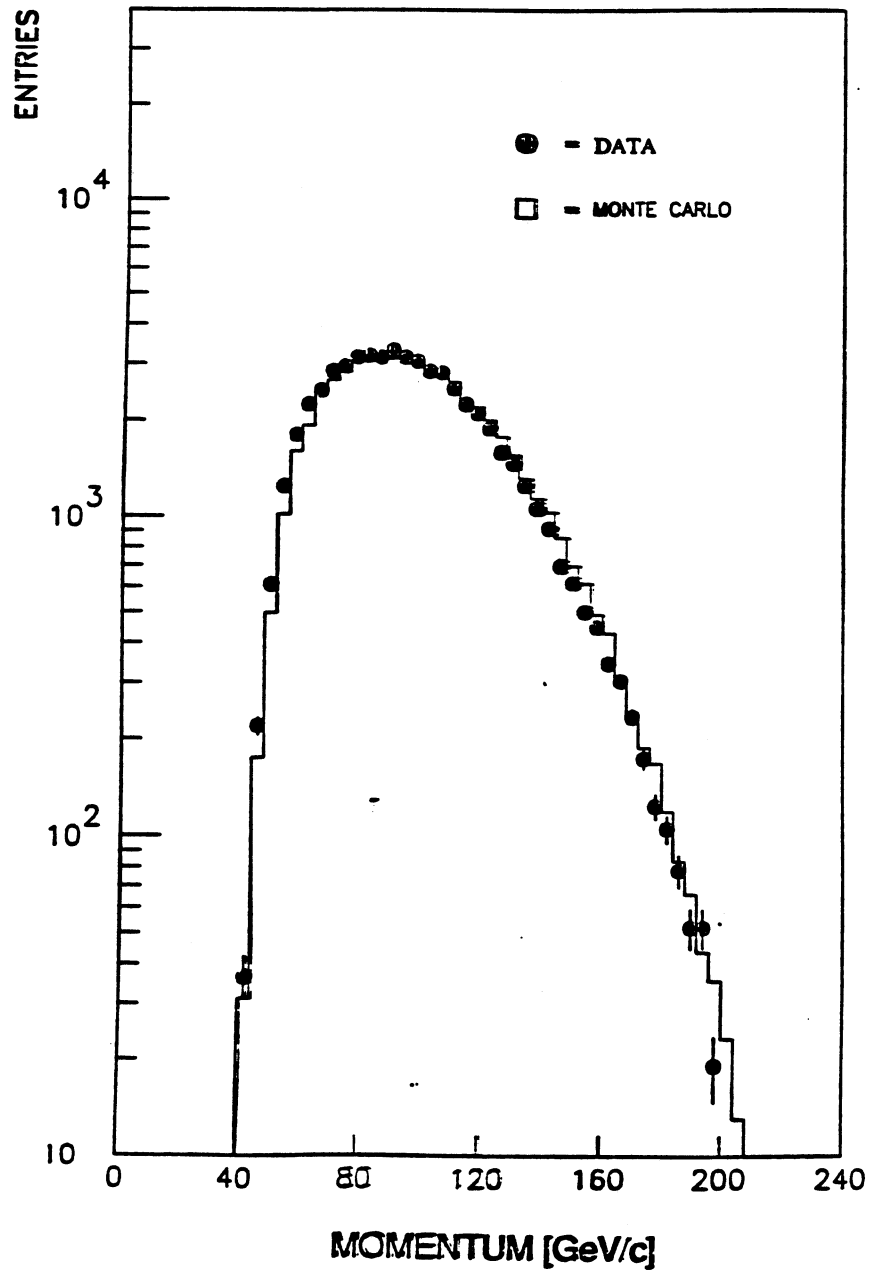
Figure 41: K_S momentum distribution.
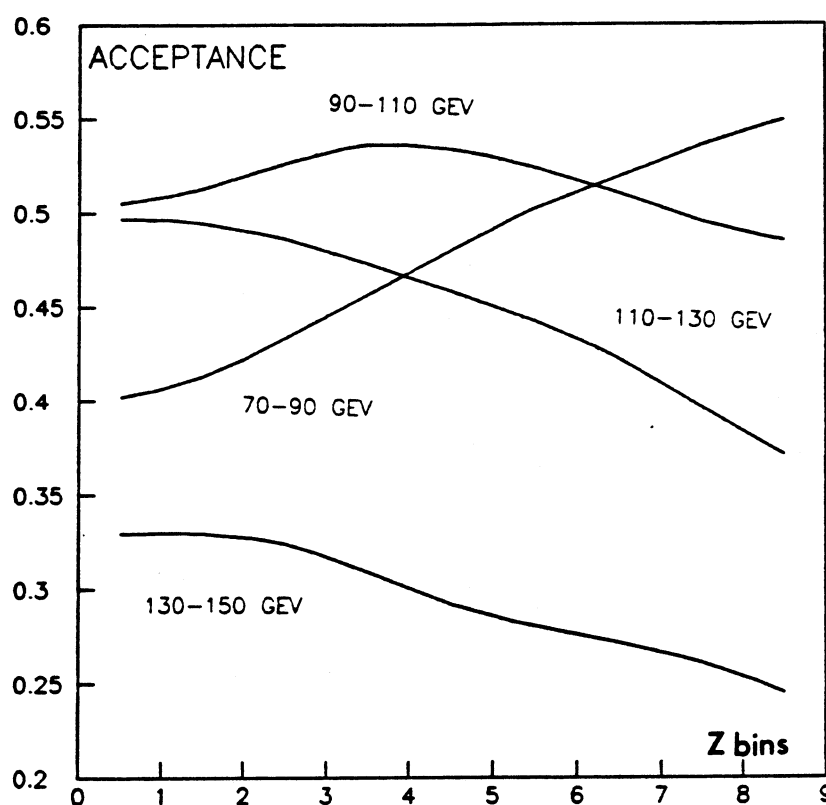
Figure 42: Acceptance for $K_L \to 2\gamma$.

From Figure 42 it is clear that our acceptance for two − body decays is excellent. Figure 43 shows the comparatively poorer acceptance for $2\pi^0$.

A comparison of data with monte carlo will be made in the analysis chapters. It is appropriate to make the following points here. There is no absolute way of knowing if a monte carlo calculates the correct acceptances; it is only possible to see how well the monte carlo describes events which are accepted compared with the real data. In addition after the data have been corrected with the acceptances one can make certain physics checks. For example, one should obtain a flat vertex distribution in K_L, because the lifetime of that particle is much longer than the decay region, $c\tau = 15.54$ m. However the possibility of a systematic effect in the acceptances cannot be easily dismissed.
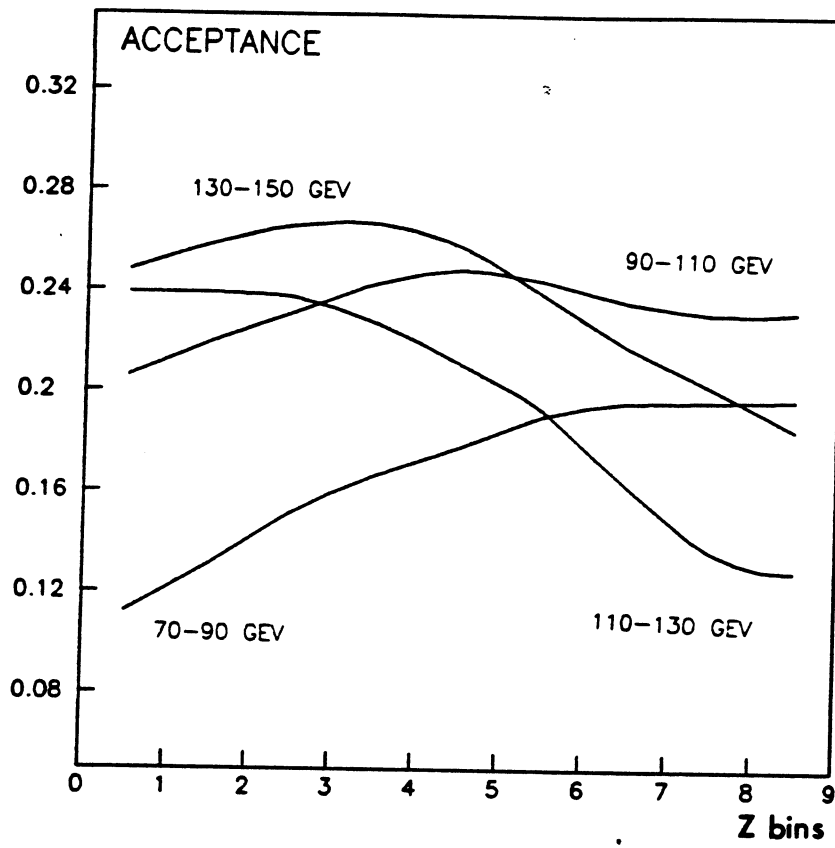
Figure 43: Acceptance for $K_L \to 2\pi^0$.

7. THE MEASUREMENT OF $\Gamma(K_L \rightarrow 2\gamma)/\Gamma(K_L \rightarrow 2\pi^0)$

The apparatus and trigger for the experiment allow both $2\pi^0$ and 2γ events to be accepted simultaneously. However an online microprocessor is used to reject the large number of events where greater than four photons are found. Because the signal and normalisation events are recorded simultaneously in the same neutral beam any hardware rate dependent effects largely cancel in the ratio. The detector acceptances are quite different for the two decays and have to be calculated with a monte carlo simulation of the experiment. The branching ratio is then simply given by :

$$B = \Gamma(K_L \rightarrow \gamma\gamma)/\Gamma(K_L \rightarrow \text{all}) = \frac{N_{2\gamma} \times \varepsilon_{2\pi^0} \cdot B(2\pi^0)}{N_{2\pi^0} \times \varepsilon_{2\gamma}} \quad (1)$$

Where $N_{2\gamma}$ denotes the number of $K_L \rightarrow 2\gamma$ events observed, $N_{2\pi^0}$ denotes the number of $K_L \rightarrow 2\pi^0$ events observed, $\varepsilon_{2\gamma}$ and $\varepsilon_{2\pi^0}$ are the monte carlo acceptances for the signal and normalisation and $B(2\pi^0)$ is the branching ratio for $K_L \rightarrow 2\pi^0$ determined from previous experiments.

7.1 The cuts

The cuts applied to the reconstructed events in order to produce the DST's have been very loose. Additional cuts are required, in order to reject the remaining backgrounds. We now discuss these cuts in turn, comparing data distributions which have passed·all the cuts with monte carlo. Throughout we adopt the philosophy that we have collected the largest data sample of 2γ events in the world and can afford to make cuts which, whilst rejecting good events, optimise the signal to background ratio. We are most concerned here with controlling the systematic errors.

7.1.1 The centre of gravity cut.

Figure 44 and Figure 45 shows the plots of the first moment versus Z for 2γ and 4γ events respectively, where Z is obtained from the kaon mass constraint. The beam penumbra is clearly seen at 6 cm. We allow a margin for error and cut at 7 cm. The region with centre of gravity (COG) greater than 7 cm. can be used for estimation of the background. The background is clearly seen to fall with Z, as predicted in chapter four.

7.1.2 The vertex cut.

We choose to work only in the Z region where the acceptance is nearly flat. From studies of $K_L \to \pi^+\pi^-$ there is evidence that there are kaons with a high p_T close to the K_L collimator and presumably incoherently regenerated K_S produced by interaction of the beam with it. There is no way of measuring p_T in $K_L \to \pi^0\pi^0$, except by the Dalitz decays of which too few are available. Therefore the region close to the collimator is not used. It is also convenient to work in a region defined by train positions, because for the measurement of R these are the natural units, and the same region size can be used for both measurements. The fiducial volume is defined to start at the collimator position of station 5, and end at station 41 of the XTGV. That is about 80% of the total decay volume is used; 5 < Z < 48 m. where Z is measured from the K_L collimator.

7.1.3 The total energy cut.

The energies used are 70 − 150 Gev because the acceptance is nearly flat in this range. In addition K_S produced in the target give a non negligible flux of $K_S \to 2\pi^0$ decays above 150 GeV and these would have to be subtracted. In fact at 200 GeV we are in the interference region, that is the number of K_L and K_S decays to two pions is equal. In Figure 46 and 47 the kaon energy for accepted events is compared for 2γ and $2\pi^0$ with monte carlo.
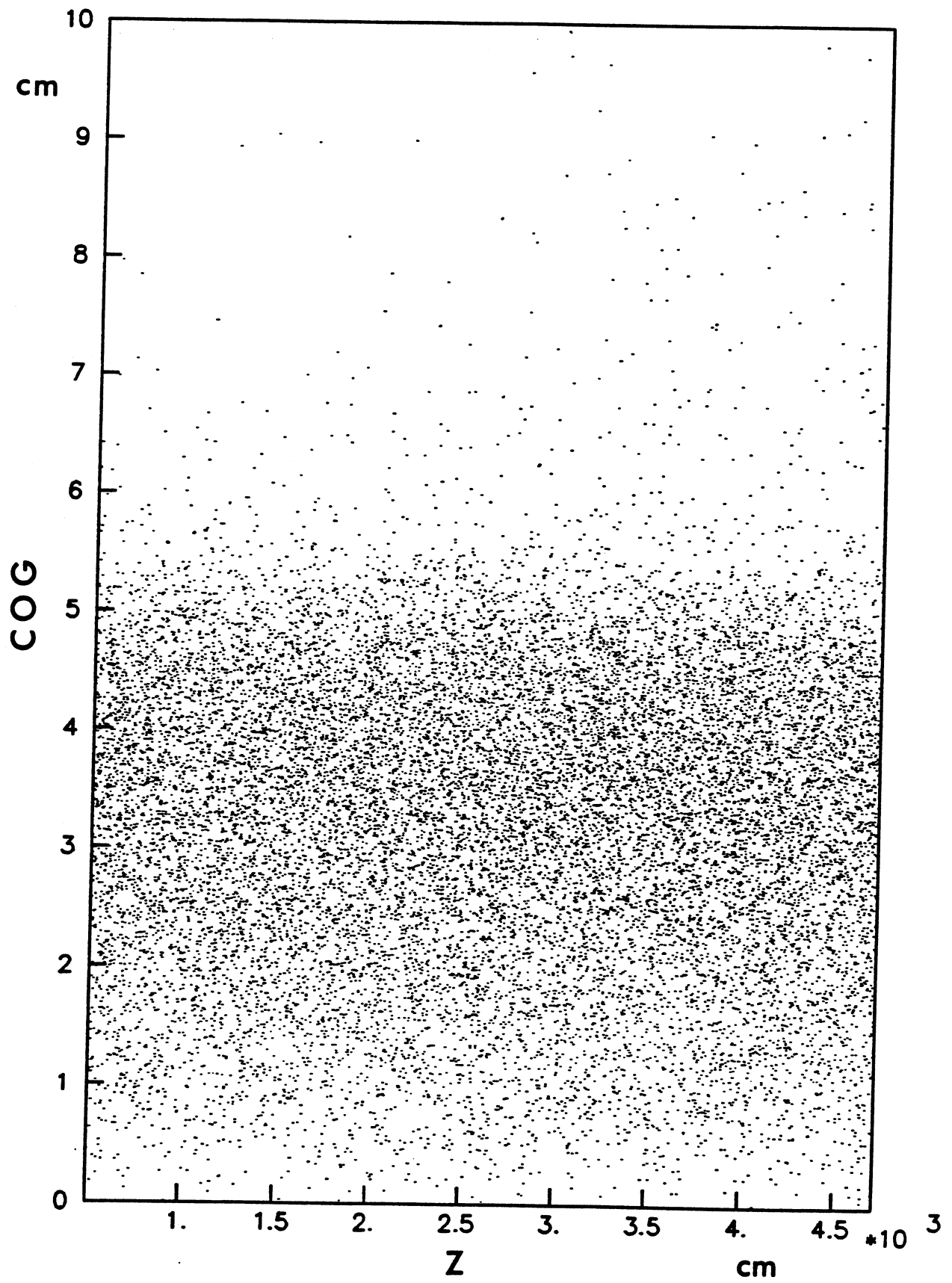
Figure 44: First moment versus Z for $K_L \to 2\gamma$.
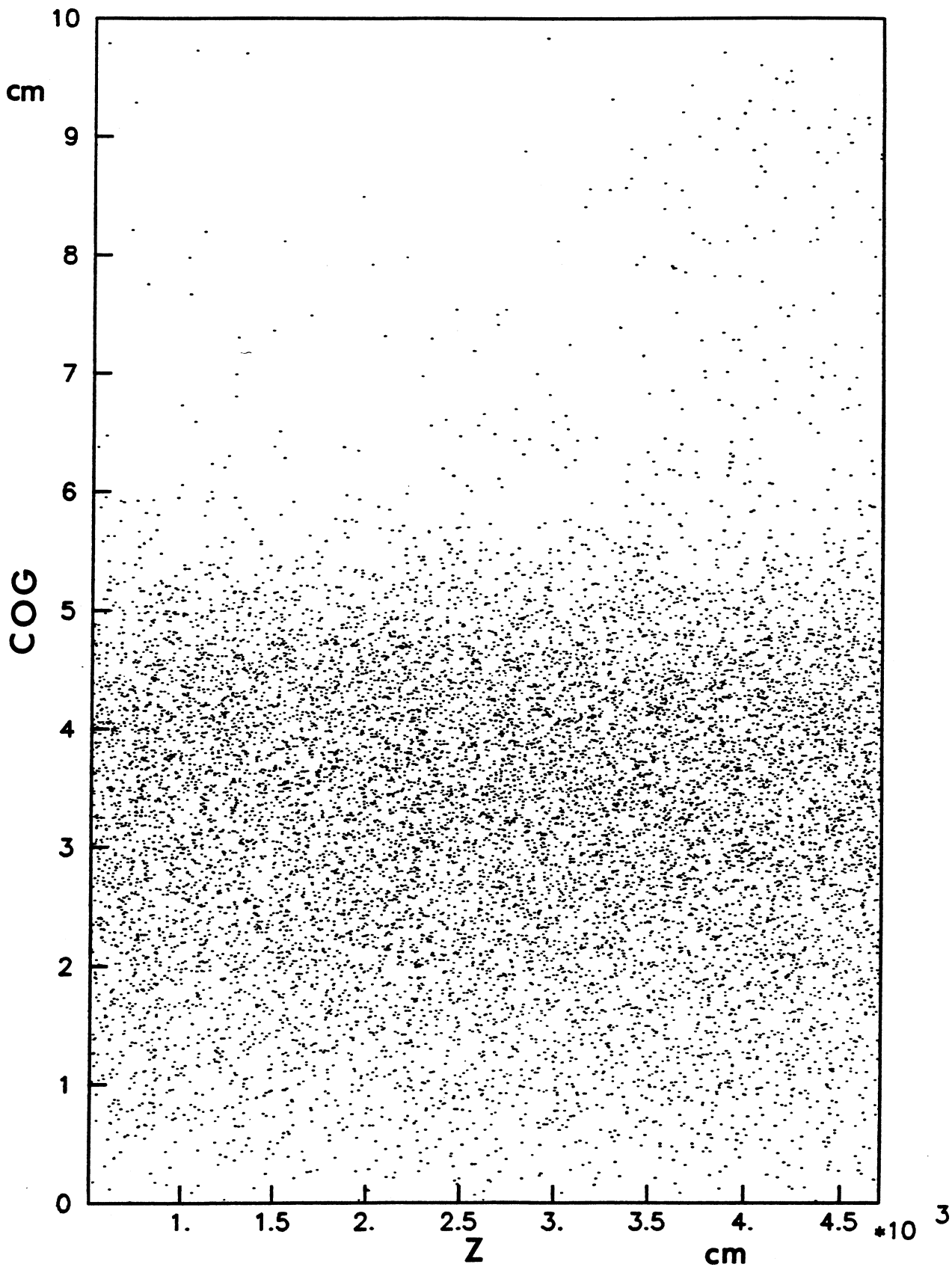
Figure 45: First moment versus Z for $K_L \to 2\pi^0$.

93

As there are always undetected photons in events which constitute the background, these events are, on average, softer than the signal. By demanding greater than 70 GeV for an event the signal to background ratio is improved.

7.1.4 The minimum photon energy cut.

This is not a critical cut for 2γ. Geometrically, there is almost no acceptance for $\gamma\gamma$ events with an energy ratio above four, therefore at 70 GeV γ's below 15 GeV are rare. The cut is at 10 GeV. However the $2\pi^0$ background can have $\gamma\gamma$ pairs of energy ratios over a wider range so the cut has an effect in reducing the background.

For $2\pi^0$ decays the requirement that each photon has greater than 5 GeV is very severe. The mass resolution is dominated by the energy of the lowest photon in an event. With this cut the background from $3\pi^0$ is more easily distinguished. In Figure 48 and 49 the minimum energy photon of each event is plotted for 2γ and $2\pi^0$ for monte carlo and data.

7.1.5 The maximum photon energy cut.

The ADC channels are designed not to saturate for $2\pi^0$ decays which, for a kaon energy of 200 GeV have a mean photon energy of around 50 GeV. The 2γ decays have a very different γ energy spectrum. There is evidence that the ADC'S saturate above 100 GeV as shown in Figure 50 , where the maximum ADC channel for a shower is plotted against the total energy. As there are four projections this quantity should be approximately equal to one quarter of the total energy; therefore the cut is at 100 GeV.

More importantly, the calorimeter is not calibrated for single particles above 80 GeV which corresponds to the highest energy electron beam data taken. It is therefore possible to introduce systematic uncertainties by using γ energies beyond the calibrated energy range.
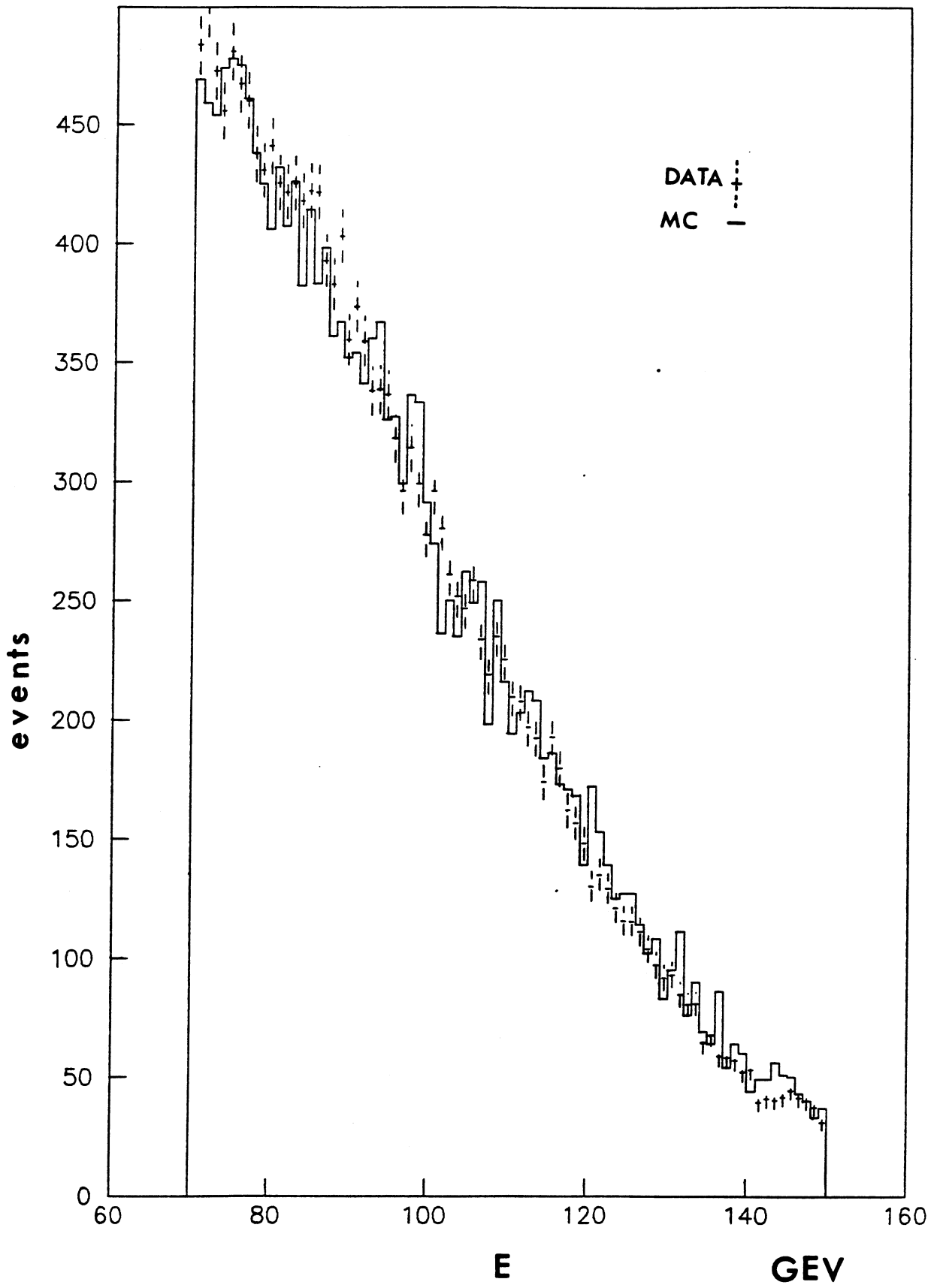
Figure 46: Total energy for 2γ events in data and monte carlo.

95
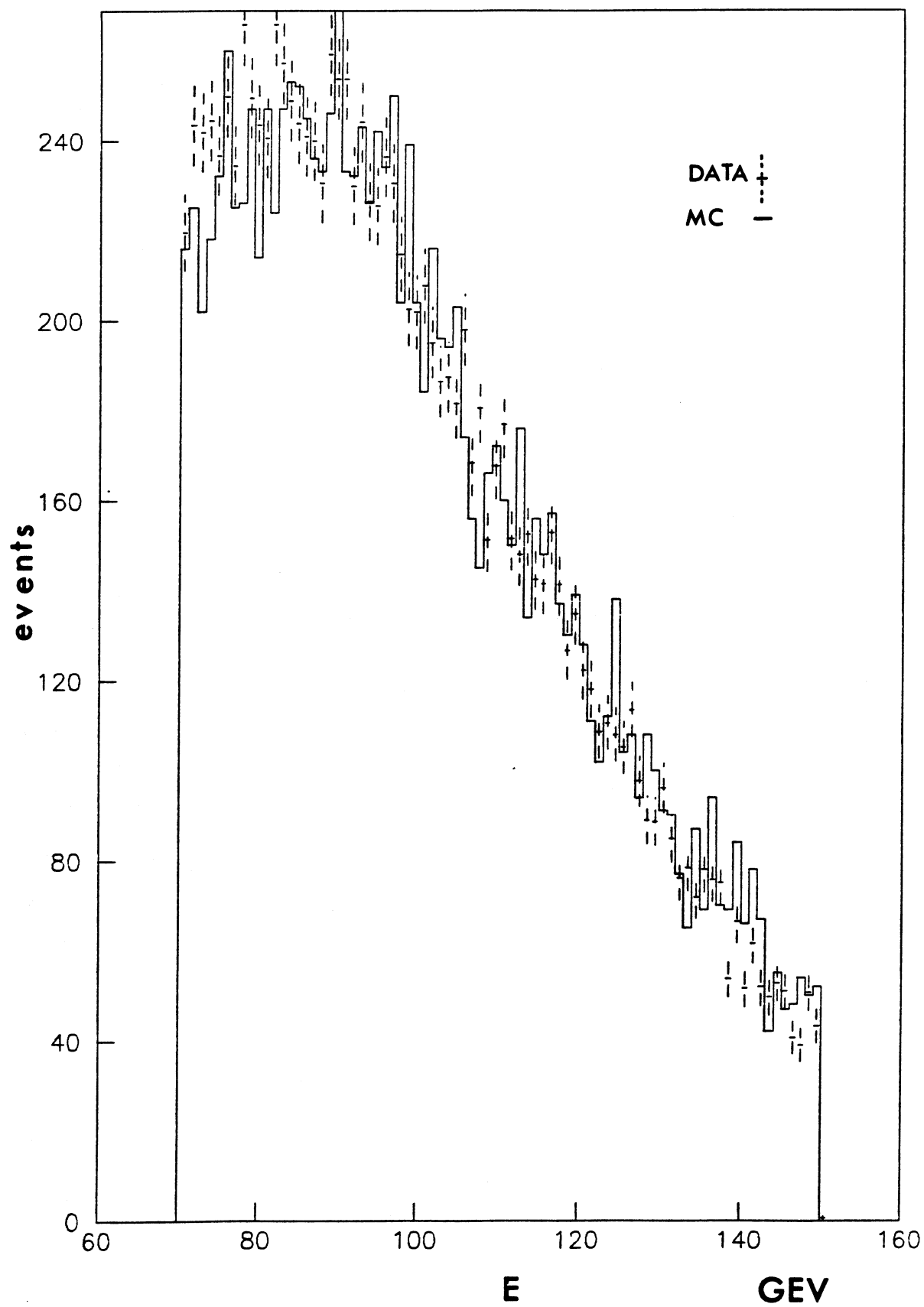
Figure 47: Total energy for $2\pi^0$ events in data and monte carlo.
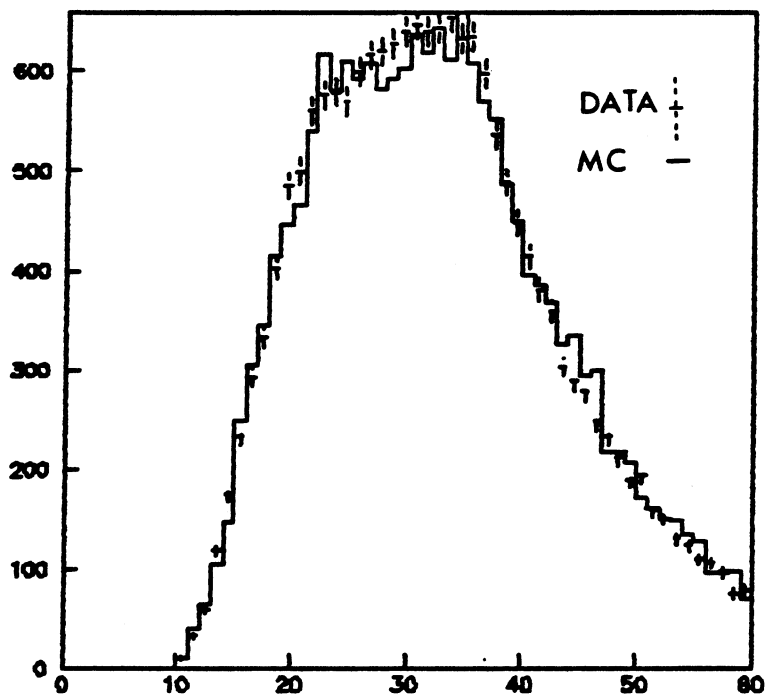
Figure 48: Lowest energy γ for 2γ events in data and monte carlo.
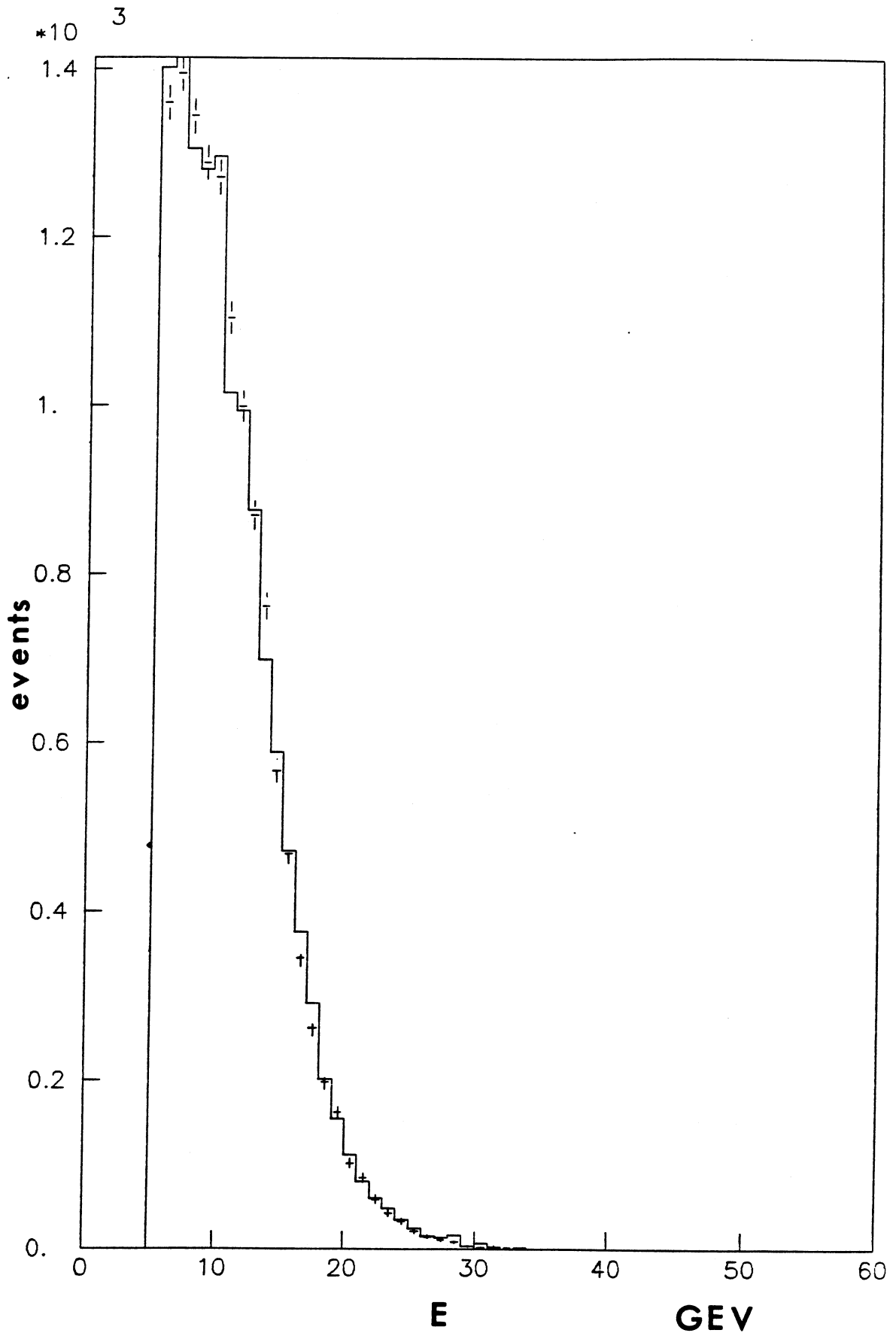
Figure 49: Lowest energy γ for 2π⁰ events in data and monte carlo.
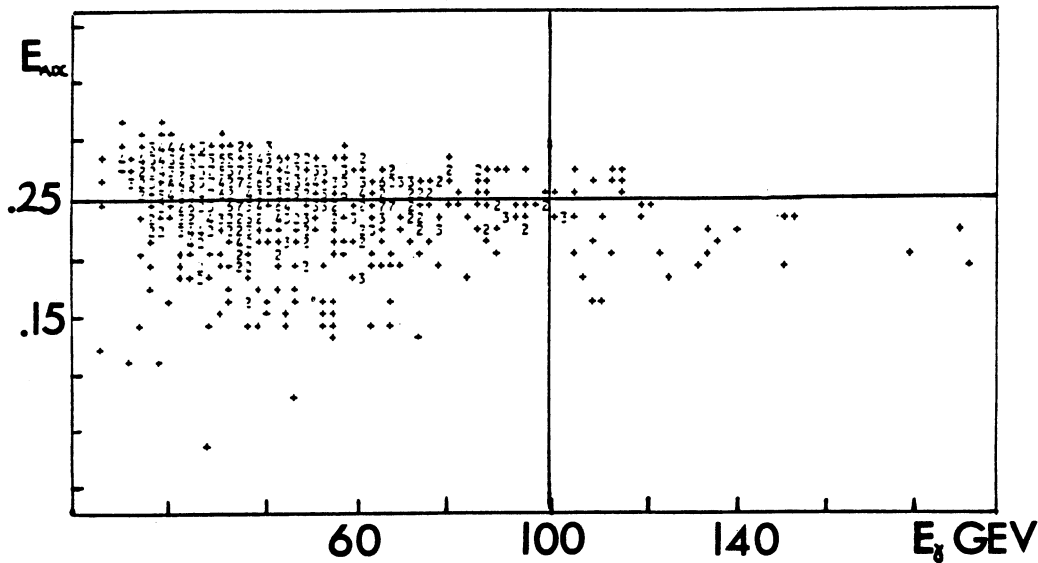
Figure 50: ADC saturation.

At higher photon energies the additional complication of leakage is also of considerable importance. The leakage is known to rise logarithmically with increasing photon energy, but it has not been well−measured. The data and monte carlo for the maximum energy photon in 2γ and $2\pi^0$ events is shown in Figure 51 and Figure 52

7.1.6 The radial cut.

The radial region is chosen such that from any decay vertex in the decay volume, a photon can travel in a straight line without traversing more than the minimum amount of material presented by the vacuum and helium tanks, windows and chamber foils etc., to the detector thereby ensuring that the photon energy is well measured. Though for two body decays the radial distribution is well−centred in the active area of the detector, for $2\pi^0$ about 10% of the data is lost with this requirement. Figure 53 shows the constraints which determine the choice : $16 < r < 118$ cm.

The calorimeter is constructed in two halves which are joined at $X = 0$. At the join the photon energy is not well measured. All events which have a photon in the region $|X| < 0.5$ cm. are rejected in the analysis. In Figure 54 and 55 the radial distributions are shown for the photon closest to the beam−pipe and furthest from it for $2\pi^0$ and 2γ events.
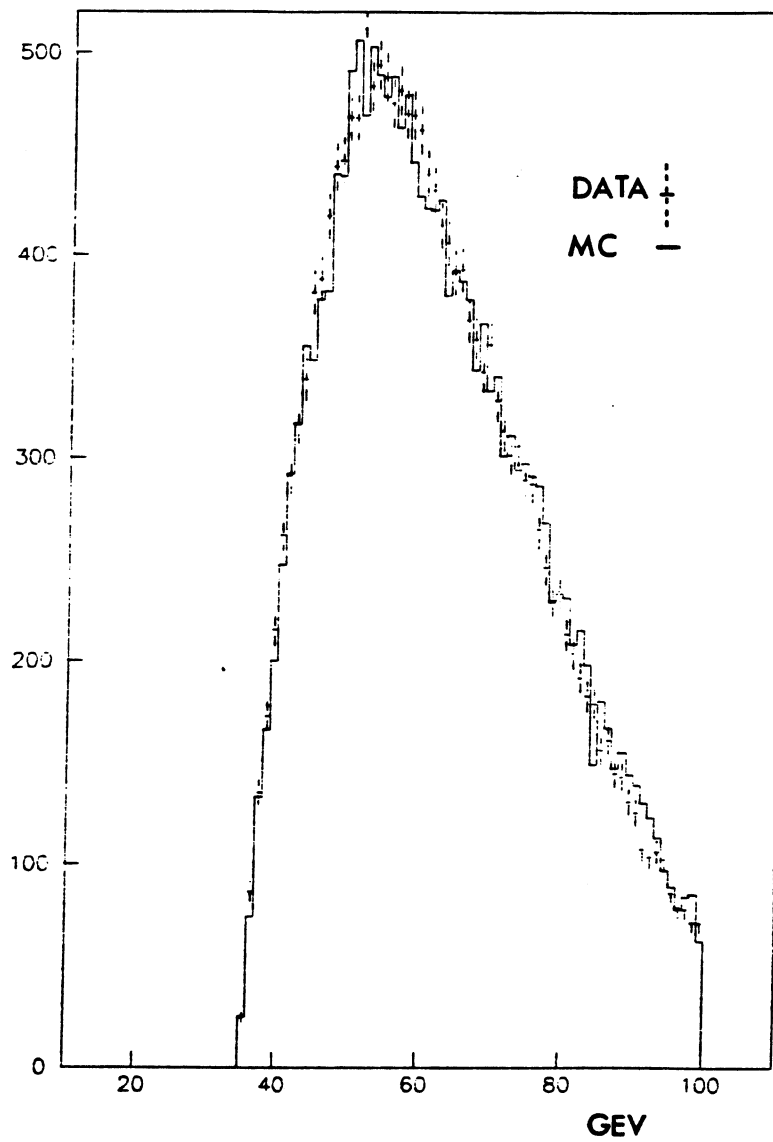
Figure 51: Maximum energy γ *for* 2γ *in data and monte carlo.*
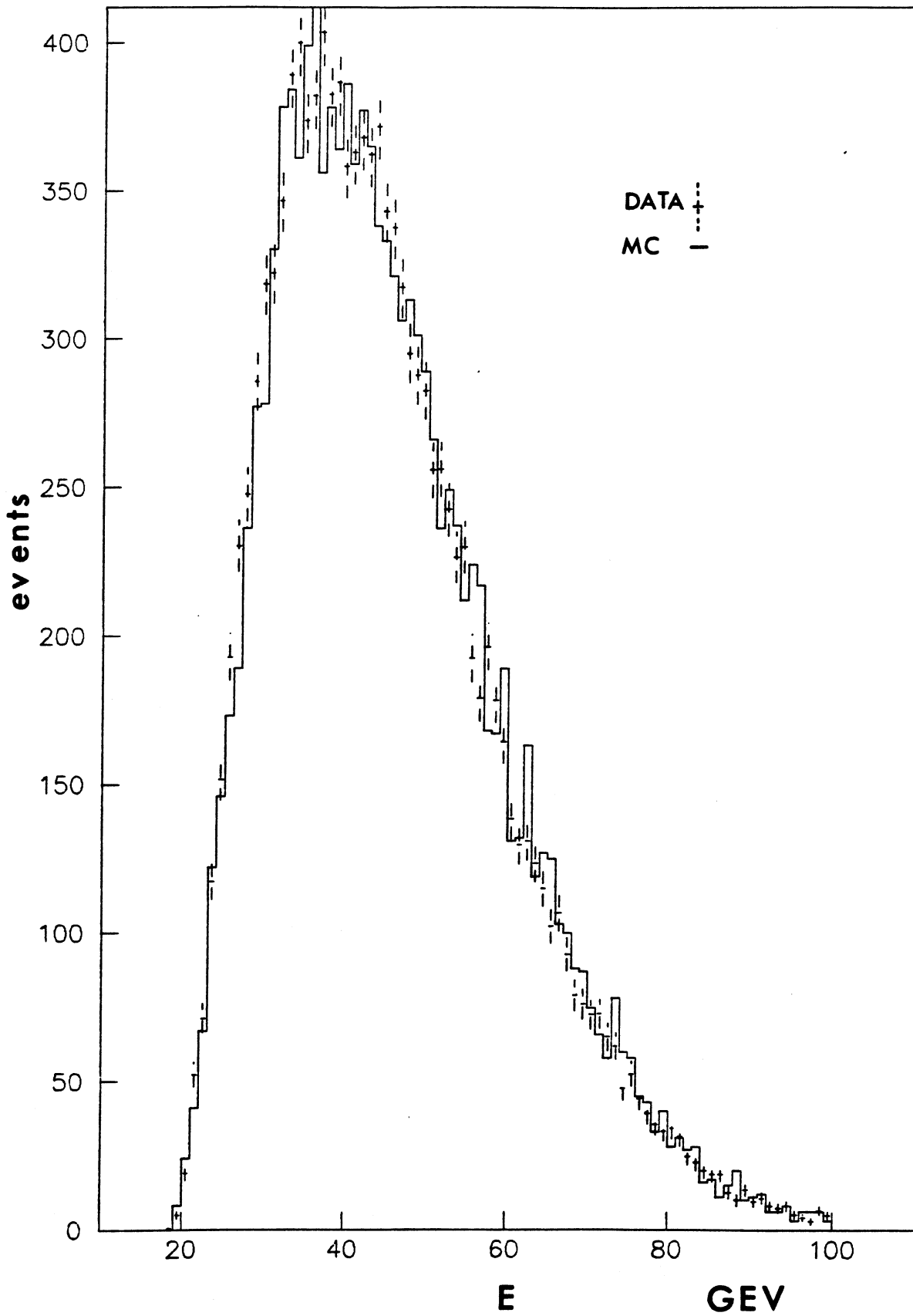
Figure 52: **Maximum energy γ for 2π⁰ events in data and monte carlo.**

101

WCI   LAC

flange

Figure 53:   Definition of the detector active area for this analysis.

7.1.7 Fiducial detector cuts corresponding to the trigger for 2γ events.

The peak−finder is used in the trigger in two ways. In order to veto single track events, two peaks in the vertical view are required at the fast trigger level. As there are several dead areas in the calorimeter, which could not detect gammas, the peak−finder channels corresponding to these areas are not considered in the trigger. If a γ from a 2γ event hits one of the dead regions the event is therefore rejected by the trigger. In addition, there is a group of dead peak−finder channels which correspond to a live area in the calorimeter, identified by looking at a special run with the peak−finder removed from the trigger.

To deal with these areas of the detector which were either inefficient or completely dead because of   defects, we reject any event with a photon in these regions. For the acceptance calculation, these same regions are excluded. Further, in order to resolve peaks, the peak−finder requires that there is a channel between two peaks which has significantly less energy than either of the peaks themselves. Therefore events which have a decay plane which is close to parallel with the X−axis, will not be resolvable by the peak−finder. As the beam size at the detector is six centimetres, there should be a substantial number of these events in the region : $|X| < 6$ cm. By requiring that ΔX is
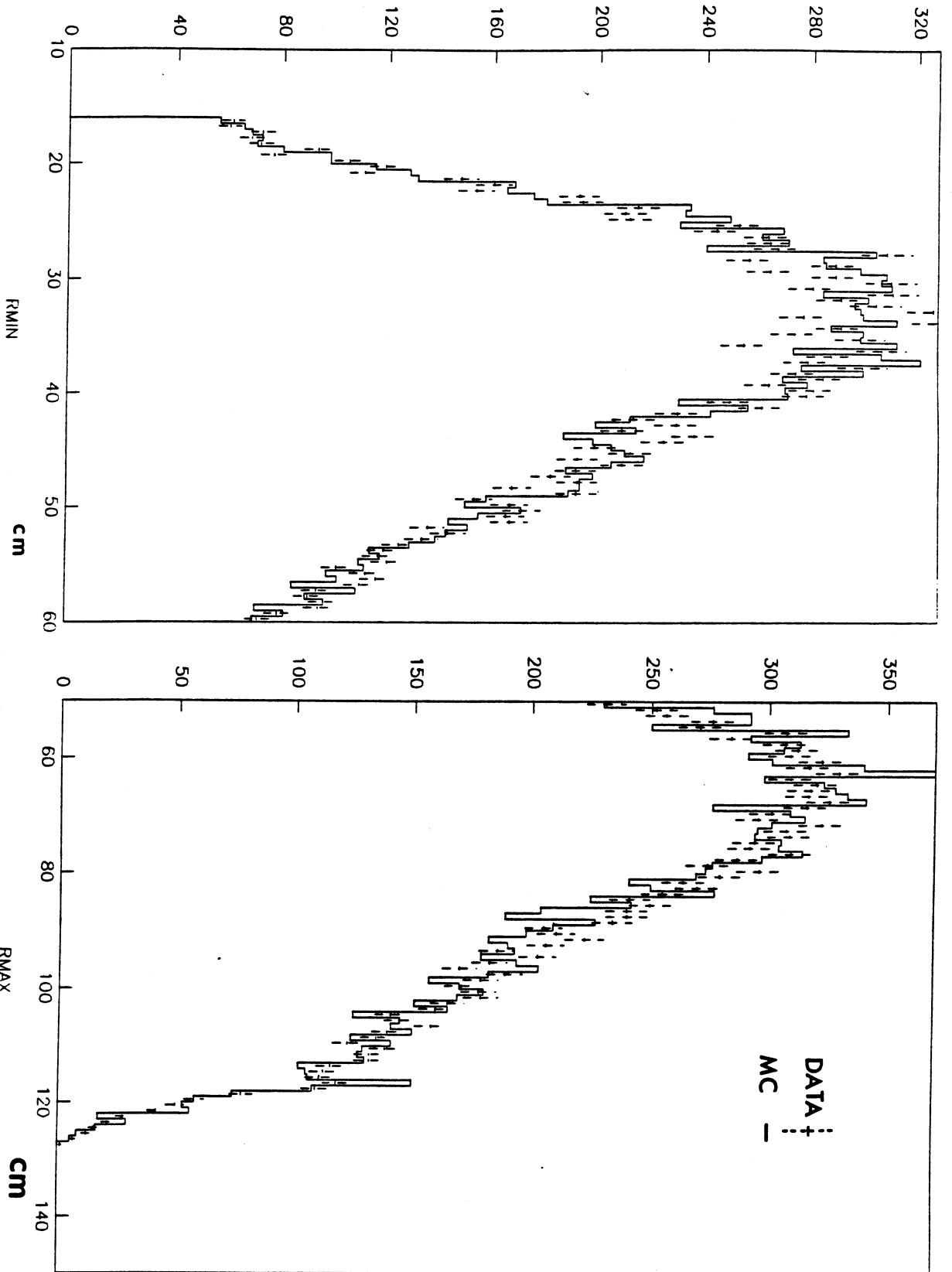
Figure 54: Radial distributions for 2γ events in data and monte carlo.
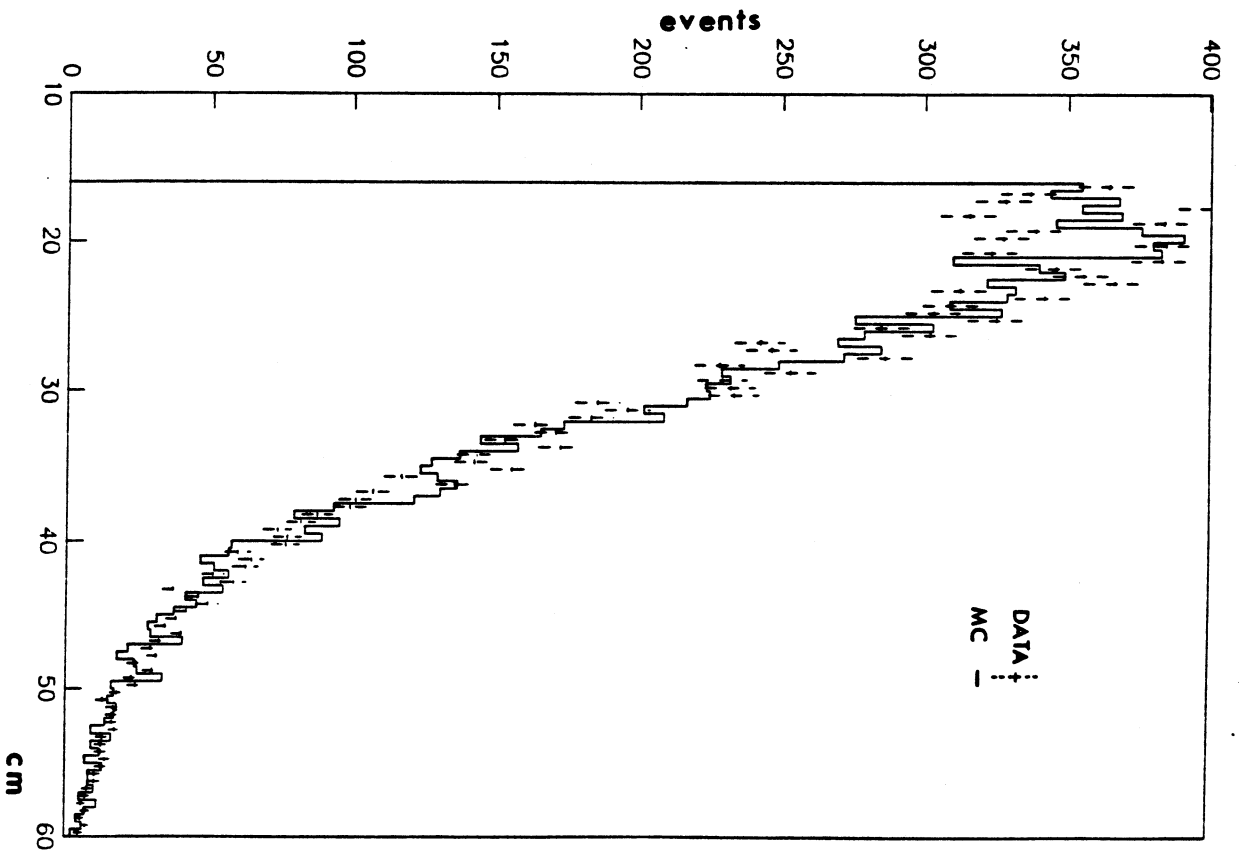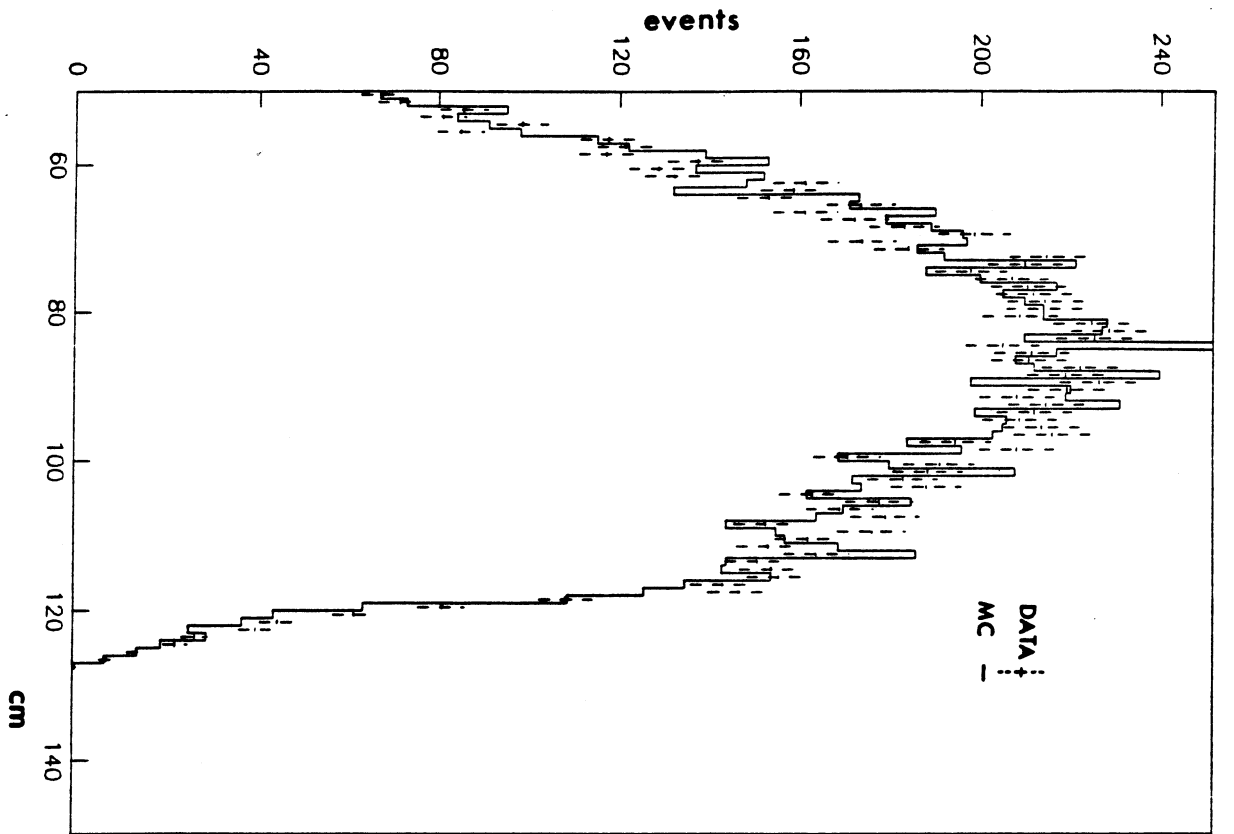
Figure 55: Radial distributions for 2π events in data and monte carlo.

greater than 2.5 cm. in the calorimeter for each event, full efficiency of the peakfinder is ensured. In the monte carlo the same criterion is applied. The amount of data lost by these cuts both for K_L and K_S is shown in Table 5 .

Table 5: Data losses due to dead areas in the calorimeter.

K_L	$2\pi^0$	2γ
Total events	102614	49303
Fiducial Detector Cuts	0	7.3%
Central strip	3.3%	1.4%
Events remaining	99258	45958

K_S	$2\pi^0$	2γ
Total events	45130	2746
Fiducial Detector cuts	0	8.8%
Central strip	3.6%	1.2%
Events remaining	43500	2504

In Figure 56 the azimuthal distribution of 2γ events which pass all cuts is shown, the dashed line is the monte carlo prediction if no account is made of the various trigger and detector inefficiencies. The solid line shows how well the monte carlo distribution simulates the data after all inefficient regions are taken into account.

The effects of the peakfinder also have to be considered for $2\pi^0$ decays. If there are more than four photons, that is eight energy clusters in two projections, the 168/E processor rejects the event. This condition was only implemented in the filter algorithm after thorough testing had demonstrated that less than one per mille of all $K_S \rightarrow 2\pi^0$ events were rejected by it. A similar loss is expected for K_L
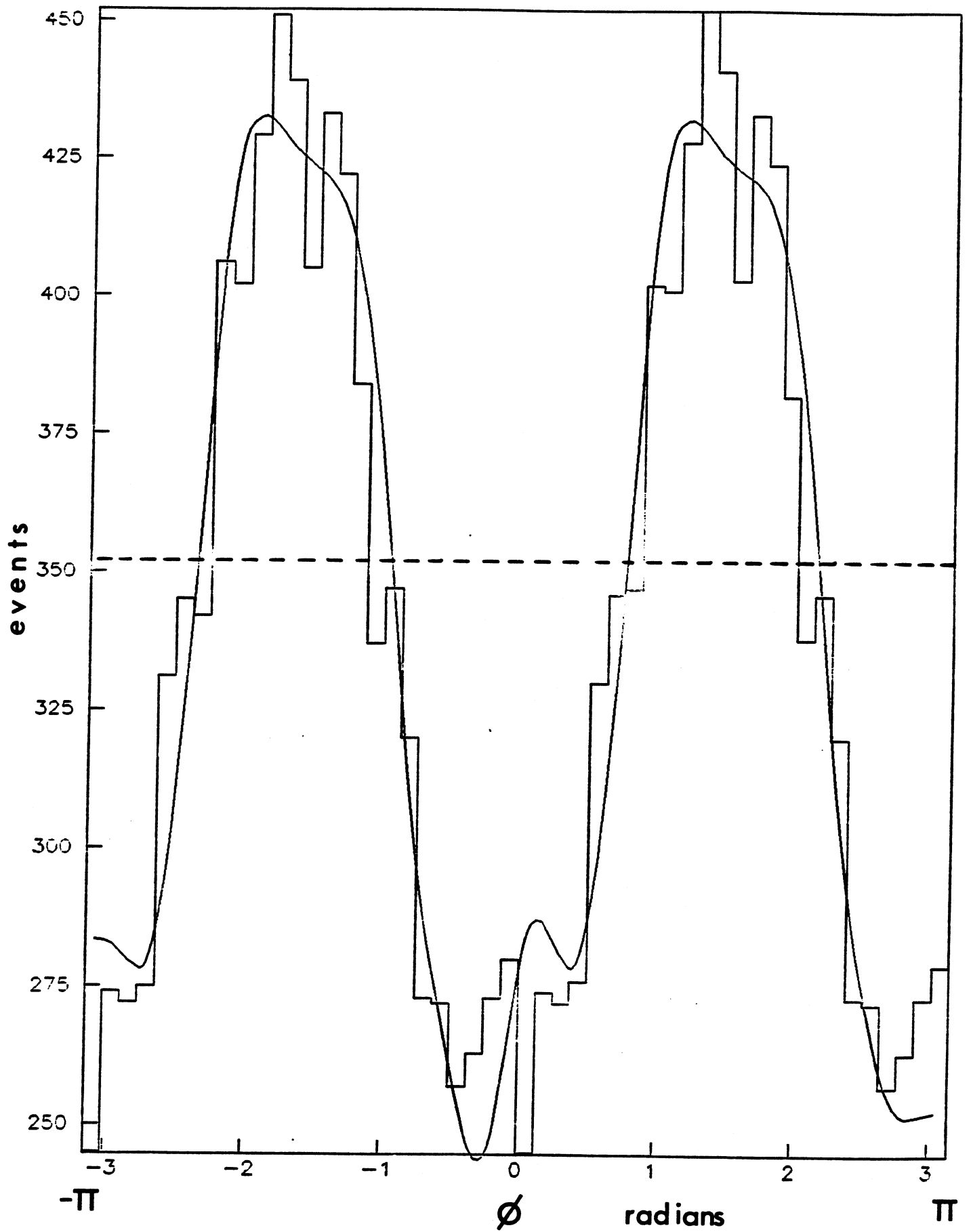
Figure 56: The angular distribution of 2γ events.

7.1.8 The mass cut.

The mass distribution for the two pairs of photons in a 4γ event which give the best χ^2 in a fit to the m_{π^0} are shown in Figure 57 and 58 for K_L and K_S respectively. A $3\pi^0$ background is clearly visible in the K_L plot. The calorimeter resolution dictates the mass resolution and determines the cut. In the $m_{\pi^0} - m_{\pi^0}$ space the masses are correlated along the line :

$$m_1 + m_2 = 2m_{\pi^0}$$

For ease of background subtraction we introduce the mass variable μ :

$$\mu = \{ (m_1 + m_2 - 2m_{\pi^0})/ 4 \text{ MeV} \}^2 + \{ (m_1 - m_2)/ 12 \text{ MeV} \}^2$$

The cut is at $\mu < 1$ which defines an ellipse of area μ with major axis along the line $m_1 + m_2 = 2m_{\pi^0}$ centred at m_{π^0}, and minor axis $m_1 - m_2$ centred at 0. The ellipse corresponds to a cut in the mass peak at $\pm 2.5\sigma$.

7.1.9 Shower separation cut

The resolution of the photon reconstruction algorithm has been measured by overlaying by software combinations of events where the photon separations are known. The reconstruction is found to be fully efficient for photons separated by greater than four centimetres. The radial separation of all showers is required to be greater than five centimetres. As it is kinematically unlikely for any showers to be closer than this, the loss of good events by this cut is negligible. The cut has no effect whatsoever on 2γ events.

7.1.10 Contamination of the data by non $- K^0$ decays

In this section the possibility is considered that some of the events in our data sample are not kaon decays. In particular there is a possible background in 2γ from events where a neutron is detected in coincidence with a single photon.

Figure 57: The m_{π^0} peak in K_L

$K^0_L \to \pi^- \pi^0$

M(PI0) vS M(PI0)

GEV

GEV

108
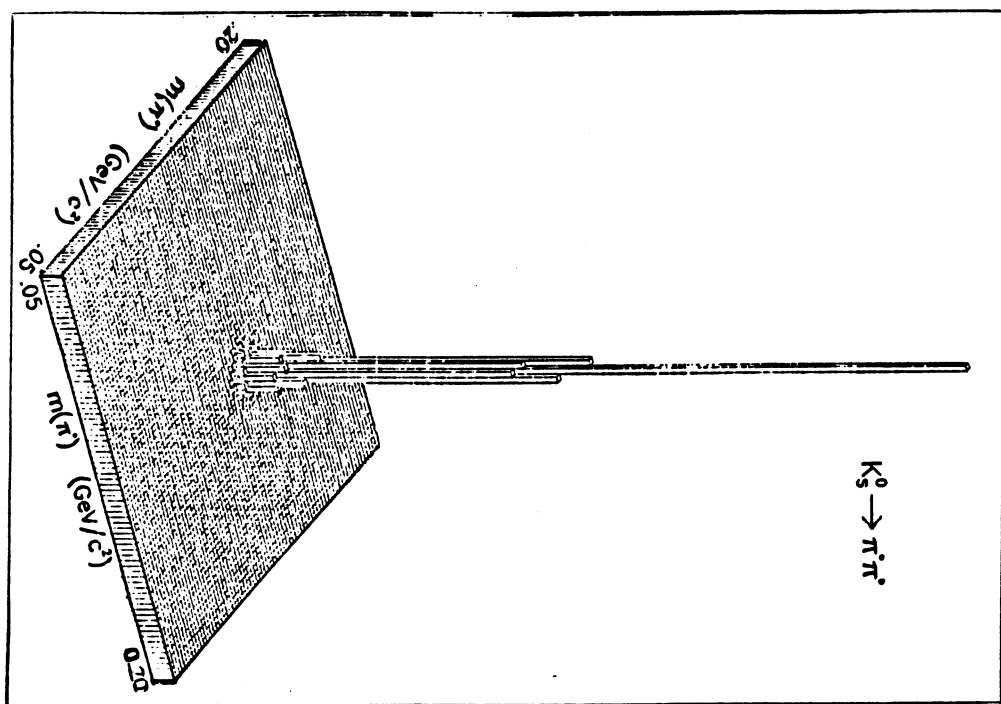
Figure 58: The m_{π^0} distribution in K_S
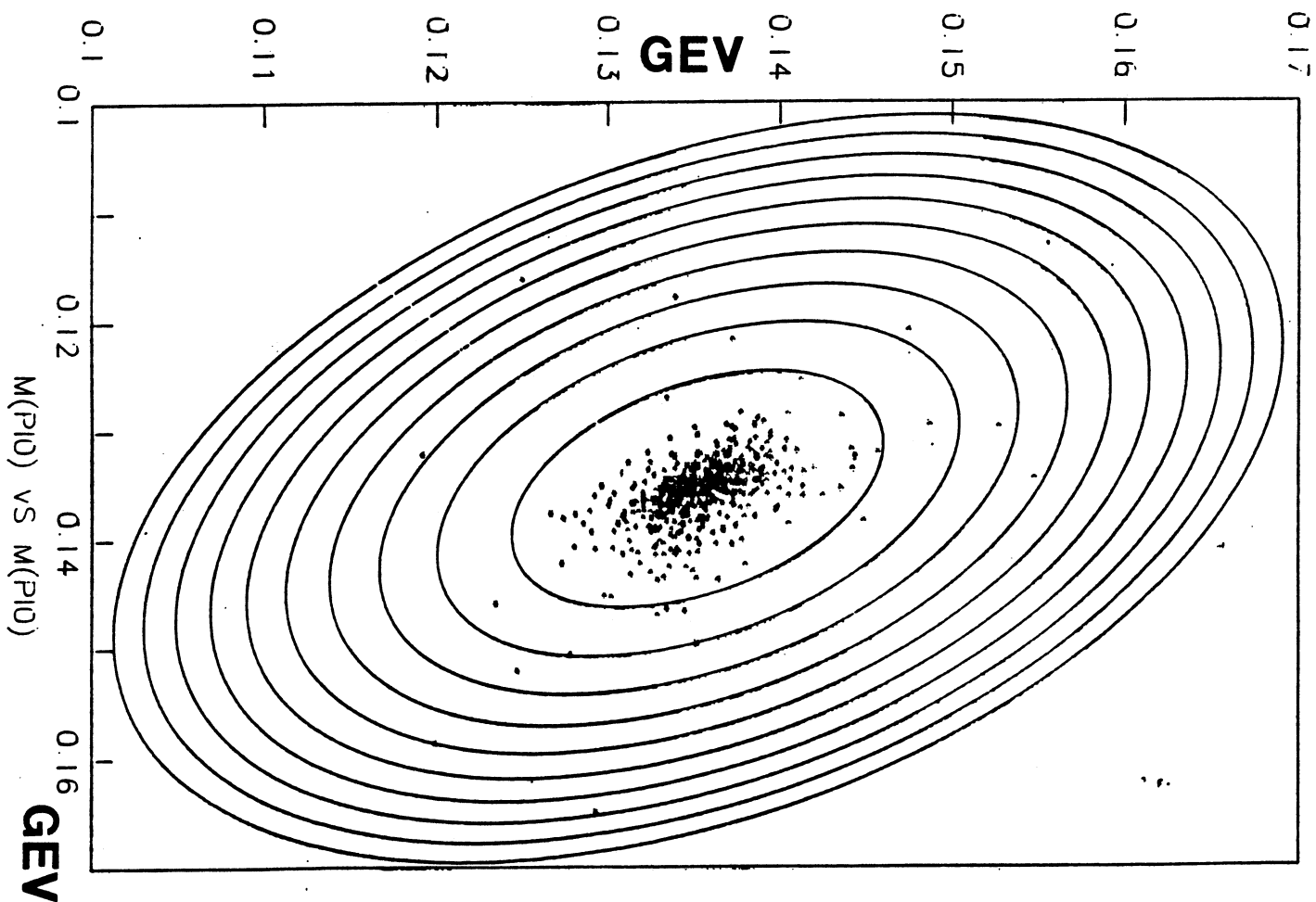
A hadron can be differentiated from a photon by the presence of hadronic energy, the longitudinal shower development in the calorimetry and the shower width. If the hadron is charged there will also be a correspondence between a track in the chambers and energy in the detector.

Using the ADC contents, the width of a shower has been calculated for a subsample of the data. The width is defined as :

$$X_n = \Sigma_{i=1,N} E_i \, x_i^n \quad \text{and} \quad Y_n = \Sigma_{i=1,N} E_i \, y_i^n$$

$$<X>^2 = X_2/X = -(X_1/X_0)^2$$

$$<Y>^2 = Y_2/Y_0 - (Y_1/Y_0)^2$$

$$\text{Width} = \sqrt{(<X>^2 + <Y>^2)}$$

where the sum is over four channels either side of the peak channel in the front half of the calorimeter. In Figure 59 and 60 the width distribution for γ's from $K_S \rightarrow 2\pi^0$ and hadrons from $K_S \rightarrow \pi^+\pi^-$ are given. The width of γ's from the 2γ sample, and the Z dependence is plotted in Figure 61. There is clear evidence for background of a few per mille at Z close to the detector. There is no evidence of a similar effect in the $2\pi^0$ sample. The events with large width were examined and found to have a vertex and one broad track. They had been mistakenly treated as 2γ candidates because they had failed the charged reconstruction as one or both tracks had space−points close to a ring and the neutral trigger was satisfied. The events are clearly K_{e3} decays.

To remove this contamination no event is accepted for analysis if the following condition is satisfied :

HITS IN WC1 > 2 .and. HITS IN WC2 > 2

Events which satisfy this condition have a Z distribution which falls quickly with no events in the first half of the decay volume.

110
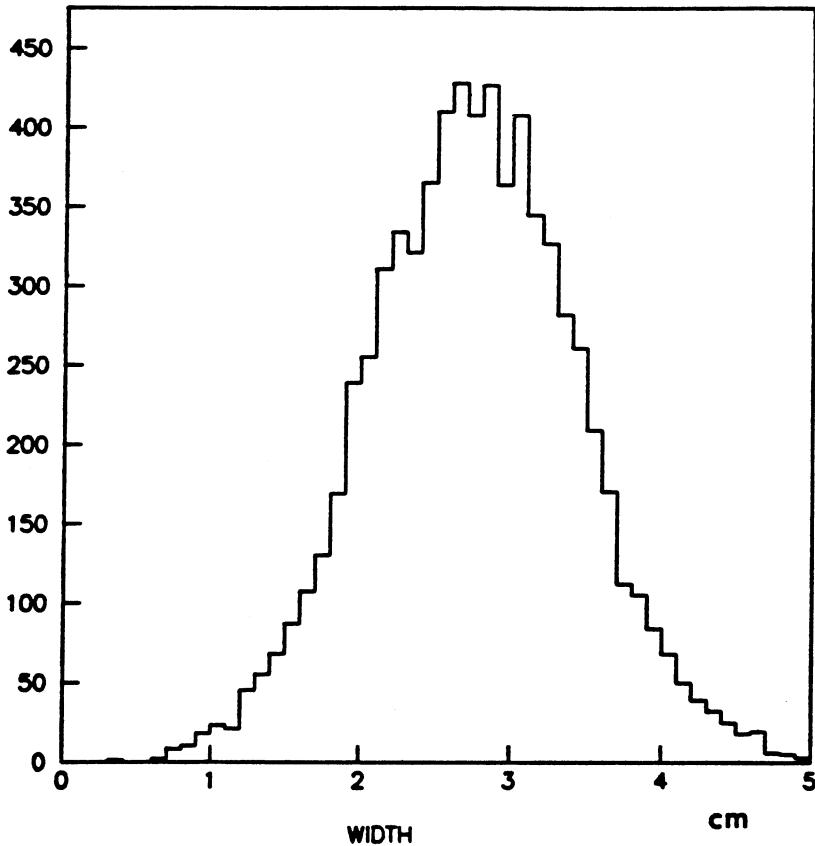
Figure 59: Width distribution for hadrons in $K_S \to \pi^+ \pi^-$.

We may use the width distribution to place an upper limit on hadron contamination of the γ sample. Ten thousand $K_S \to \pi^+ \pi^-$ events where at least one pion deposited greater than 10 GeV in the electromagnetic calorimeter were selected. The width was calculated for the pion which showered in the calorimeter. In 85.6% of the events the width was in the range $1.0 >$ W or W > 2.2 cm. In ten thousand 2γ candidates no event was found in this width range. At 90% C.L. we observe < 2.3 events. The hadron contamination of the photon sample is therefore $< 5 \times 10^{-5}$.

7.1.11 Effects of the cuts on the data

The distributions of the quantities used in cuts have all been in good agreement between monte carlo and data. This gives confidence to the claim that the acceptance of the signal and the normalisa-
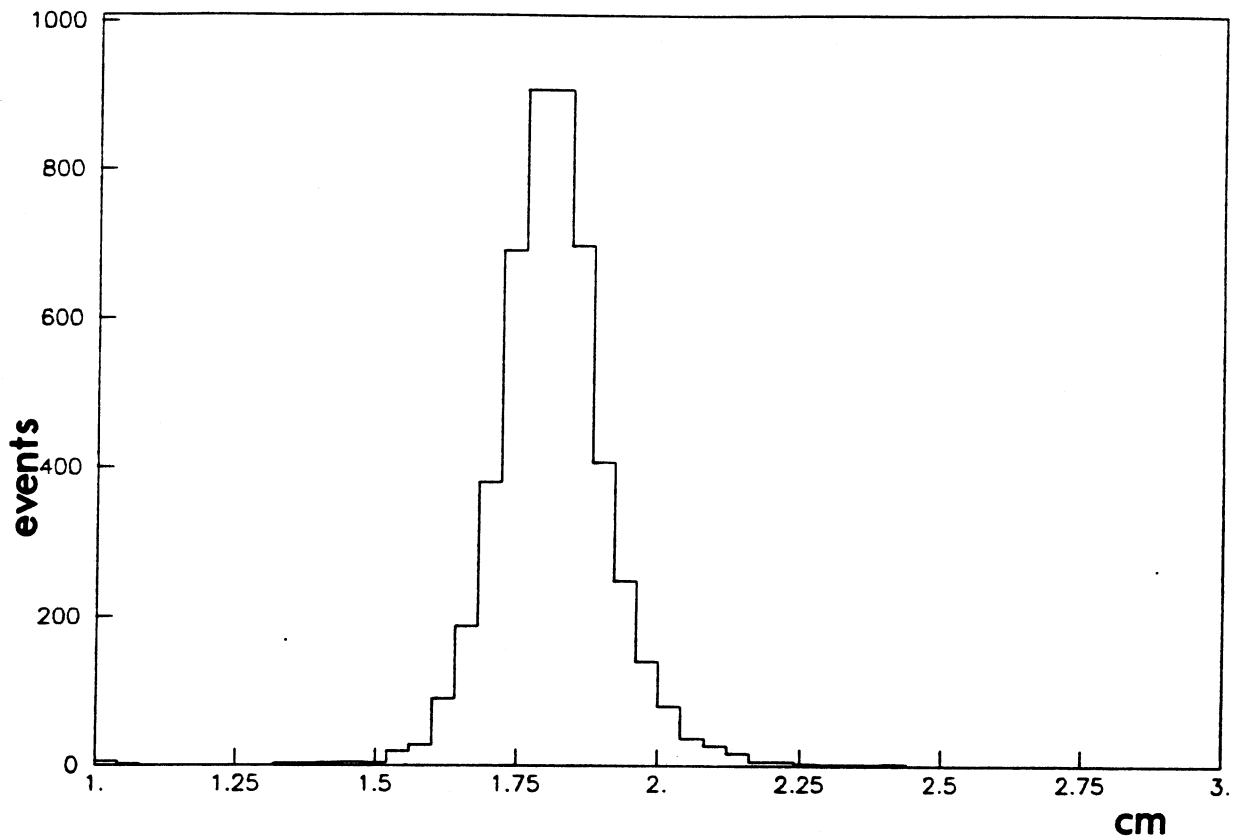
Figure 61: Width of photons in $K_S \to 2\pi^0$.

tion are well understood. The cuts described are now applied to the data. The effect of each cut applied independently to the data is shown in Table 6 .

7.1.12 Binning the data

The fiducial volume is divided into nine Z bins; each of the first eight are four K_S stations long (4.8 m.) while the last is one station shorter. The energy range is divided into four bins of 20 GeV each. The choice of these bin sizes is made so that the results obtained here can be used directly to determine R.
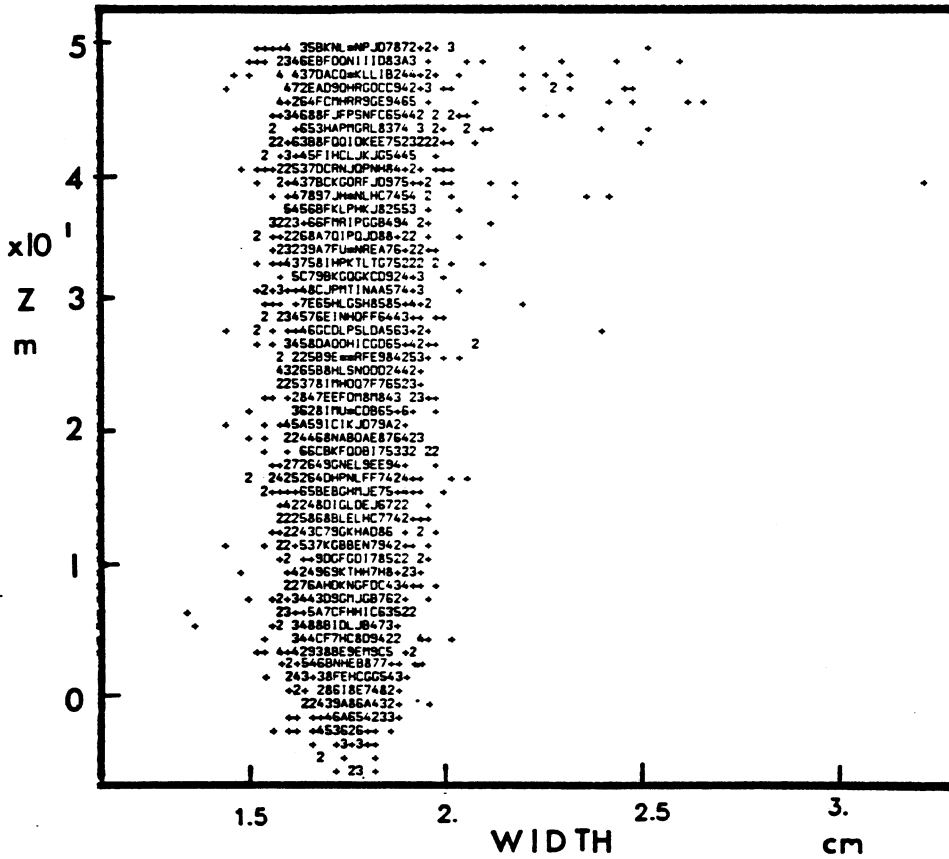
Figure 61: *Vertex dependence of the width for* $K_L \to 2\gamma$.

7.2 Subtraction of the background in $2\pi^0$.

The $2\pi^0$ background is from $3\pi^0$ where two photons are undetected. The four remaining photons which minimise the χ^2 function are distributed uniformly in $m_{\pi^0} - m_{\pi^0}$ space in the region close to m_{π^0}. This is demonstrated in Figure 62. The background is estimated reliably by a simple extrapolation into the region $\mu < 1$. To make a bin by bin subtraction the region $5 < \mu < 15$ is used, which is an area bounded by two concentric ellipses ten times larger than the signal area. Events in this region which satisfy all other cuts are binned in E and Z. After division by ten the background is subtracted from the bin contents. The inner ellipses used in the background subtraction are shown in Figure 63 .The Z dependence of the background is shown in Figure 64 .

Table 6: K_L *analysis*

	$2\pi^0$	2γ
total events	99258	49303
minimum photon energy	18.1%	9.1%
inner radial cut	12.1%	4.7%
outer radial cut	2.9%	1.8%
c.o.g. cut	25.8%	2.5%
total energy cut	37.8%	38.2%
Z - cut	39.8%	29.5%
mass cut	62.5%	−
shower separation	0.2%	−
projection separation	−	0.3%
events passing	12765 (12.9%)	18509 (40.3%)

7.3 Subtraction of background in 2γ

The background is from $2\pi^0$ where two photons are undetected. The remaining 2γ are distributed in the first moment out to about 6 cm. This fact is used to extrapolate from the region > 7 cm. into the signal region, as shown in Figure 66 .

As there are too few events at > 7 cm. in the data to obtain the background as a function of E and Z, the bin correction must be made with the help of monte carlo. Generated $2\pi^0$ decays which have only two detected photons are distributed in E and Z, weighted according to the ratio of observed $2\pi^0$ events in the monte carlo and data. A subtraction is then made to each bin. The monte carlo prediction for the Z dependence of the background is given in Figure 65 .

114
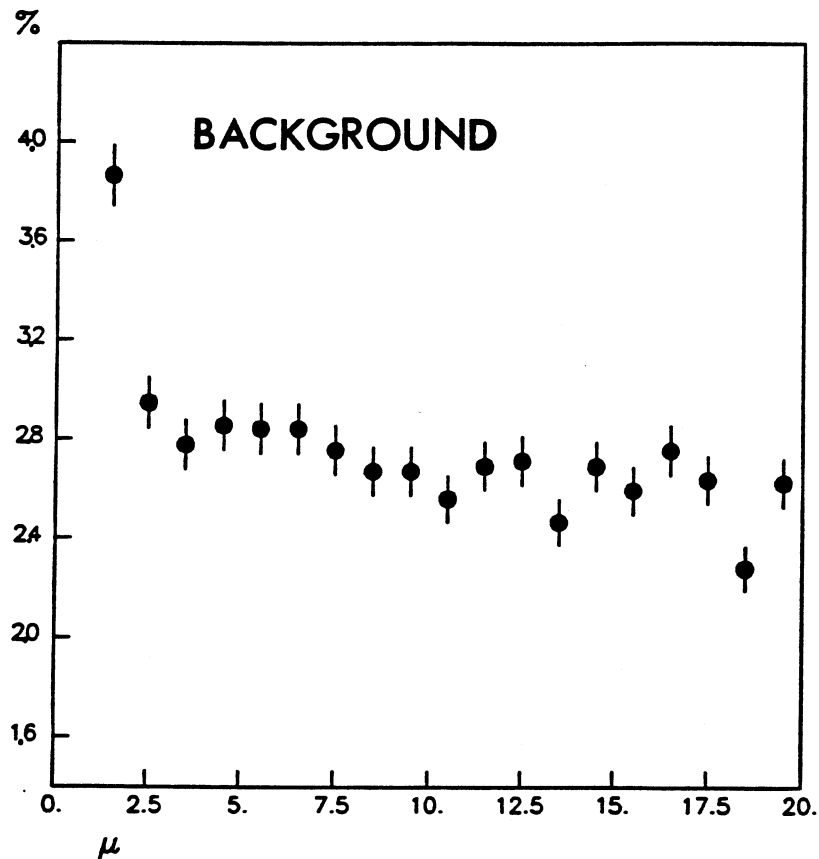
Figure 62: The μ mass distribution for K_L

7.4 Calculation of P and B

All the components necessary to calculate P are now assembled. Equation (1) is used to calculate the global value for P :

$$P = \{ (18509 - 104)/ (12765 - 363) \} \times (0.20144/0.46489) = 0.643 \pm 1.1 \% \pm 0.5 \%$$

where the statistical error includes a 0.5 % contribution from the finite number of events generated in the monte carlo. The value of B using the world average branching ratio for $K_L \rightarrow 2\pi^0$ is :

$$B = 0.643 \times 9.4 \times 10^{-4} = 6.04 \times 10^{-4}$$

Alternatively using all 36 bins a weighted mean is obtained :

115
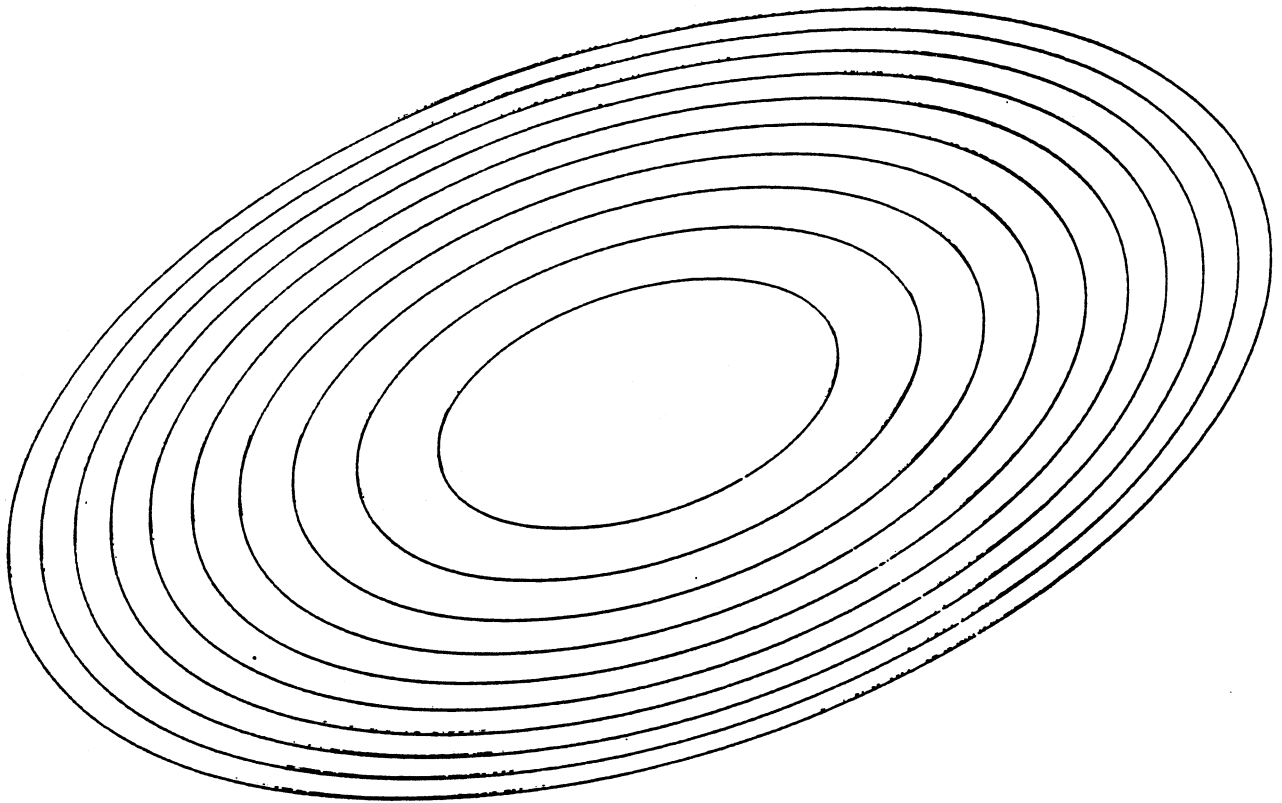
Figure 63: Ellipses used in background subtraction

$$B = 6.03 \pm 0.07 \times 10^{-4}$$

In Figure 67, the 36 individual determinations of the branching ratio are shown. The results are gaussianly distributed about their mean. There is no evidence for a Z−dependence, indicating that the backgrounds which are a strong function of Z have been correctly subtracted. This is also supported by the corresponding plots for the signal and normalisation taken separately. In Figure 68 the branching ratio as a function of energy is shown. No energy dependence is seen.
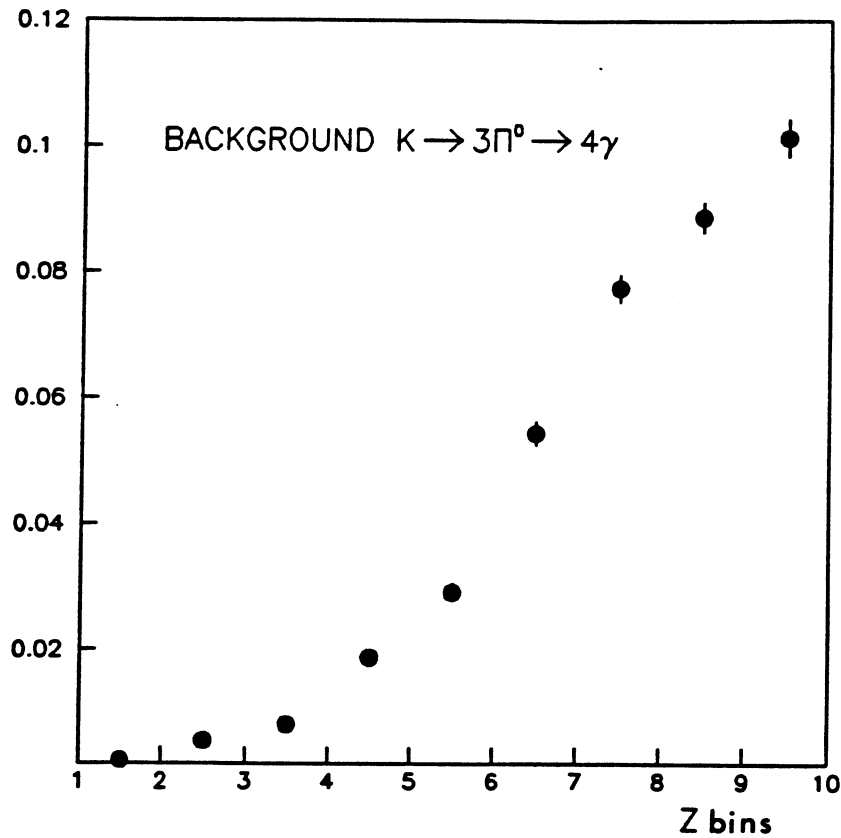
Figure 64: *The Z dependence of the $2\pi^0$ background*

7.5 Consistency requirements

The use of the mass constraint explicitly assumes that the 2γ events observed which satisfied all cuts are $K_L \rightarrow 2\gamma$. We have never proved that this is indeed the case, we have asserted instead that they can be nothing else. There are two consistency checks which one can perform. The assumption that the events are kaon decays has not constrained either the first moment distribution or the energy spectrum. In Figure 69 the first moment distribution of $2\pi^0$ and 2γ events is overlaid. The distributions are identical. In Figure 70 the acceptance corrected decay spectrum is shown for $2\pi^0$ and 2γ events. Both event types have the same spectrum indicating that they have both come only from K_L decays.

117
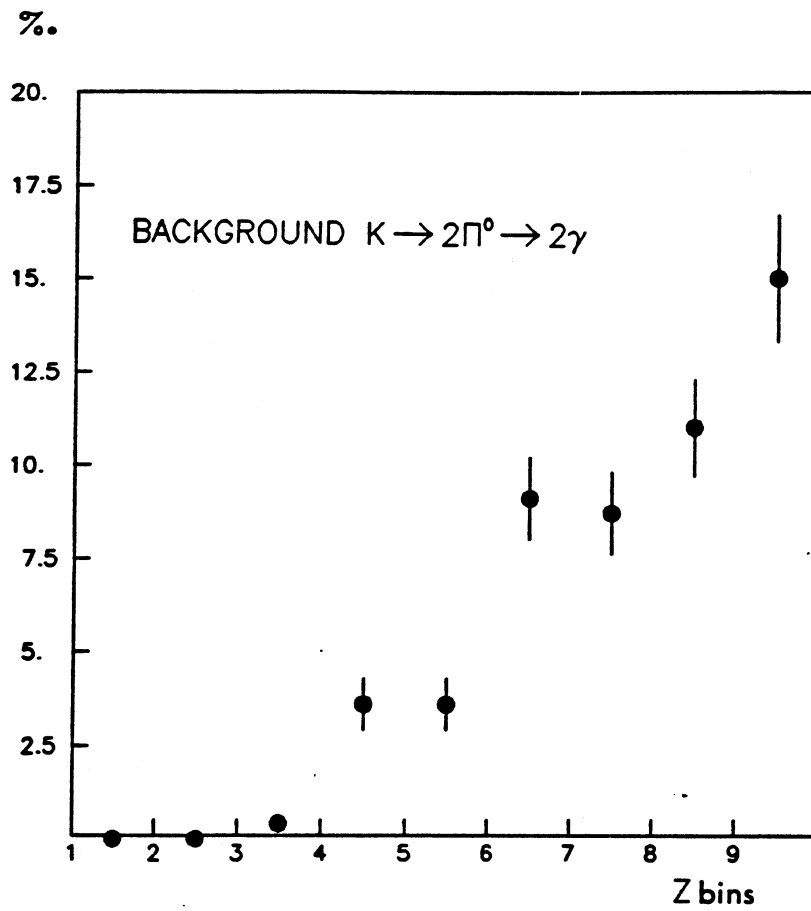
Figure 65: Z dependence of 2γ background

7.6 Corrections and systematic errors

We now turn to a consideration of possible systematic errors in the result and to corrections which have yet to be taken into account.
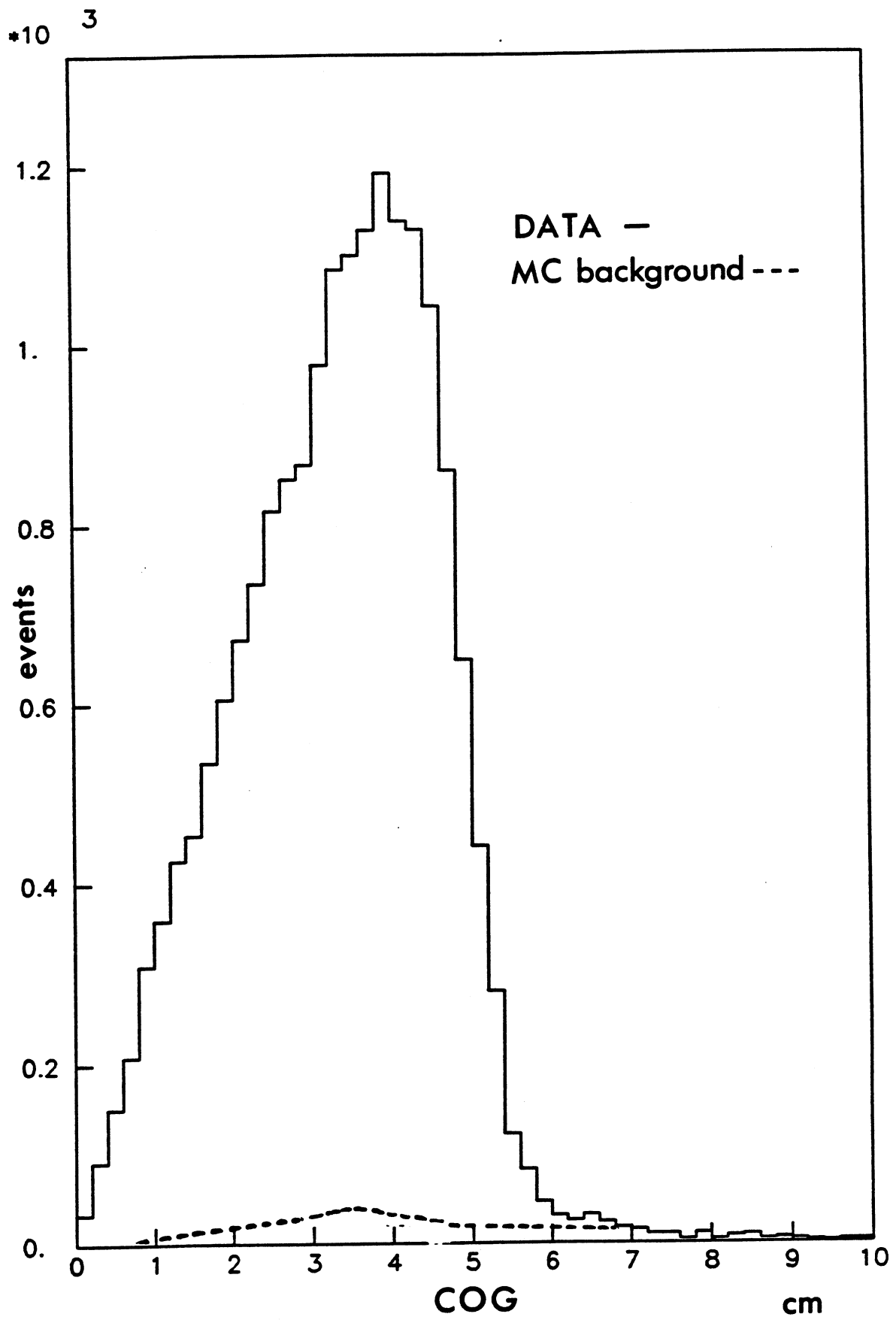
Figure 66: First moment distribution of $K_L \rightarrow 2\gamma$

118a

$$\Gamma(K \rightarrow 2\gamma)/\Gamma(K \rightarrow ALL)$$

70–90 GEV

90–110 GEV

110–130 GEV

130–150 GEV

Z bins
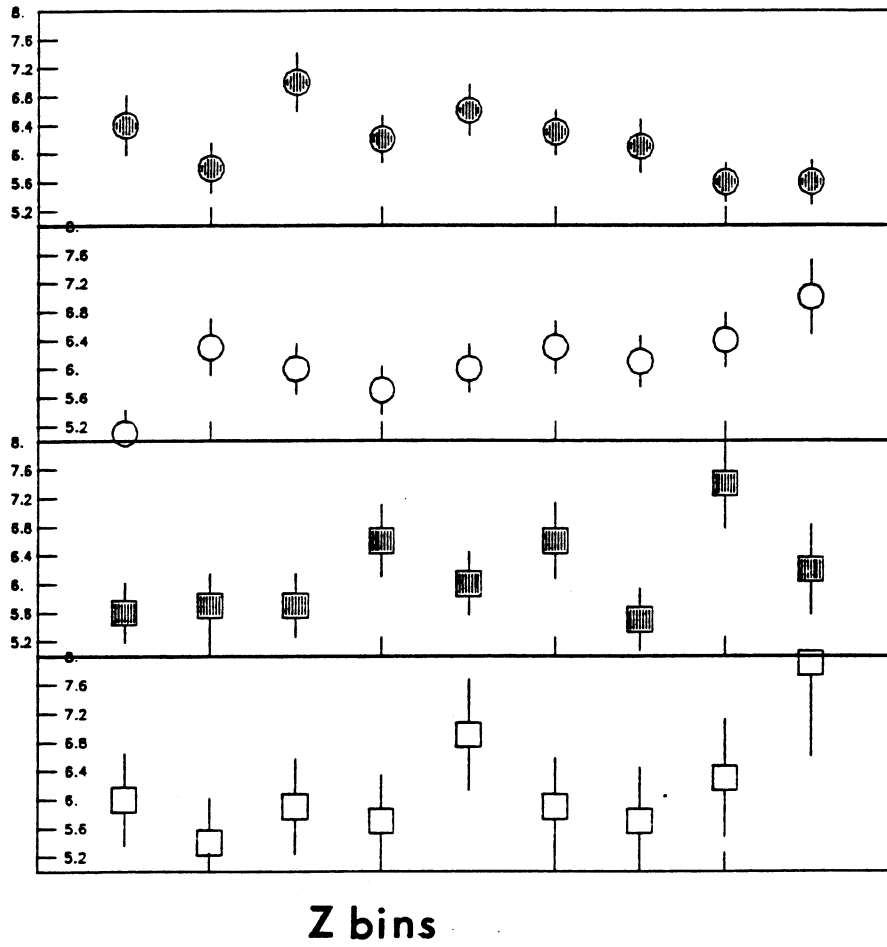
Figure 67: 36 determinations of B.
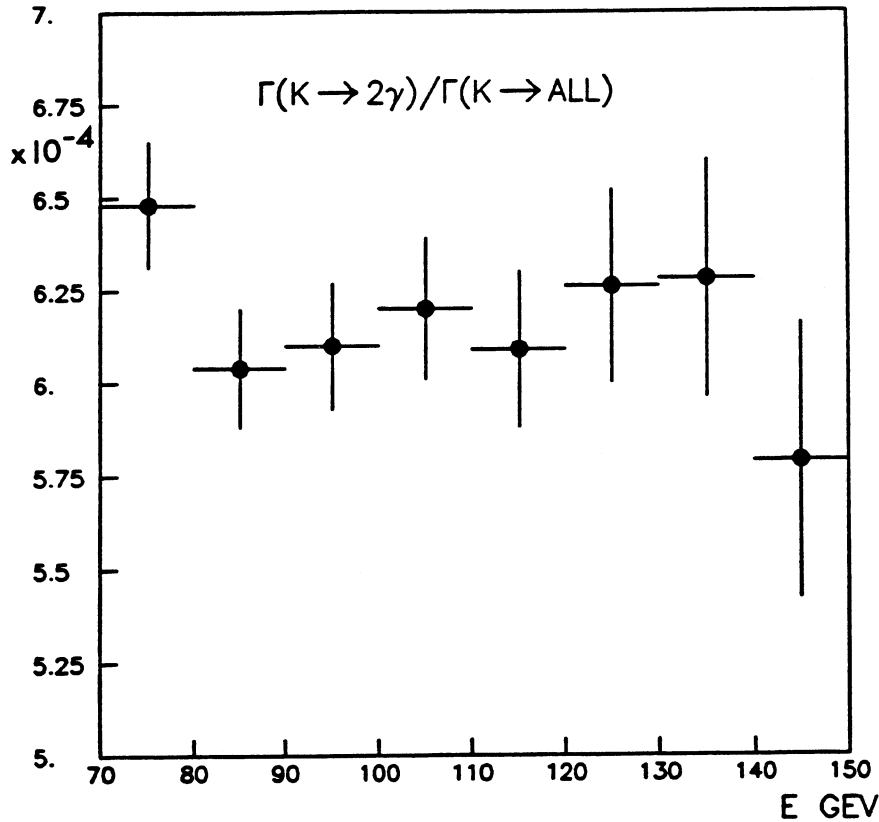
Figure 68: Energy independence of B.

7.6.1 The Dalitz correction to $K_L \to 2\gamma$

It has been demonstrated that a background exists in the two gamma sample of events which have two hits in each chamber coming from K_{e3} decays. These events have been explicitly excluded from the data sample as there is no obvious way of calculating how many K_{e3} decays of this type to expect. This cut will also reject two genuine classes of 2γ event; double conversions and Dalitz decays.

The conversion probability for photons in the helium tank and Kevlar window before the first chamber, has been determined using reconstructed $K_S \to 2\pi^0$ decays to be 0.6%. Therefore the probability that two photons convert in the same event is $\cong 4 \times 10^{-5}$, which is completely negligible.

The branching ratio $\Gamma(K_L \to e^+e^-\gamma)/\Gamma(K_L \to \text{all})$ has never been measured. We have calculated this branching ratio by evaluating the integral given in [39] for the Dalitz decay of a pseudoscalar meson to two photons obtaining :
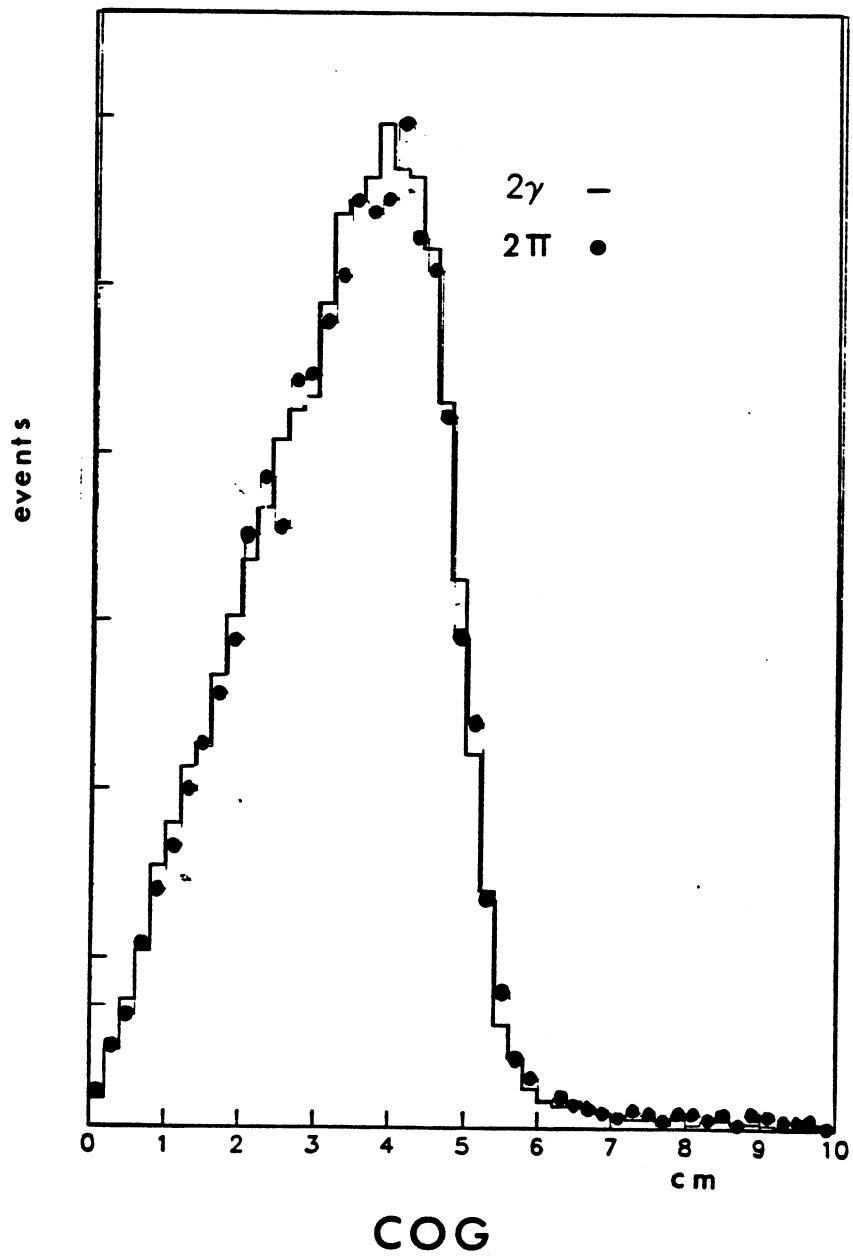
Figure 69: Comparison of first moments for $2\pi^0$ and 2γ
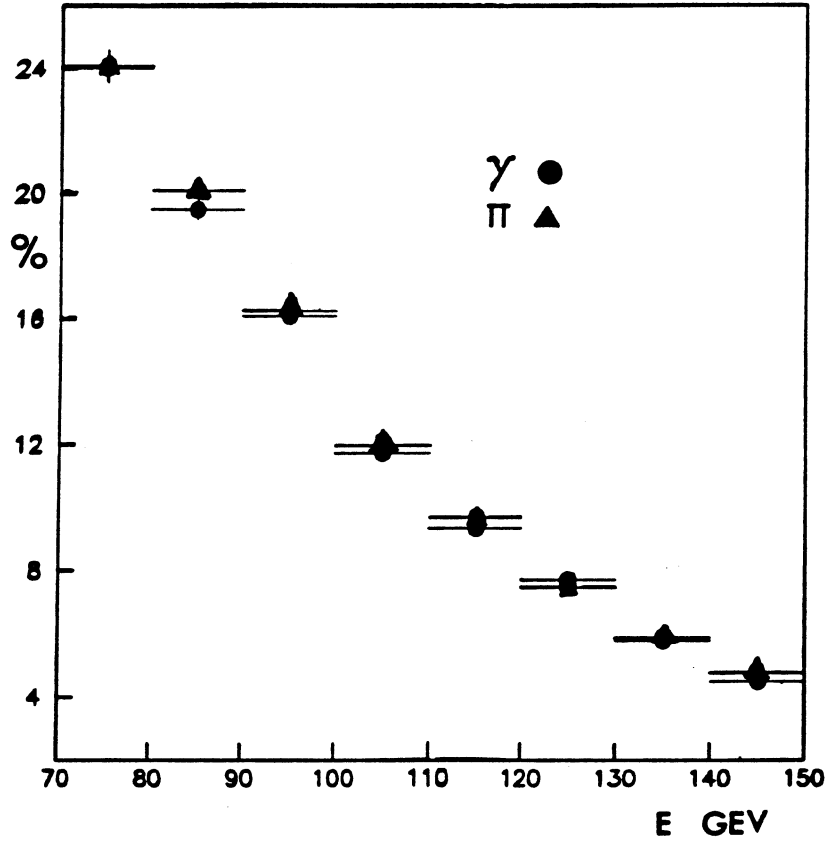
Figure 70: *Comparison of the decay spectrum for $2\pi^0$ and 2γ*

$$\Gamma(K_L \to \gamma e^+ e^-)/\Gamma(K_L \to 2\gamma) = 4\alpha/3\pi \, \int_{2m}^{M} (1-x^2/M^2)^3(1-4m^2/x^2)^{0.5} \, (1+2m^2/x^2) \, dx/x$$

$$= (4\alpha/3\pi) \, 5.12 \cong 1/61$$

whilst for the $\pi^0 \to \gamma e^+ e^-$:

$$= (4\alpha/3\pi) \, 3.82 \cong 1/81$$

where m and M are the electron and pseudoscalar meson masses respectively, and x is the mass of the virtual photon. Using the world average $B(K_L \to 2\gamma)$, this result gives a branching ratio of :

$$\Gamma(K_L \to \gamma e^+ e^-)/\Gamma(K_L \to \text{all}) = 8.0 \times 10^{-6}$$

The heavier pseudoscalar mesons have larger Dalitz branching fractions because the virtual photon may be more massive. The electron pair opening angle in the laboratory peaks at zero degrees and is proportional to the mass of the virtual photon. For the K − Dalitz decay the opening angle distribution has a large angle tail. We have therefore probably lost most of the Dalitz decays by placing a condition on the chambers. As we can only calculate the Dalitz process theoretically we prefer to estimate the number of Dalitz decays that remain in our sample after cuts and subtract these. This will mean however that our final measurement will expressly exclude the Dalitz process.

A monte carlo is used to calculate the number of Dalitz decays that should be subtracted. The wire chamber cluster resolution is not well known. It is thought that two clusters can be distinguished if the distance between the centre of each cluster is greater than three wire spacings, that is 1.8 cm. The resolution of the calorimeter is dictated by the reconstruction program which has a resolution of four centimetres. There are therefore four categories of event to consider which would satisfy a trigger; in three both electrons and the photon are accepted in the calorimeter. The possibilities are; the electron pair are resolvable in both the wire chambers and the calorimeter, or only in the wire chamber, or in neither device. The final permutation involves one electron missing the detector. In all cases we consider the photon has been accepted by the detector. The last two categories will not give two hits in each chamber, moreover the final category can also be expected to fail other cuts as one of the decay products is undetected. The Dalitz decay where the opening angle of the electron pair is smallest will remain in our 2γ sample.

In Table 8 the result of a monte carlo is shown as a function of chamber cluster resolution.

Table 8: K − Dalitz subtraction

Dalitz events generated 16000

Corresponding $K_L \rightarrow 2\gamma$ + Dalitz = 976000

Wire resolution	events passing cuts	‰ of total
3	1235	2.7
5	1411	3.1

The average of the two results is the correction to be subtracted. The systematic uncertainty in the correction is 0.4‰.

7.6.2 Dalitz correction to $K_L \to 2\pi^0$

The branching ratio $\Gamma(\pi^0 \to e^+e^-\gamma)/\Gamma(\pi^0 \to \text{all})$ is experimentally determined to be $\cong 1/81$. In the decay $K_L \to 2\pi^0$ we therefore expect that the probability of a Dalitz decay is $\cong 1/41$. When the two electrons are resolvable at the calorimeter the event has five clusters, and would not be expected to give a good m_{π^0} solution. If the electrons are not resolvable however, the event should pass all cuts. We calculate, with the aid of monte carlo, how many Dalitz decays are in the final sample. As we wish to normalise to $K_L \to 2\pi^0$ which is defined to include the secondary Dalitz decay, the Dalitz decays which have been rejected by the chamber condition are corrected for. The correction, which is determined for a variable chamber cluster resolution is shown in Table 9 .

Table 9: Dalitz correction for $2\pi^0$

Dalitz events generated 17000

Corresponding $K_L \to 2\gamma$ + Dalitz = 671500

Wire resolution	events passing cuts	Loss % of total
3	444	2.2
5	628	2.0

We take the mean (2.1%) as the correction for the loss of Dalitz decays and 2‰ as the systematic error in the correction.

7.6.3 Correction to the monte carlo efficiency

From an inspection of the mass distributions for $K_S \to 2\pi^0$ decays, where there is no background from $3\pi^0$, and monte carlo $K_L \to 2\pi^0$ a difference, shown in Figure 71, between the two is found. The mass resolution appears to be better in the data than in the monte carlo. The decay spectrum is harder for K_S than K_L, therefore the average mass resolution should be better in K_S. By extrapolating the

background linearly in K_L data one can however see that the mass peak has a similar shape in K_L and K_S, indicating that the difference in the decay spectra can be neglected. The situation is summarised in Table 10
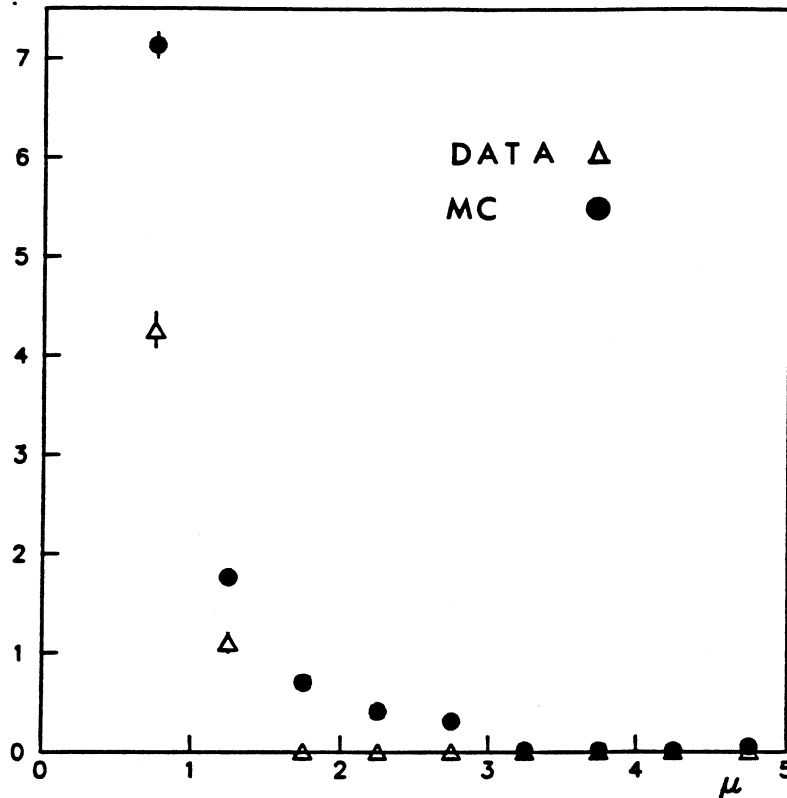
Figure 71: Monte carlo and data mass resolution

Table 10: Mass distributions for monte carlo and data

Event type	$\mu < 1$	$\mu < 2$	$1 < \mu < 2$
$K_S \to 2\pi^0$ (data)	97.2 %	98.9%	1.7%
$K_L \to 2\pi^0$ (MC)	95.7 %	98.1 %	2.6%
$K_L \to 2\pi^0$ (data)	—	—	1.6%

The monte carlo acceptance will be too low by a factor 97.2/95.7 = 1.016 the normalisation must be reduced by this factor. The correction therefore increases the size of B. The reason for the discrepancy between monte carlo and data is not certain; however from scanning monte carlo events a correlation is observed between events which fail the mass cut and the lateral separation between the photons of the combination with a bad mass. When two photons are close in the calorimeter an algorithm

is used to share the energies before digitisation. This algorithm does not appear to model the data accurately enough.

The systematic error in this correction has been estimated by comparing the difference between monte carlo and data when the mass cut is varied. The error is found to be 0.5%.

7.6.4 Correction for residual non − linearity in energy scale

From electron beams at five energies, after all corrections to the electron energies have been applied offline, there remains a energy dependent difference between the nominal beam energy and the measured energy. The effect is shown in Figure 72.
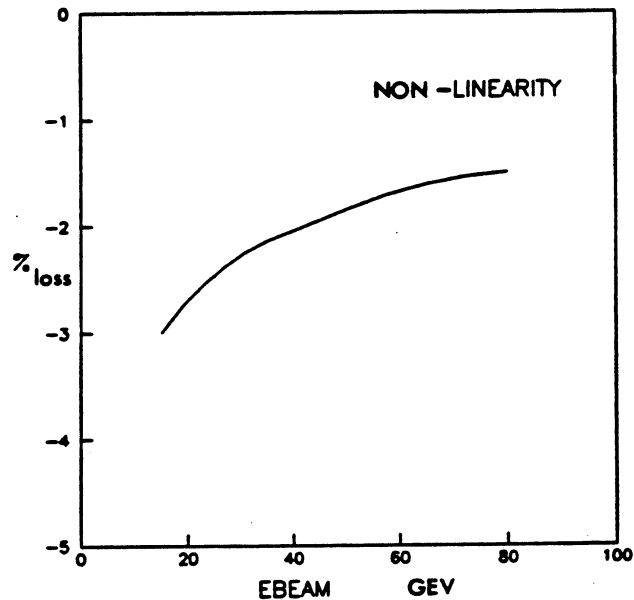
Figure 72: Non − linearity of the energy scale from electron data.

The effect has at least two possible origins. The electron beams were interchanged quite frequently, starting at one energy and later returning to it. The hysteresis in the momentum selection magnet is not taken into account, therefore the reproducibility of the energy of the beam is questionable. Alternatively the effect is a residual non − linearity.

As it is impossible to disentangle the two effects of non−linearity and hysteresis at the present time, no correction has been applied to the data to restore the energy scale. The contribution of this effect to the systematic error has been investigated in the following way. The discrepancy between nominal and measured energy has been approximated to a linear correction :

$$E_{cor} = -2.833 \times 10^{-4} . E_{\gamma} + .0070833$$

This correction is applied to all photon energies in the monte carlo before the standard cuts are made. The acceptances consequently change. The larger correction is to 2γ, reflecting the wider energy range of the photons in that decay compared to $2\pi^0$. The overall systematic effect is 0.55 % in the value of B. The details are summarised in Table 11

Table 11: Monte carlo simulation of non−linearity

Event type	2γ	$2\pi^0$	ΔB
acceptance	0.46489	0.20144	−
acceptance with correction	0.46899	0.20208	−
acceptance change	+.88%	+.32%	− 0.55%

7.6.5 Reconstruction efficiency

The efficiency of the reconstruction program is determined by taking a set of monte carlo generated events and passing them through two different analysis chains. In the first chain the photons are smeared, the digitisation is simulated and the events are passed through the reconstruction program. In the second chain the photons are only smeared. The ratio of events which survive the two analyses is the reconstruction efficiency, which was found to be 99.1 % for $2\pi^0$ and 99.8 % for 2γ.

This reconstruction inefficiency is already included in the acceptance calculations as the data and monte carlo events have both passed through the first chain described. A possible objection might now be raised; all that has been measured is the reconstruction efficiency for monte carlo events. To investigate the possibility that the monte carlo events are in some sense cleaner than the data, 400 events from the complete data tapes were taken from random K_S stations at random times throughout the data-taking period. These events were selected in a minimum bias fashion, requiring only that each event had at least 60 GeV of electromagnetic energy determined by adding all ADC channels, and that the event was not on the DST. The events were scanned by eye with the aid of a computer event display. No good $2\pi^0$ event was found in the sample which consisted mainly of 3γ events and scattered kaon decays. The sample corresponded to 700 good $2\pi^0$ events on the DST, and therefore to a reconstruction inefficiency of $<0.3\%$ at 90% CL. As a further test, 100 events were selected without the electromagnetic energy requirement, and no good $2\pi^0$ event was found.

There remains the possibility that spurious events do exist, unsimulated by MCCP, which pass the cuts for the DST but fail one or more of the final cuts. It has been shown that the reconstruction program is very efficient, and that there is no gross difference between monte carlo and data events which could lead to the rejection of the latter. We conclude that any remaining systematic is smaller than the reconstruction inefficiency and ascribe a systematic error of 0.5% to the monte carlo reliability.

7.6.6 Systematics in background subtraction of 2γ

The monte carlo predicts less background, by a factor of two, than appears present from the first moment plot in the region outside the signal. The origin of this extra background is unclear and therefore the extrapolation into the signal region is uncertain. However the monte carlo is able to predict accurately, to within 20%, the number of 3γ events in the total data sample, and the level of background from $3\pi^0$ in the $2\pi^0$ sample. As a check on the method of subtracting background using the

first moment, the same method was used to predict the $3\pi^0$ background. The background with this method was 330 events under the peak, compared to 363 using the simpler mass variable.

In the monte carlo simulation of the 2γ background, one third of the background is due to split photons. The algorithm to repair split photons is not ideal. The moment distribution of 5γ events is broader by a centimetre than that from ordinary $2\pi^0$ decays. The algorithm can also change 3γ events from a $3\pi^0$ event into 2γ. As previously explained the $3\pi^0$ background is outside our fiducial volume, however the when the photons are incorrectly merged the event can have an artificially large effective mass. Other possible sources of two photons are the K_S component in the K_L beam and the possibility that $K_L \rightarrow \pi^0 2\gamma$ which has never been observed has a non$-$negligible branching ratio. The process is thought to be heavily suppressed however. Studies of the events at large moments show a correlation with activity in the first chamber indicating that the wire chamber cut was insufficient to remove all the charged background. We describe this background uncertainty with a systematic error calculated assuming that the extra background is the same shape in the signal region as that which we have already subtracted, the error is then 0.5%.

7.6.7 Accidentals

Using the region $Z < 10$ m. accidentals can be isolated in 3γ events if two of the three photons give a good 2γ solution. Two types of event are found in this region; 70% are due to split photons and the remainder are assumed to be accidentals. The rate is computed to be 0.5%. The spectrum falls quickly with a negligible fraction of photons above 4 GeV.

The accidental rate is independent of event type. For 2γ the $E_\gamma > 10$ GeV requirement reduces the accidental contamination to negligible proportions. In $2\pi^0$ the requirement is only $E_\gamma > 5$ GeV; however the additional constraint of a good mass solution again suggests that accidentals may be neglected. There is no correction applied for accidentals.

7.6.8 Summary of corrections to measurement of B

All corrections are collected in Table 12. Corrections are shown with their sign which refers to the effect on numerator or denominator of B. The non − linearity sign however refers to B. The correction for conversions is an upper limit estimate for the number of converted photons which are resolvable at the LAC due to multiple scattering and fail the cuts in consequence. The source of each correction is given in brackets.

Table 12: Corrections to B.

	correction	systematic
event loss from mass cut(data)	+ 1.6%	0.5%
background in 2γ (data)	−	− 0.5%
Dalitz $2\pi^0$ (MC)	+ 2.1%	0.2%
Dalitz 2γ (MC)	− 3‰	0.2%
Non − linearity(MC)	−	− 0.55%
reconstruction efficiency(data)	−	0.5%
conversion(stat)	−	0.1%

7.7 The final result.

All these corrections are now applied to the raw values obtained for P and B. The sign of the corrections is well established. We add all the systematic contributions determining P and B to be :

$$P = \Gamma(K_L \to \gamma\gamma)/\Gamma(K_L \to 2\pi^0) = 0.643 \times \{-.3\%/(1.6\%+2.5\%)\}\pm(.5 + .5 + .2 + .05 + .5 + .5 + .1)\%$$

$$= 0.643 \times \{1/1.04452\} \pm 2.3\%$$

$$= 0.616 \pm .006 \pm .014$$

To calculate B we note that the world average branching ratio for $K_L \rightarrow 2\pi^0$ is :

$$B(K_L \rightarrow 2\pi^0) = \Gamma(K_L \rightarrow 2\pi^0)/\Gamma(K_L \rightarrow all) = (9.4 \pm 0.18) \times 10^{-4}$$

so that :

$$\Delta B/B = 19 \%$$

To avoid this large systematic error we use the recent experimental results from Adair [32] and Winstein [1] to calculate a more precise weighted average for $B(K_L \rightarrow 2\pi^0)$. We recall :

$$|\eta_{+-}|^2 / |\eta_{00}|^2 = \frac{\Gamma(K_L \rightarrow \pi^+\pi^-)}{\Gamma(K_S \rightarrow \pi^+\pi^-)} \frac{\Gamma(K_S \rightarrow 2\pi^0)}{\Gamma(K_L \rightarrow 2\pi^0)}$$

The lifetimes cancel, the expression becomes :

$$|\eta_{+-}|^2 / |\eta_{00}|^2 = \frac{B(K_L \rightarrow \pi^+\pi^-)}{B(K_S \rightarrow \pi^+\pi^-)} \frac{B(K_S \rightarrow 2\pi^0)}{B(K_L \rightarrow 2\pi^0)}$$

We use the PDG values for the branching ratios :

$$B(K_L \rightarrow \pi^+\pi^-) = (2.03 \pm 0.05) \times 10^{-3}$$

$$B(K_S \rightarrow 2\pi^0) = 0.3139 \pm 0.0024$$

$$B(K_S \rightarrow \pi^+\pi^-) = 0.6861 \pm 0.0024$$

and the relation :

$$|\eta_{+-}|^2 / |\eta_{00}|^2 = 1 + 6\epsilon'/\epsilon$$

$$\epsilon'/\epsilon = -0.0046 \pm 0.0058 \Rightarrow |\eta_{+-}|^2/|\eta_{00}|^2 = 0.9724 \pm 0.035 \quad \text{(Winstein)}$$

$$\epsilon'/\epsilon = 0.0017 \pm 0.0083 \Rightarrow |\eta_{+-}|^2/|\eta_{00}|^2 = 1.010 \pm 0.050 \quad \text{(Adair)}$$

we obtain :

$$B(K_L \rightarrow 2\pi^0) = (9.55 \pm 0.42) \times 10^{-4} \quad \text{(Winstein)}$$

$$B(K_L \rightarrow 2\pi^0) = (9.2 \pm 0.51) \times 10^{-4} \quad \text{(Adair)}$$

$$B(K_L \rightarrow 2\pi^0) = (9.41 \pm 0.32) \times 10^{-4} \quad \text{(weighted average)}$$

$$\Delta B/B = 3.4\%$$

Alternatively, using the world average value :

$$|\eta_{+-}|^2 = (2.273 \pm 0.022 \times 10^{-3})^2 \quad \text{(PDG)}$$

$$|\eta_{00}|^2 = (5.31 \pm 0.22) \times 10^{-6} \quad \text{(Winstein)}$$

$$|\eta_{00}|^2 = (5.12 \pm 0.27) \times 10^{-6} \quad \text{(Adair)}$$

$$|\eta_{00}|^2 = (5.23 \pm 0.17) \times 10^{-6} \quad \text{(weighted average)}$$

and the average for $B(K_S \rightarrow 2\pi^0)$ to obtain :

$$B(K_L \rightarrow 2\pi^0) = (9.54 \pm 0.32) \times 10^{-4}$$

As the second derivation of $B(K_L \rightarrow 2\pi^0)$ involves one less independent measurement, it is systematically more reliable and will be used in this work. The difference between the two methods of extracting $B(K_L \rightarrow 2\pi^0)$ differ by more than 1.3% which is within the errors quoted for each result individually. Finally the value of B is :

$$B = \Gamma(K_L \rightarrow \gamma\gamma)/\Gamma(K_L \rightarrow \text{all}) = (5.87 \pm 0.06 \pm 0.12 \pm 0.20) \times 10^{-4}$$

Where the first error is statistical, the second systematic and the third an external systematic from $B(K_L \to 2\pi^0)$. This is to be compared with the value obtained using the previous world average :

$$B = \Gamma(K_L \to \gamma\gamma)/\Gamma(K_L \to all) = (\ 5.78 \pm 0.06 \pm 0.11 \pm 1.11\ ) \times 10^{-4}$$

We defer a discussion of this result until chapter nine.

8. THE MEASUREMENT OF THE RATIO $\Gamma(K_S \to 2\gamma)/\Gamma(K_L \to 2\gamma)$

8.1 Introduction

In this chapter we present a measurement of R. Previous experiments have always attempted to measure the branching ratio of $K_S \to 2\gamma$. We determine R by the double ratio technique which has the advantage that it does not depend, to first order, on a monte carlo calculation. To introduce the technique we first recall its more familiar use in the measurement of $|\eta_{+-}|^2/|\eta_{00}|^2$.

8.2 Determination of $[\eta_{+-}]^2/[\eta_{00}]^2$ by the double ratio technique

The most common use of the double ratio technique is in the determination of ε'/ε. As in chapter 2 we write the amplitudes as:

$$\eta_{+-} = <\pi^+\pi^- | K_L> / <\pi^+\pi^- | K_S>$$

$$\eta_{00} = <\pi^0\pi^0 | K_L> / <\pi^0\pi^0 | K_S>$$

In terms of experimentally measured quantities we actually determine:

$$|\eta_{+-}|^2 = \Gamma(K_L \to \pi^+\pi^-) / \Gamma(K_S \to \pi^+\pi^-)$$

$$|\eta_{00}|^2 = \Gamma(K_L \to \pi^0\pi^0) / \Gamma(K_S \to \pi^0\pi^0)$$

$$|\eta_{+-}|^2/|\eta_{00}|^2 = R_{2\pi}$$

Let N be the number of events observed in a given energy and z bin. Let ε be the efficiency for detecting a given mode. Then $R_{2\pi}$ is determined simply from counting events:

$$R_{2\pi} = \frac{N(K_L \to \pi^+\pi^-)\varepsilon(K_L \to \pi+\pi-) \quad N(K_S \to 2\pi^0)\varepsilon(K_S \to 2\pi^0)}{N(K_S \to \pi^+\pi^-)\varepsilon(K_S \to \pi+\pi-) \quad N(K_L \to 2\pi^0)\varepsilon(K_L \to 2\pi^0)}$$

because to first order the efficiency, which is largely geometrical, cancels if the momentum spectrum and vertex distributions are the same, explicitly:

$$\epsilon(K_L \to \pi^+\pi^-) = \epsilon(K_S \to \pi^+\pi^-)$$

$$\epsilon(K_S \to 2\pi^0) = \epsilon(K_L \to 2\pi^0)$$

A typical second order effect which does not completely cancel between K_L and K_S is the finite beam size. Whilst this effect is important for a precise determination of ϵ'/ϵ it will not be considered further for this application of this technique to two photons.

8.3 The double ratio technique applied to R

Using notation similar to the previous section, we construct the following two identities:

$$|\eta_{\gamma\gamma}|^2 \cdot |\eta_{00}|^2 = \frac{\Gamma(K_S \to 2\gamma).}{\Gamma(K_L \to 2\gamma)} \frac{\Gamma(K_L \to 2\pi^0)}{\Gamma(K_S \to 2\pi^0)}$$

$$|\eta_{\gamma\gamma}|^2 \cdot |\eta_{00}|^2 = \frac{N(K_L \to 2\pi 0).\epsilon(K_L \to 2\pi^0)}{N(K_L \to 2\gamma).\epsilon(K_L \to 2\gamma)} \frac{N(K_S \to 2\gamma).\epsilon(K_S \to 2\gamma)}{N(K_S \to 2\pi^0).\epsilon(K_S \to 2\pi^0)}$$

With the same cancellations as before :

$$\epsilon(K_L \to 2\gamma) = \epsilon(K_S \to 2\gamma)$$

$$\epsilon(K_S \to 2\pi^0) = \epsilon(K_L \to 2\pi^0)$$

Equating the first two identities yields on rearrangement :

$$R = |\eta_{\gamma\gamma}|^2 = \frac{N(K_S \to 2\gamma)\, N(K_L \to 2\pi^0)}{N(K_S \to 2\pi^0)\, N(K_L \to 2\gamma)} \cdot \frac{1}{|\eta_{00}|^2}$$

Whilst the K_L and K_S momentum spectra are identical at the target, the difference between their respective lifetimes produces quite different momentum spectra and vertex distributions for the decays in the fiducial volume. The XTGV ensures that the distribution of decays throughout the volume is approximately the same for K_S and K_L. For the acceptance to cancel, for any given decay mode, between K_L and K_S it is necessary to calculate R in momentum bins small enough for the spectra to be similar. We therefore transform the identity just obtained into a sum over 36 bins in momentum and vertex :

$$R = \frac{1}{n} \cdot \frac{1}{|\eta_{00}|^2} \Sigma_{i=1,n} \frac{S_i}{L_i} \qquad (3)$$

where n is the number of bins, and L_i and S_i are the ratios of 2γ to $2\pi^0$ events observed in the ith bin in the K_L and K_S beams respectively.

8.4 The method of extraction of $K_S \to 2\gamma$

There is no useful additional information about the photons from K_S decay. From the K_L study , and from naive theoretical expectations we anticipate the main source of background will be $2\pi^0$ decays and the branching ratio to be low. The $K_S \to 2\pi^0$ decay is copious, to compare the situation with K_L consider the background to signal ratio:

$$\frac{\text{background}}{\text{signal}} = \frac{B(K_L \to 2\pi^0)}{B(K_L \to 2\gamma)} \cdot \frac{\epsilon(K_L \to 2\pi^0 \to 2\gamma)}{\epsilon(K_L \to 2\gamma)}$$

136

$$\frac{\text{background}}{\text{signal}} = \frac{B(K_S \rightarrow 2\pi^\circ)}{B(K_S \rightarrow 2\gamma)} \frac{\varepsilon(K_S \rightarrow 2\pi^0 \rightarrow 2\gamma)}{\varepsilon(K_S \rightarrow 2\gamma)}$$

The background has already been measured in K_L to be about 1%, using this and an estimate for $B(K_S \rightarrow 2\gamma)$ we obtain:

$$\frac{\text{Ratio of background to signal in } K_S}{\text{Ratio of background to signal in } K_L} = \frac{3 \times 10^{-1} \times 1}{2 \times 10^{-6} \times 2} \approx 10^5$$

therefore :

$$\text{Ratio of background to signal in } K_S \approx 10^3$$

To work in the same fiducial volume as in K_L would mean facing the impossible task of extracting a signal from a background 1000 times larger. The situation can be improved by working only in the effective mass region from which $2\pi^0$ decays are excluded. We recall that this region corresponds to a effective $\gamma\gamma$ mass of 458 MeV. To use this region a new variable ζ is introduced. This quantity is defined in Figure 73.

ζ is simply a measure of the departure from a kaon mass which any pair of photons possess assuming the decay had occurred at the end of the collimator. Alternatively, $(1-\zeta)$ is a measure of the fractional mass a pair, has with respect to the kaon mass, if it decayed at the end of the collimator. For a $K_S \rightarrow 2\gamma$ decay at the collimator $\zeta = 0$, assuming no measurement error.

For clarity consider an example. A kaon decays at the collimator into $2\pi^0$. Only two of the photons are detected with an effective mass of 400 MeV. The train is at station 21 :

The shift will be $\Delta Z = 1 - (400/500) = 1/5$

At station 21 this is $\Delta Z = 20$ m.

Therefore $\zeta = 0.2$

Let the train move to station 41 :
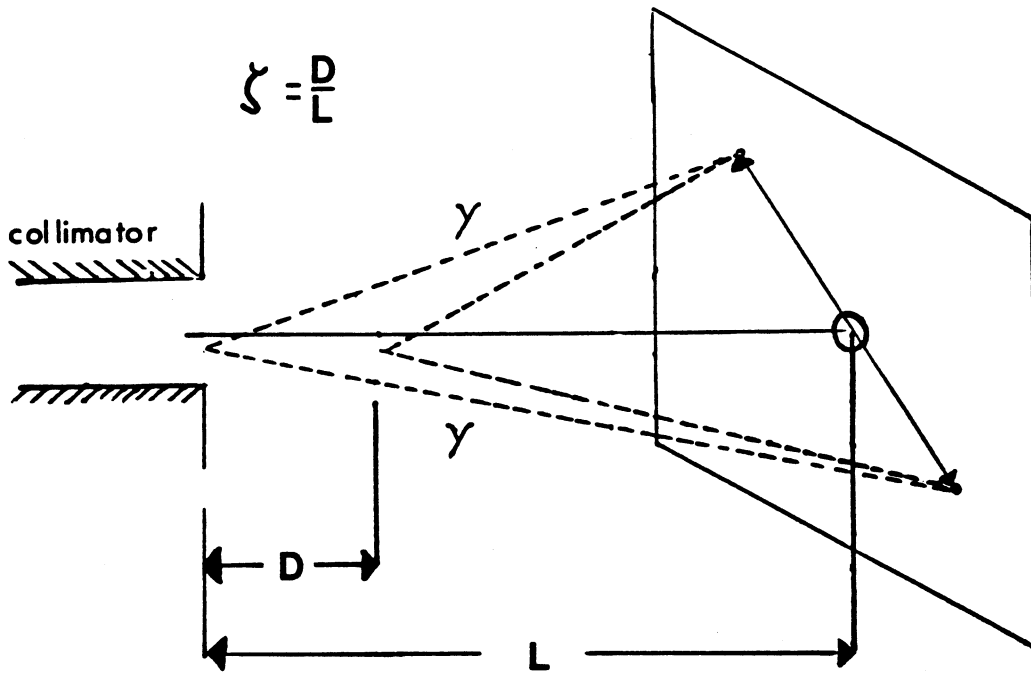
Figure 73: The definition of ς.

The shift will be $\Delta Z = 1 - (400/500) = 1/5$ as before

At station 41 this is $\Delta Z = 16$ m.

Therefore $\varsigma = 0.2$ as before

A vertex cut would admit a different amount of background at each station, the advantage of using ς is that it is K_S station invariant.

One could instead use the K_S lifetime, but there are several reasons for not doing so. The lifetime is much more sensitive to the energy scale than ς. That ς does not depend on the kaon momentum complements the fact that the kinematical region from which $2\pi^0$ decays are excluded is also energy independent.

ς is bounded for a kaon decay from below by vertex resolution, and from above by the detector itself. The possible values of ς are $-0.05 < \varsigma < 1$. The region without background corresponds to

138

$\zeta < 0.08$, which is one K_S lifetime at station 21 at 100 GeV, indicating that only about 30% of the flux will be rejected by this cut.

We determine ζ for each $2\pi^0$ and 2γ decay. By cutting at the same value of ζ for both modes, the signal is normalised correctly. In Figure 74 the ζ distribution is given for $K_S \rightarrow 2\pi^0$, events at negative values are from vertex resolution and anti−counter inefficiency. Figure 75 is the same plot for 2γ events. The vertex shift is evident.

8.5 The experimental determination of R

The denominator of equation (3) has already been determined. The L_i are just the raw numbers of events which were used in the 36 determinations of P. Using exactly the same cuts as in the K_L analysis, with the additional cut in ζ, we obtain the S_i . The effects of each cut applied independently to the data is shown in Table 13.

The L_i and S_i are listed in Table 14 and Table 15. Only six 2γ events satisfy all the cuts. These events were each scanned, with the aid of an event display. The events are indistinguishable from typical $K_L \rightarrow 2\gamma$ events. The events are shown in a plot of z versus first moment in figure 76.

We now evaluate equation (3). The 36 potential terms are reduced to only six. The weighted mean of the Adair [32] and Winstein [1] experiments is used in preference to the old world average for $|\eta_{00}|^2$, as it is more precise. The factor of one fifth appearing in the sum allows for the downscaling of $K_S \rightarrow 2\pi^0$ events during the DST production.

$$|\eta_{00}|^2 \; = \; 5.23 \pm 0.17 \; \times \; 10^{-6} \quad \text{(weighted average)}$$

to obtain :
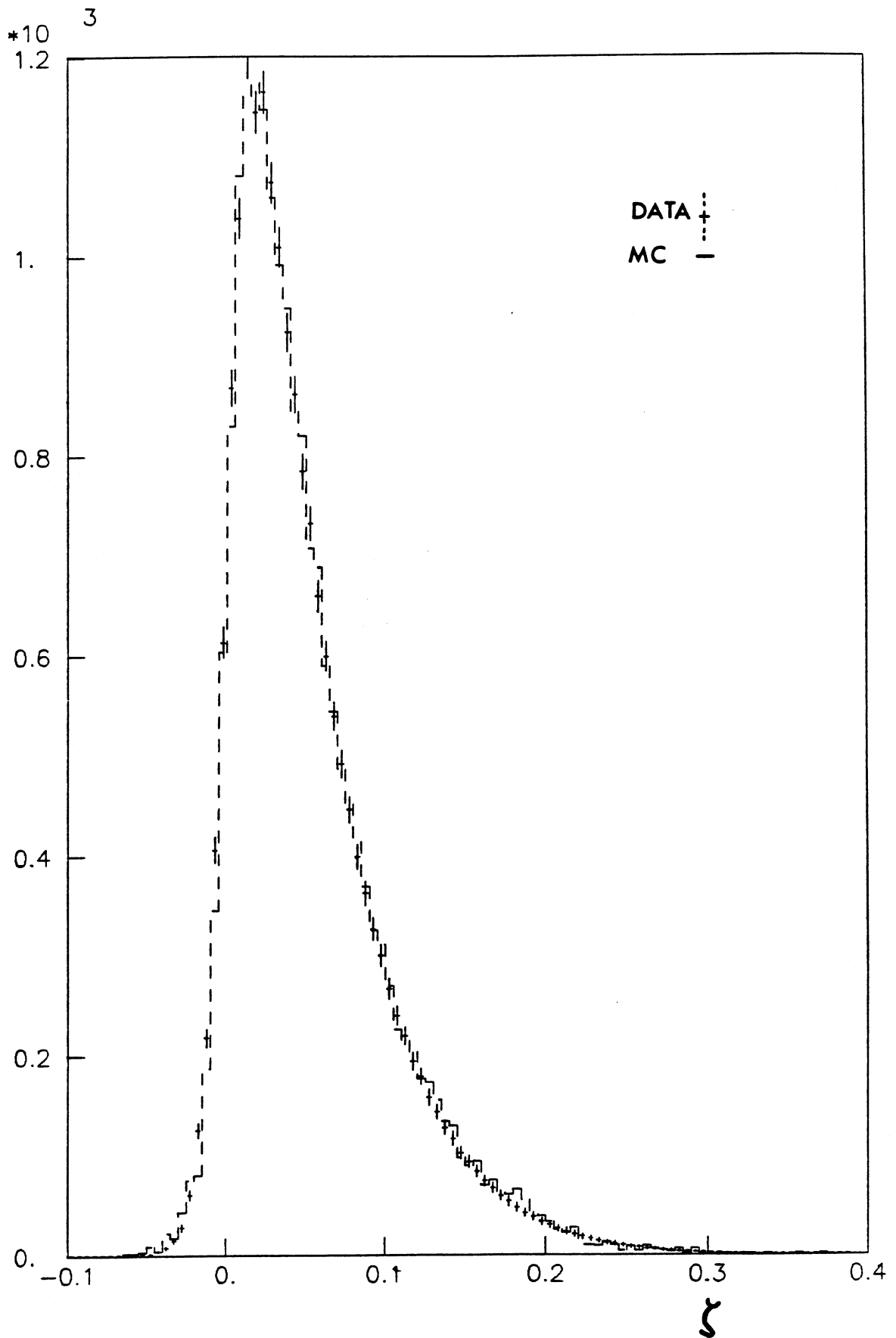
Figure 74: ζ for $K_S \to 2\pi^0$
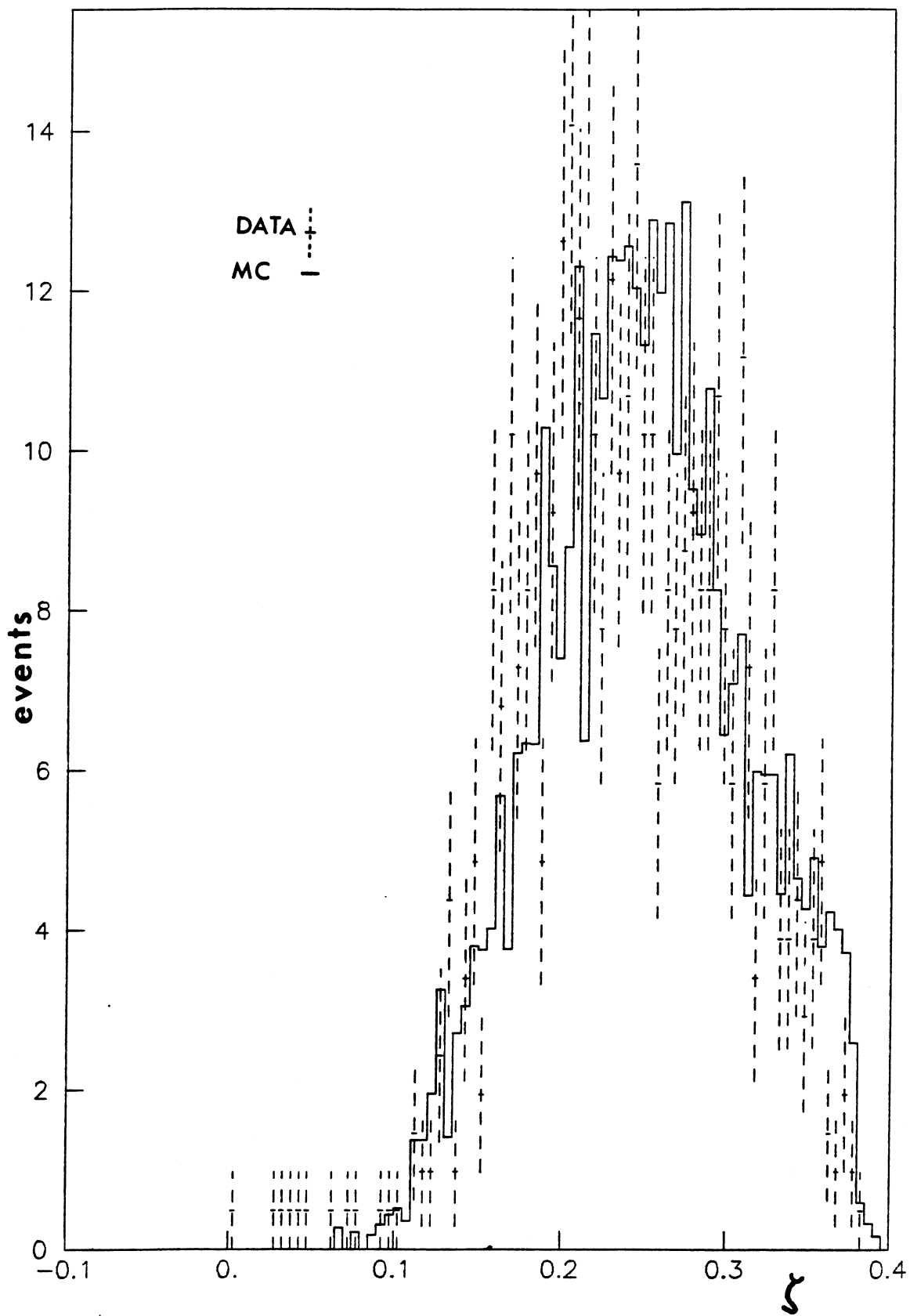
Figure 75: ζ for 2γ events

Table 13: K_S analysis

	$2\pi^0$	2γ
total events	43500	2504
minimum photon energy	27.2%	8.4%
inner radial cut	13.3%	4.7%
outer radial cut	2.1%	0.6%
c.o.g. cut	0.7%	9.8%
total energy cut	23.6%	31.7%
ζ	35.2%	31.0%
mass cut	7.2%	—
shower separation	0.4%	—
projection separation	—	.0.5%
events passing	12790 (29.4%)	6 (0.2%)

$$R = (0.0015 + 0.0013 + 0.0013 + 0.0018 + 0.0022 + 0.0011) \times (1/36) \times (1/5) \times (5.23 \times 10^{-6})$$

$$R = 9.8$$

8.6 Subtraction of the K_L background

At the target the number of K_L and K_S are equal, because the K^0 and $\bar{K}^0$ which are produced by the strong interaction at the target are linear superpositions of K_S and K_L in equal proportions. The K_S beam, whilst dominated by K_S decays, especially close to the target, has a K_L content which is approximately flat throughout the decay region. Therefore $K_L \to 2\gamma$ decays will be present in the K_S

Table 14: The L_i in the determination of R.

GEV	1	2	3	4	5	6	7	8	9 Z bins
70–90	$\frac{809}{330}$	$\frac{799}{409}$	$\frac{879}{416}$	$\frac{954}{531}$	$\frac{993}{503}$	$\frac{1060}{606}$	$\frac{1010}{592}$	$\frac{1060}{685}$	$\frac{830}{487}$
90–110	$\frac{595}{439}$	$\frac{629}{415}$	$\frac{676}{446}$	$\frac{633}{489}$	$\frac{718}{527}$	$\frac{679}{469}$	$\frac{677}{480}$	$\frac{678}{453}$	$\frac{436}{283}$
110–130	$\frac{387}{328}$	$\frac{370}{323}$	$\frac{346}{306}$	$\frac{381}{309}$	$\frac{365}{334}$	$\frac{352}{261}$	$\frac{326}{278}$	$\frac{327}{216}$	$\frac{214}{162}$
130–150	$\frac{156}{204}$	$\frac{141}{173}$	$\frac{149}{169}$	$\frac{142}{183}$	$\frac{156}{157}$	$\frac{139}{158}$	$\frac{113}{112}$	$\frac{130}{97.5}$	$\frac{88}{62.7}$

beam, indistinguishable from $K_S \to 2\gamma$ decays. The number of events expected from this source can be calculated by at least two methods.

The more precise method uses the $K_S \to 2\pi^0$ events. To each event a weight is assigned; the probability that the event travelled the observed distance from the target before decaying:

$$P_S = \exp(-(md_T/E\ c\ \tau_S))$$

where d_T is the distance of the vertex of the event from the K_S target. The probability that a K_L decayed at the same position to $2\pi^0$ is:

$$P_L = \exp(-(md_T/E\ c\ \tau_L)) \times (1/P_S) \times (|\eta_{00}|^2) \times 5$$

The observed ratio of $K_L \to 2\pi^0$ events to $K_L \to 2\gamma$ events, has already been determined for the measurement of B. Using the mean value of L_i the number of 2γ events from K_L is :

$$N_L = P_L \times L_i$$

Table 15: The S_i in the determination of R.

GEV	1	2	3	4	5	6	7	8	9 Z bins
70–90	$\frac{1}{265}$	$\frac{0}{355}$	$\frac{0}{392}$	$\frac{0}{435}$	$\frac{0}{478}$	$\frac{0}{325}$	$\frac{0}{269}$	$\frac{0}{347}$	$\frac{0}{220}$
90–110	$\frac{0}{465}$	$\frac{1}{504}$	$\frac{0}{585}$	$\frac{1}{576}$	$\frac{0}{597}$	$\frac{0}{388}$	$\frac{1}{327}$	$\frac{0}{354}$	$\frac{1}{222}$
110–130	$\frac{0}{507}$	$\frac{0}{492}$	$\frac{0}{501}$	$\frac{0}{512}$	$\frac{1}{497}$	$\frac{0}{340}$	$\frac{0}{230}$	$\frac{0}{212}$	$\frac{0}{131}$
130–150	$\frac{0}{357}$	$\frac{0}{368}$	$\frac{0}{368}$	$\frac{0}{306}$	$\frac{0}{325}$	$\frac{0}{216}$	$\frac{0}{124}$	$\frac{0}{130}$	$\frac{0}{70}$

Because we have used the data directly we have not needed to make any assumptions about the flux, the spectrum or the acceptance. The method predicts :

$$N_L = 2.13 \times 1.48 = 3.2 \pm 0.05$$

$K_L \rightarrow 2\gamma$ background events.

It is possible to measure the K_L content of the beam directly; detecting $3\pi^0$ decays which can only be produced by K_L in the limit of CP − conservation. We determine the ratio of 2γ to 6γ events in the K_L beam then select 6γ events in the K_S beam to predict the $K_L \rightarrow 2\gamma$ events in the same ζ region. We observe 40 events leading to :
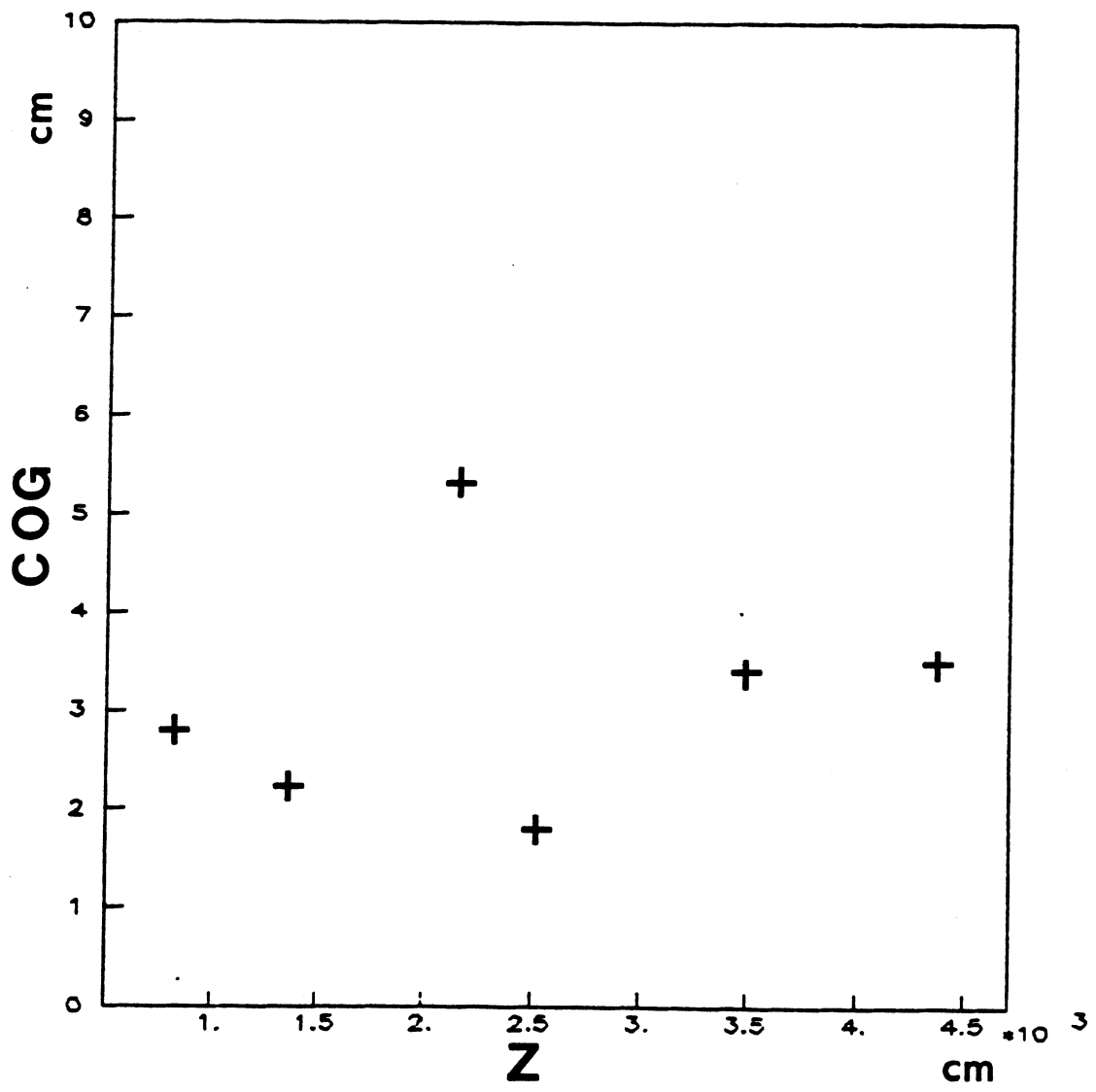
Figure 76: Z vs. first moment for K→γγ events in the K_S beam.

$$L_6 = N(K_L \rightarrow 2\gamma) / N(K_L \rightarrow 3\pi^0)$$

$$N(K_L \rightarrow 2\gamma \text{ in} K_S) = L_6 \times N(K_L \rightarrow 3\pi^0 \text{ in } K_S)$$

$$(3.5 \pm 0.6) = 0.087 \times 40$$

The results from the two methods are in good agreement. Subtracting the weighted mean of the two backgrounds from the global value of R gives :

$$6 - (3.2 \pm 0.03) = 2.8 \rightarrow R = 4.7$$

Small numbers are dominated by poisson statistics. Both the signal and the background will fluctuate. If the mean expectation for the signal and background are S and B respectively, the probability of observing C events is :

$$P(C) = \{\exp[-(S+B)].(S+B)^C)\} / C!$$

This is a poisson distribution with mean $(S+B)$. Integrating the distribution from 0 to 6 we obtain :

$$\text{at } 90\% \text{ C. L. } 6 \rightarrow 10.53$$

That is the mean of the distribution is 10.53, the corresponding value of S is :

$$S = 10.53 - 3.2 = 7.33 \rightarrow R < 12.0$$

More correctly, using Bayes Theorem [40], if the probability distribution of S, P(S), before the measurement was made is uniform, P(C) is proportional to P(S). With negligible error in the mean value of the background, the probability of observing an S greater than some value A with 90% C.L. is :

146

$$P(S) = N \ P(C)$$

$$0.1 = {}_A\!\int^{\infty} P(S) \ dS$$

$$A = 7.16 \Rightarrow R < 11.7$$

This is the final result. It should be compared with the previous upper limit of $R < 474$.

The result may be used to constrain ϵ as explained in chapter two :

$$0 \leq |\epsilon_1|^2 \leq 1/R \quad \text{and} \quad 0 \leq |\epsilon_2|^2 \leq R$$

$$0 \leq |\epsilon_1|^2 \leq .085 \quad \text{and} \quad 0 \leq |\epsilon_2|^2 \leq 11.7$$

alternatively for the superweak case :

$$0 \leq |\epsilon|^2 \leq .085$$

Theoretically, if R is as large as 10 experiments designed to measure the partial rate difference Δ (t) will be unable to differentiate between the superweak and Kobayashi – Maskawa models of CP violation. Whilst this result represents a substantial improvement on previous measurements it is not at a level sufficient to indicate whether experiments in the future measuring Δ (t) will be valuable.

9. PREVIOUS MEASUREMENTS

9.1 Past determinations of 2γ decays.

There have been nine previous measurements of $K_L \to 2\gamma$ and five measurements of $K_S \to 2\gamma$. All were made between 1968 and 1973 except the FERMILAB result from 1984. These results together with the current work are given in Table 16 and Table 17. The column labelled quoted result refers to a paper which only gave a rate ratio rather than the branching ratio B.

Table 16: Previous determinations of $\Gamma(K_L \to \gamma\gamma)/\Gamma(K_L \to all)$

experiment	2γ events	Normalization	quoted result$\times 10^{-3}$	B $\times 10^{-4}$
Todoroff	32	$\pi\mu\nu,\pi e\nu,\pi^+\pi^-\pi^0$		6.7 ± 2.2
Arnold	16	$3\pi^0$	2.5 ± 0.7	5.4 ± 1.5 *
Banner	115	$3\pi^0$	2.24 ± 0.28	4.8 ± 0.6 *
Kunz	90	$3\pi^0$		5.5 ± 1.1
Barmin	28	$3\pi^0$	2.13 ± 0.43	4.6 ± 1.0 *
Enstrom	23	$\pi\mu\nu,\pi e\nu,3\pi^0$		4.5 ± 1.0
Repellin	≈ 100	$K_S \to 2\pi^0$		5.0 ± 1.0
Banner	≈ 4000	$K_L \to 2\pi^0$		4.54 ± 0.84 †
Norton	≈ 8000	$3\pi^0$	2.836 ± 0.058	6.10 ± 0.32 *
this result	≈ 18000	$K_L \to 2\pi^0$	0.62 ± 0.014	5.87 ± 0.24

* using world average for $\Gamma(K_L \to 3\pi^0)/(K_L \to all)$

† using their value $|\eta_{00}|^2/|\eta_{+-}|^2 = 1.05 \pm 0.14$

It is appropriate to compare the previous measurements with this result. Five of the experiments have measured $\Gamma(K_L \to \gamma\gamma)/\Gamma(K_L \to 3\pi^0)$ and so a comparison can only be made after a conversion of the rate ratio into a branching ratio. This process results in a systematic error larger than the systematic error in Norton's case. It is quite surprising that so many of the K_L decay channels have been so

Table 17: *Previous determinations of* $\Gamma(K_S \to \gamma\gamma)$

experiment	2γ events	Branching ratio $\times 10^{-3}$	R*
Banner	0	21.0	24900
Repellin	0	2.2	2609
Banner	0	0.71	842
Morse	0	2.0	2372
Barmin	0	0.4	474
this result	0	0.01	11.7

* using old world average 4.9×10^{-4}

All results are at 90% C. L.

Figure 77: *History of* η_{+-}

$\Gamma(K \rightarrow 2\gamma)/\Gamma(K \rightarrow ALL)$

$x10^{-4}$

9

8

7

6

5

4

3

[5] [7] [8] [6] [9] [11] [10] [12] [1] **REF**

2σ

this
result
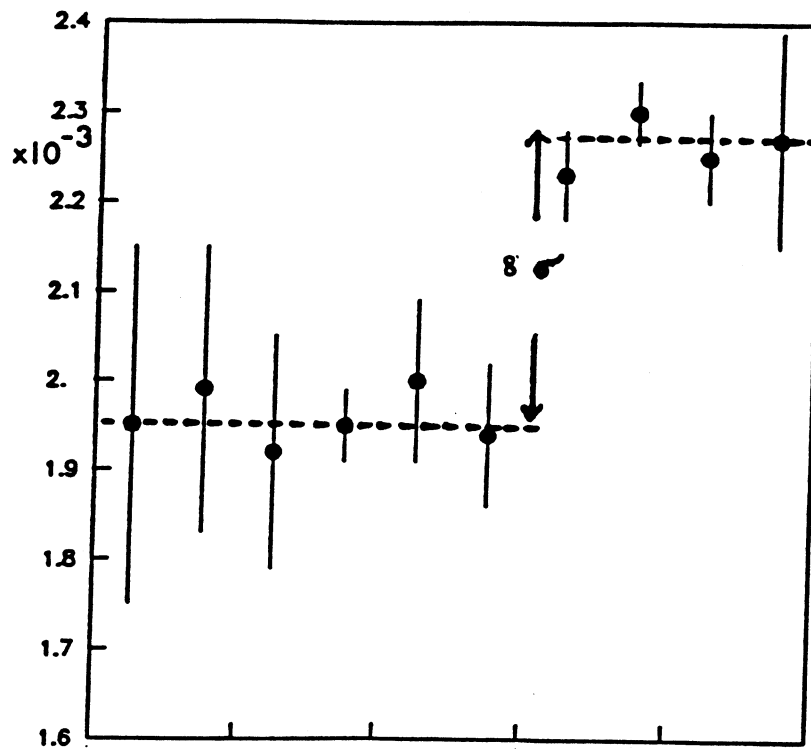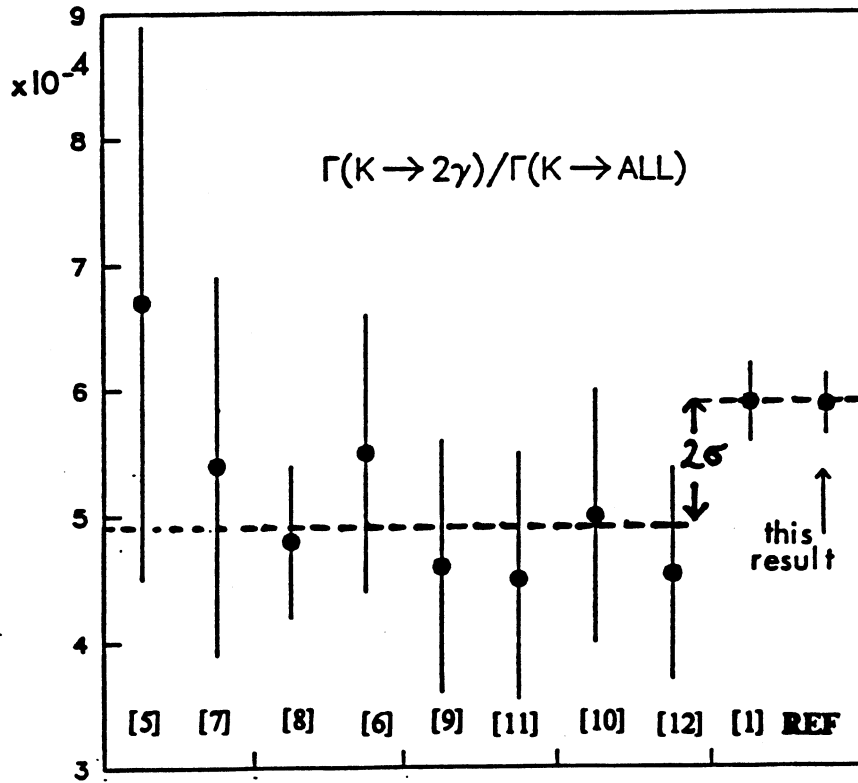
Figure 78: History of $\Gamma(K_L \rightarrow 2\gamma)/\Gamma(K_L \rightarrow all)$

poorly measured. It would certainly be valuable to have more precise determinations of the neutral modes.

Criegee et al. [5] were the first group to detect the decay $K_L \rightarrow 2\gamma$ at Brookhaven in 1966 in an experiment dedicated to that mode only. They employed an optical spark chamber (OSPC) to measure the coordinates of the photons which converted in the chambers, and lead — scintillator shower detector to measure energies. From the opening angles of the two photons in the best plane through the two tracks, and the energies, the invariant mass was calculated. The poor mass resolution ($\Delta m/m \approx 100$ MeV) of the experiment meant a a strong dependence on monte carlo to subtract the background from $2\pi^0$ and $3\pi^0$ decays in which only two photons were detected. The initial result was later replaced by the thesis of Todoroff [5] whose value is shown in Table 16 .

Cronin et al. [6] working at the Princeton Pennsylvania Accelerator (PPA), used a different technique. Only one gamma ray was detected and converted to an electron positron pair in each event. Energies of the pair were determined in an OSPC in a magnetic field. Independently, the momentum of the parent kaon was determined by a time of flight system (TOF). This enabled the observed photon to be transformed to the cms system of the kaon. As shown in chapter four the kinematics in that frame are quite different for the three neutral decay modes. The energy resolution in the cms was determined from the monochromatic 2γ decay to be 15%. The kinematical cutoffs in E_{cm} where used to separate the three processes. In the original paper several events are found with $E_{cm} > 260$ MeV, which were not understood. The result was later replaced by the thesis of Kunz [6].

Using a heavy liquid bubble chamber (HLBC) at CERN, Arnold et al. [7] measured photons converted in the liquid, from a neutral beam incident on the chamber. The energies were deduced both from the total track length and the observed curvature in the magnetic field. The invariant mass of the event was determined with a resolution of 20%. All events with an invariant mass greater than 350 MeV were considered as candidates. The normalistion to $3\pi^0$ events taken simultaneously.

Barmin et al. [9] at ITEP used the same technique as Arnold. Even the letter reporting the result is remarkably similar.

Banner et al. [8] performed an experiment measuring $\Gamma(K_L \to 2\pi^0)/\Gamma(K_S \to 2\pi^0)$ in order to obtain $|\eta_{00}|^2$ at the PPA. The detector was also able to accept 2γ decays. The principle, which was the same as Cronin et al. in 1966, involved transforming the photons to the rest frame of the kaon, however in this experiment the second gamma was also measured in a separate spark chamber. Because of the low energy of the photons, only the position of the second gamma was used, the vertex being determined by projecting the well–measured track back to an intersection with the beam. The signal was extracted by cutting in E_{cm} and the coplanarity angle. The coplanarity is defined as the cosine of the opening angle, θ, between the two gamma rays in the cms frame. The $2\pi^0$ background is flat in coplanarity and this was used to extract a small observed background.

In order to investigate possible neutron induced backgrounds in the detector a regenerator was inserted in the beam. This enabled a measurement of $K_S \to 2\gamma$ to be made. For this study only the region close to the regenerator was used for the signal, the same cuts were used as in K_L. In addition the TOF information reavealed the presence of beam interactions in the regenerator which were cut. In a plot of E_{cm} vs. $\cos\theta$ the region where the K_L signal had peaked now contained 1 event.

Using $3\pi^0$ events obtained from the regenerator run compared to the number of the same events in the free run the relative exposures of the two runs could be determined. The observed 2γ events in the free run were scaled with this ratio to predict 1.1 events in the K_S data. A further background from incoherently regenerated $2\pi^0 \to 2\gamma$ was put at 0.8 events. At the 90% CL, 2 events remained after background subtractions. The result was fairly insensitive to assumptions about interference between K_L and K_S as 64% of all the K_S observed arose from incoherent regeneration.

Enstrom et al. [11] at SLAC also used OSPC to determine tracks of the photon and a TOF system to obtain the kaon momenta. The two tracks were fitted to a pair of straight lines which formed a common vertex at their point of intersection with the beam. A coplanarity plot then extracted the data from the $2\pi^0$ background. In a special run, the detector accepted charged decay products also to determine the absolute K_L flux which was used for the normalization.

Banner et al. [12] used an OSPC at Brookhaven. The main aim of the experiment was a determination of $|\eta_{00}|^2$. With an uranium regenerator in the beam both gamma rays were detected but only one, which was converted into an electron pair was well measured. The energy resolution was $\Delta E/E = 2.5\%$ and with good angular resolution a cut in P_T was made on line. The vertex was found by projecting the converted photon back to the very thin ribbon beam. The kaon mass however could only be calculated by requiring that the magnitude of the transverse momentum vector of the unconverted gamma be equal an opposite to the converted gamma. By binning the data in z and the supplement of the angle between the transverse momentum vector of the two gamma rays, the contributions from $K_S \to 2\pi^0$ and $K_L \to 2\gamma$ could be be isolated and subtracted from the small angle small z bin where most

152

$K_S \rightarrow 2\gamma$ could be expected to lie. The 53 events observed in this bin have to be compared with the 40.5 $2\pi^0$ and 22.2 K_L events expected, thus -9.7 events were observed. The normalisation was to the $K_L \rightarrow 2\gamma$ events observed.

It should be remembered that in traditional determinations of η_{00} the regenerator amplitude is approximately equal to the length of the K_L decay region divided by the K_L decay length averaged over the momentum spectrum, in order to provide equal intensities of K_L and K_S to maximise interference. This is of course a far from ideal situation for identifying $K_S \rightarrow 2\gamma$ decays :

$$N(K_S 2\gamma)/N(K_L 2\gamma) = B(K_S \rightarrow 2\gamma)/ B(K_L \rightarrow 2\gamma) \quad |\rho|^2/(L/\Lambda_L)$$

where the notation is transparent and the assumption that acceptances cancel has been made for simplicity. When the last term on the r.h.s. is less than or equal to unity trying to observe $K_S \rightarrow 2\gamma$ is extremely difficult if theoretical predictions are to be believed. Unfortunately this was exactly the situation Banner et al and most other previous experiments have been in, the 90% CL for their negative observation is shown in the table.

From the run without a regenerator in the tank 4000 K_L events were found, the only normalisation available was 120 $2\pi^0$ decays found in the η_{00} experiment. The quoted result for B explicitly removes $|\eta_{00}/\eta_{+-}|^2$, in order to separate the error due to the uncertainty in $B(K_L \rightarrow 2\pi^0)$.

Using the HLBC at ITEP Barmin et al. [2] produced K^0's in the chamber from a π^- beam. The converted gamma tracks were extrapolated back to form a common vertex, energies were determined by total track length. 15 candidates with an invariant mass greater than 300 MeV were found. The contribution from $2\pi^0 \rightarrow 2\gamma$ was predicted to be 16.3 events, whilst the contribution from $K_L \rightarrow 2\gamma$ decaying in the chamber was negligible. At 90% CL $21.4 - 16.3 = 5.1$ events, after acceptance correction a maximum likelihood fit gave 5.7 events. From the number of $K_S \rightarrow 2\pi^0$ decays observed corrected for acceptance and scanning efficiency and the branching ratio for $2\pi^0$ the 2γ branching ratio was determined. Since no $K_L \rightarrow 2\gamma$ events were expected the result was independent of any assumption about interference. It was this experiment that set the limit on R until the present work.

Morse et al. [4] determined $K_S \rightarrow 2\gamma$ using a deuterium bubble chamber at Brookhaven exposed to a beam of charged kaons. The neutral kaons were produced in the chamber in charge exchange interactions. The photons were converted in stainless steel cones in the liquid. If two converted photons were seen they were projected back to the charge exchange vertex and transformed into the kaon centre of mass determined by a fit to the charge exchange products. A background from K^+ scattering, and from π^+ in the beam had to be corrected for. After allowing for detection efficiency and background subtraction 0 ± 7 events were found. From $2\pi^0$ and $\pi^+\pi^-$ events found in the same scan the branching ratio could be determined.

Repellin et al. [10] at CERN used an OSPC behind a regenerator. The K_S intensity relative to K_L was 0.6%. Gamma ray energies were determined by spark−counting. A cut in the transverse momentum removed $3\pi^0$ decays. Due to the presence of both K_L and K_S decays in the chamber Repellin was able to calculate both branching ratios, using the region close to the regenerator for the latter. The K_L mass peak was only clearly visible in the downstream region. The main systematic error arose from background subtraction of $K_S \rightarrow 2\pi^0 \rightarrow 2\gamma$ which was uncertain by a factor of two due to the poor energy resolution. The regeneration amplitude was uncertain for copper at the energy used and the result quoted explicitly factors it out.

The measurement of Norton [1] has a considerable number of advantages over the previous measurements. Performed at FERMILAB in an experiment designed to measure $|\eta_{00}/\eta_{+-}|^2$, the high energies, $60 - 140$ GeV, of the beam and the superior statistics make the measurement much easier. All the photon energies were measured in a lead glass electromagnetic calorimeter with a resolution of $\{0.06/E + 0.02\}^{0.5}$. One gamma is converted in a lead plate and tracked by scintillator and drift chambers to the calorimeter. The decay vertex is determined by projecting the track from this gamma back to its instersection with the line between the neutral beam production target and the centre of gravity of the γ rays at the lead glass. The momentum of every photon in a decay is therefore measured, and the invariant mass can be calculated. To decrease background in the 2γ mode to about

10 %, cuts in the centre of gravity, and closest distance of approach between the line made by the converted photon and the path travelled by the kaon are made.

This was the only experiment to allow for the energy dependence of the pair production cross section in lead. Norton estimates that for Banner et al. the pair production cross section changed by a factor of two. The normalisation was to $3\pi^0$ taken simultaneously. The acceptance for $3\pi^0$ and 2γ were different by a factor of 42. The acceptance was very sensitive to to the gamma ray conversion probability. It was necessary to make a cut in the distance between photon showers in the lead glass. The $3\pi^0$ normalisation was checked by calculating the $2\pi^0$ branching ratio, and more stringently by calculating $|\eta_{00}/\eta_{+-}|^2$. The result obtained by Norton was in good agreement with the final result for that quantity published by the experiment.

This experiment shares the advantages of high energies and large statistics with Norton. In Table 18 a comparison between the two experiments is made. The technique of converting a photon to determine the momentum has some attendant complications. The energy is always less well$-$measured as the electron pair emit bremstrahlung. Whilst the conversion probability in lead is known, account must also be taken of the Dalitz process which has a different amplitude for $K_L \rightarrow 2\gamma$ and $K_L \rightarrow 3\pi^0$. This is never mentioned in Norton's work. The momentum measurement also involves the efficiency of the drift chambers.

Recently [41] a correction for the Dalitz process made to Norton's final result has been communicated to us. With this correction the result of Norton changes :

$$B = 6.1 \pm 0.32 \times 10^{-4} \text{ (without Dalitz correction)}$$

$$B = 5.9 \pm 0.31 \times 10^{-4} \text{ (with Dalitz correction)}$$

Norton was forced to make a cut in the closest distance of approach between the converted gamma ray track and the kaon trajectory to reject a large accidental background. The lead glass was less

well calibrated at the edges where only 2γ events deposited energy. The $2\pi^0$ final state is considerably easier to reconstruct than $3\pi^0$. The principle advantage Norton has over this result is the measurement of the invariant mass. This is of particular benefit in the less clean conditions of the FERMILAB experiment.

Table 18: Comparison of this experiment with FERMILAB

	CERN	Norton
Acceptance 2γ	46 %	1.5%
Acceptance nπ^0	20 %	0.036%
Background 2γ	< 1%	10%
Background nπ^0	2.8%	4%

The result we have obtained for the branching ratio of $K_L \rightarrow \gamma\gamma$ is approximately two standard deviations above the world average and in excellent agreement with the recent FERMILAB result. However the result is not seriously in disagreement with any of the previous results taken individually. The weighted average of Norton and this result, is two standard deviations from the world average, this difference should be contrasted with the eight standard deviation change in the mean value of m_{+}! calculated from determinations prior to, and after 1973. In Figure 77 and Figure 78 the changes in the world average with time are shown. It is widely believed that the post 1973 experiments are superior by virtue of their higher statistics and better technology and hence the world average no longer includes the earlier experiments, however no reason is known for the discrepancy in the two sets of results. Certainly the energy in the later experiments was always greater than 5 GeV whilst the early measurements were at lower energies. Higher energies make the measurement easier, however either one concludes that there is an energy dependent effect in which case more low energy determinations are needed or that the PDG is correct and that superiority accounts for the difference. Nevertheless all measurments save the first were made with a knowledge of

previous results and these results clearly seem to have influenced the later determinations. This phenomena is often seen to occur in science and is, we believe, inevitable. It does not constitute a problem as long as a result which differs considerably from previous results is still accepted for publication.

REFERENCES

[1]   R.H.Bernstein et al., Phys.Rev.Lett. 54 ,1631 (1985). M.W.M.Norton, Ph.D.Thesis, University of Chicago, 1984 (unpublished) for the determination of $K_L \rightarrow \gamma\gamma$. R.H.Bernstein, Ph.D.Thesis, University of Chicago, 1984 (unpublished) for a full description of the apparatus.

[2]   V.V.Barmin et al., Phys. Lett. 47B, 463 (1973)

[3]   Glashow, S.L., J. Iliopoulos, and L. Maiani, Phys. Rev. D 2, 1285 (1970).

[4]   R. Morse et al., Phys. Rev. Lett., 28, 388 (1972).

[5]   L. Criegee et al., Phys. Rev. Lett., 17, 150 (1966). replaced by: J. Todoroff Ph.D Thesis, University of Illinois (unpublished) (1967).

[6]   J.W. Cronin et al., Phys. Rev. Lett., 18, 25 (1967). replaced by: P. F. Kunz Ph.D. Thesis, Princeton University (1968) (unpublished)

[7]   R.Arnold et al., Phys. Lett., 28B,.56 (1968)

[8]   M. Banner et al., Phys. Rev., 188, 2033 (1969)

[9]   V. V. Barmin et al., Phys. Lett., 35B, 604 (1971)

[10]   J. P. Repellin et al., Phys. Lett., 36b, 601 (1971)

[11]   J. Enstrom et al., Phys. Rev., D4, 2629 (1971)

[12]   M. Banner et al., Phys. Rev. Lett., 29, 237 (1972).

[13]   D. Cundy et al., proposal P174, CERN/SPSC/81 − 110 (1981)

[14]   L. Wolfenstein, Phys. Rev. Lett., 13, 380 (1964)

[15]   B. Guberina, and R. Peccei Nucl. Phys. B163, 289 (1980)

[16]   J. Ellis, M. K. Gaillard, and D. V. Nanopoulos, Nucl. Phys. B109, 213 (1976)

[17]   L.Adiels et al., CERN/PSCC/85− 6, PSCC/P− 82 (1985), Proposal for experiment P5195 at CERN.

[18]   M. Kobayashi, and T. Maskawa, Prog. Theor. Phys. 49, 652 (1973)

[19]   M.K.Gaillard and B.W.Lee, Phys.Rev.D10 (1974) 897

[20]   Zenaida E.S.Uy, Phys.Rev.D29 (1984) 574; D27 (1983) 300; D19 (1979) 1623 ; D3 (1971) 234.

[21]   K. Nishijima, Fields and Particles (benjamin, New York, 1969); and the correction to the calculation in: F.J. Yndurain, Prog. Theor. Phys. 48, 261 (1972).

[22]   B. R. Martin et al., Phys. Rev., D2, 179 (1970).

[23]   Particle Data Group, Review of particle properties, Rev. Mod. Phys. 56, Number 2 Part 2 (1984).

[24]   I. Ma, and A. Pramudita, Phys. Rev., D24, 2476 (1981)

[25]   B.R. Martin and E. de Rafael Nucl. Phys., B8, 131 (1968).

[26]   N.Cabibbo and E.Ferrari, Nuovo Cimento 18, 928 (1960).

[27]   L. L. Chau and H. Y. Cheng, Phys. Rev. Lett., 54, 1768 (1985) N.Cabibbo and E.Ferrari, Nuovo Cimento 18, 928 (1960).

[28]   L. L. Chau, Phys. Rep. 95, (1983).

[29]   J.Dreitlein and H.Primakoff, Phys.Rev.124, 268 (1961).

[30]   J.H.Christenson,J.W.Cronin,V.L.Fitch and R.Turlay, Phys.Rev.Lett. 13,138(1964).

[31]   F.Gilman and M.Wise, Phys.Rev.D20, 2392 (1979). F.J.Gilman and J.S.Hagelin, Phys.Lett.133B, 443 (1983).

[32]   J.K.Black et al., Phys.Rev.Lett. 54, 1628 (1985).

[33]   The NA31 Collaboration, The Beam and Detector for a High−precision Measurement of CP Violation in Neutral K Decays (to be published in Nuclear Instrumentation and Methods).

[34]   The NA31 collaboration, The Fastbus Software Workshop, CERN Yellow Report, CERN85−15.

[35]   J.F.Donoghue, E.Golowich and B.R.Holstein, Phys. Lett. 135B, 481 (1984).

[36]   J.F.Donoghue and B.R.Holstein, Phys.Rev.D29, 2088 (1984).

[37]   Y.Dupont and T.N.Pham, Phys. Rev. D29, 1368 (1984).

[38]   R. Decker, P. Pav lopoulos and G. Zoupanos, CERN preprint, TH.3917−CERN (1984).

[39]   N. M. Kroll and W. Wada, Phys. Rev., 98, 1355 (1955)

[40]   O. Helene, Nucl. Instr. and Meth., 212, 319 (1983) W. T. Eadie et al., Statistical Methods in
Experimental Physics, (North−Holland, Amsterdam, 1971)

[41]   Private communication from Professor Winstein.

Acknowledgments

I am grateful to many people who have helped me during the last four years.

I was supported financially by several sources. I thank, the Science and Engineering Research Council of the United Kingdom for their studentship, Dr.David Candlin and Professor David Wallace of the University of Edinburgh for their help in obtaining a Dewar Fellowship and Dr. Heinrich Wahl of CERN for support.

For the first two years, I was engaged in constructing the muon−veto with many others. I thank the members of the University of Edinburgh mechanical workshop, who constructed the frame. The muon−veto was wrapped, tested and assembled at Rutherford Appleton Laboratory. I thank the physicists, technicians and women who helped in this task, and for making my stay in Oxfordshire so enjoyable.

At CERN, I would like to thank the members of the NA31 collaboration. In particular, Dr. Mario Calvetti, Professor Italo Mannelli and Dr. Heinz−Georg Sander with whom I worked closely and learnt a great deal.

I am especially grateful for the privilege of working with Dr. Donald Cundy, who had the original idea to look at 2γ, and without whose enthusiasm and encouragement this analysis would not have been possible.

I thank Dr. Ken Peach for his supervision over four years and for reading this thesis and suggesting numerous improvements.

I also thank Dr. Chris Bee for reading the manuscript and making helpful suggestions.

Finally I thank Dr. Daniela Bortoletto, for her love and encouragement, and the enormous contribution she made to producing this thesis.